Dr. I. Pieter Adrianus Neeteson

Having received his degree in physical engineering from the Delft Technical University, Mr. Neeteson wrote his thesis for a doctorate in technical sciences on the analysis of the bi-stable multivibrator operation (1956).

He is at present actively engaged in research work in the Philips Central Applications Laboratories in Eindhoven (Holland) on the application of semiconductors. Previous work done by him included radio and television development (he is the author of a book on television receiver design, Flywheel Synchronization of Sawtooth Generators) and investigations into ultra-high frequency receivers.

His forthcoming book in the field of semiconductors (Junction transistors in Pulse Circuits), offers the reader a thorough insight in his experiences with this nearly ideal switch, which is now applied on a larger scale.

ELECTRONIC VALVES

BOOK X

P. A. NEETESON

ANALYSIS OF BISTABLE MULTIVIBRATOR OPERATION

PHILIPS
TECHNICAL
LIBRARY

Second enlarged edition

This extended analysis of the transient behaviour of the bistable multivibrator circuit evoked such interest that within three years a second edition was necessary. This edition has been enlarged by an extra chapter, which contains some actual bistable multivibrator circuits and binary or decimal counters composed thereof.

This bistable multivibrator, although conceived by Eccles and Jordan as early as 1919, has only started within the last ten years to play an important role in electronic pulse apparatus; in this field the counting machines occupy an important position.

In designing such a circuit, it is usual to consider only the stability of the static condition, when the circuit is at rest; this is easy in view of the fact that one then only has to deal with d.c. valves. It is, however, far more difficult to derive formulae for the phenomena occurring when the multivibrator is switching over, taking into account, of course, the influence of tube-characteristics and circuit components.

ANALYSIS OF BISTABLE MULTIVIBRATOR OPERATION

ANALYSIS OF BISTABLE
MULTIVIBRATOR OPERATION

ANALYSIS OF BISTABLE
MULTIVIBRATOR OPERATION

THE ECCLES-JORDAN
FLIP-FLOP CIRCUIT

BY

P. A. NEETESON

Second enlarged edition
1960

PHILIPS TECHNICAL LIBRARY

PREFACE TO THE FIRST EDITION

The bistable multivibrator, although conceived by Eccles and Jordan as early as 1919, has only started recently to play an important role in electronic pulse apparatus; in this field, the electronic counters and computers occupy an important position.

Perhaps the initial lack of practical interest shown in this useful circuit, and the subsequent excessive attention which it evoked, account for the fact that no really thorough analysis of the circuit has until now been published.

In designing such a circuit, it is usual to consider only the stability of the static condition, when the circuit is at rest; this is easy in view of the fact that one then only has to deal with d.c. conditions. It is, however, far more difficult to derive formulae for the phenomena occurring when the multivibrator is switching over, taking into account of course the influence of tube-characteristics and circuit components. In the present book a thorough analysis of the dynamic behaviour of the bistable multivibrator is given. This investigation was prompted by a practical problem and the results proved to be useful as a guide in the development of special tubes for this application and for other circuits in this sphere of pulse techniques. A general consideration of the vacuum tube as a switch was published in the book: Vacuum Valves in Pulse Technique.

This book may be appreciated by those who feel that in the long run it is not satisfactory to apply certain circuits on the basis of technical "feeling" or practical experience, but that a thorough insight into the nature of the phenomena are necessary to realize the full potentialities of these circuits. The author is greatly indebted to Prof. Ir. B. D. H. Tellegen who supervised the thesis on which this work is based and whose critical discussions have contributed much to the value of its contents. Thanks are also due to Mr. D. J. Mitchell, M. A. for reading the English text.

July 1956   The Author

PREFACE TO THE SECOND EDITION

Taking into account that this book is based on a thesis for getting the doctor's degree in Electrical Science at the Technical University of Delft, it will be clear that no attempt for popularizing the treatment of the subject could be introduced. Therefore it is a pleasant surprise to the author that this extended analysis of the transient behaviour of the bistable multivibrator circuit evoked such interest that within a few years a second edition was necessary. It reinforces his idea that a thorough analysis of electronical circuits is necessary to help understand their operation and to stimulate the further development and design of similar or new circuits. This second edition has been enlarged by an extra chapter which contains some actual bistable multivibrator circuits and binary or decimal counters composed thereof. It is hoped that this makes the book useful to a still larger number of readers.

April 1960   The Author

CONTENTS

1. GENERAL INTRODUCTION

In modern pulse technique a certain electronic switching circuit, known as the *bistable multivibrator* or *Eccles-Jordan flip-flop* circuit, has found widespread application. The field of pulse technique covers a great variety of apparatus, which generate a certain pulse pattern, often called the "logic", or which are caused, by the input of a given pulse pattern, to perform a certain logical operation. With this kind of electronic apparatus may be classed electronic counting and computing devices, time-measuring apparatus, pulse-modulation systems, radar, television, telemetering and automatic-telephony circuits.

The basic circuit and operation principle of a bistable electronic trigger device was first indicated by Eccles and Jordan and described in the Radio Review of December 1919, pp. 143–146, under the title: "A Trigger Relay Utilising Three-Electrode Thermionic Vacuum Tubes".

It is worth while to cite the argumentation that led to their invention:

"In a well-known method of using a triode for the amplification of wireless signals an inductive coil is placed in the filament-to-anode circuit, and another coil magnetically coupled with this is introduced into the filament-to-grid circuit. This 'back-coupling', as it is sometimes conveniently called, if it is arranged in the right sense, greatly exalts the magnification produced by the tube in any alternating E.M.F. applied to the grid; for the induced E.M.F. passed back to the grid is in correct phase relation to add directly to the original alternating E.M.F. applied there. If, instead of using inductive retroaction of this kind, we attempt to use resistance back-coupling, then the retroactive E.M.F. applied to the grid is exactly opposite in phase to the original alternating E.M.F., and the amplifying action of the triode is reduced. Since, however, one triode can produce opposition in phase in the manner indicated, it is clear that two or any even number of similar triode-circuits arranged in cascade can produce agreement in phase. Hence we conclude that retroactive amplification can be obtained by effecting a back-coupling to the first grid from the second, fourth, and so on, anode circuit of a set of triodes arranged in an ohmically-coupled cascade. It is possible to take advantage of the fact above stated for obtaining various types of continuously-acting relay, but the purpose of the present communication is to describe what may be called a one-stroke relay which, when operated by a small triggering electrical impulse, undergoes great changes in regard to its electrical equilibrium, and then remains in the new condition until re-set".

The authors then describe two possible circuits, in which the principle

mentioned is incorporated. These circuits are represented in figs. 1–1 and 1–2, where E_1 and E_2 represent anode-voltage batteries, e_1 and e_2 grid-voltage batteries, no polarity being indicated in the latter. An external voltage pulse V_i is applied to the transformer T. No tube types are given. In the initial condition the hatched triode draws a large current, the other one a very small current. A positive voltage pulse on the grid of the left-hand triode starts a chain of events in the circuit which results finally in the left-hand tube drawing a large, and the right-hand tube a small current.
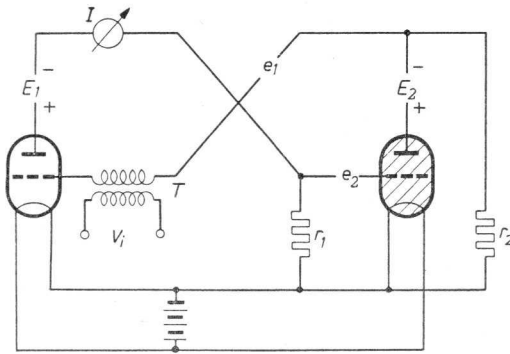
Fig. 1–1

This change is indicated by an "ammeter or a moving tongue relay", I in figs. 1–1 and 1–2.

Further, it is mentioned that "in order to restore the initial conditions it is easy to interrupt for an instant the linkage between the tubes, or to stop the operation of one or both of the tubes, as, for instance, by dimming its filament".

The change in current through the ammeter is from 0–2.5 micro-amperes, using the following values in the circuit of fig. 1–1:

$E_1 = 78$ V, $E_2 = 74$ V, $r_1 = 22000$ ohms, $r_2 = 12000$ ohms, $e_1 = 31$ V, $e_2 = 17.5$ V.

The sensitivity using a given telephonic transformer, with a telephone connected to the primary, is such that "the relay is operated with cer-

Fig. 1–2

tainty by snapping the thumb and the finger at a distance of five feet from the telephone".

The sensitivity of the circuit of fig. 1–2 could be made even greater when using the following values:

$$E = 80 \text{ V}, \, r_1 = r_2 = 100000 \text{ ohms}, \, e_1 = e_2 = 40 \text{ V}.$$

No grid leak values are given.

It is clear that the main purpose of these circuits must have been to realize a very sensitive trigger relay and that the speed of operation, more precisely the repetition frequency of the trigger action, cannot have been high if the relay circuit was brought back to its initial condition by "interrupting the linkage between the tubes or dimming their filaments". It must be admitted that 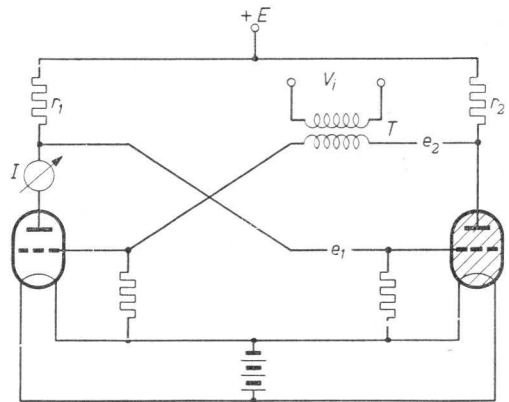the authors explicitly mention the circuits as examples of a "one-stroke relay". Now, it is the possibility of successive trigger action that renders the Eccles-Jordan circuit specially suited for application in modern high-speed electronic switching devices.

In the same way as a positive voltage pulse, applied to the grid of the non-conducting tube, switches the trigger circuit into its reverse state, a subsequent negative pulse at the same grid will return it to its initial state. Or, alternatively, a second positive pulse at the grid of the other tube will again restore the initial condition. The accompanying voltage changes at the anodes of the tubes can be used advantageously for opening or closing electronic gate-circuits. This mode of operation, characterized by the application of trigger pulses to only one grid at a time, has found wide use in a variety of pulse "logic" apparatus. A second possible way of trigger operation, however, has also found important application. In this case, pulses of the same polarity are applied to both grids simultaneously. If these trigger pulses are negative, the conducting tube will always be cut off, the other tube will become conducting. At the application of every pulse the circuit will reverse its state. After two pulses the initial condition will be restored, in other words the flip-flop changes its state with a frequency that is the half frequency of the applied trigger pulses and the circuit acts as a frequency divider. Using the anode-voltage changes of one of the tubes as trigger pulses for a next flip-flop circuit results again in a frequency reduction by a factor two. Thus, the frequency of the voltage changes in the second trigger circuit is one quarter of the frequency of the input trigger pulses. This frequency division in a binary scale is one of the basic elements that has enabled the development of modern electronic computers and counting apparatus. Counting speeds up to a pulse repetition frequency of 20 Mc/s have been obtained in four cascaded flip-flop circuits with modern double-triode tubes, especially developed for computing and counting purposes. By application of suitable feedback in a four-cascade arrangement, the division by 16 may be reduced to a division by 10. This is commonly accomplished by applying the output pulses of one or

more stages of the cascade of four bistable multivibrators to the grids of one or more other stages in such a way that in total six of the sixteen possible positions of the counter array are skipped [1]). The same may be accomplished by the application of a gate circuit [2]). Another possibility of arranging a decimal counter with the aid of bistable multivibrators is to combine a ring-counter of five multivibrators with a single multivibrator in cascade. In this way a division by five and a division by two result in a decimal system [3]) (bi-quinary system).

These methods offer the possibility of making decimal system counters and computers. Trigger pulses ("clock-pulses") having repetition frequencies up to a few megacycles per second are used in electronic computers. The fundamental trigger circuit most generally used nowadays is represented in fig. 1–3. With a proper choice of the supply voltages $+V'$ and $-V''$ and of the resistance values, it is possible to attain such grid-voltage values that one of the tubes is cut off and the other conducting. Recent publications, showing the increasing interest in this trigger circuit, amply deal with this static condition and its stability. Analysis of the transient state or dynamic condition during switching of the circuit from one static condition into the other is much more complicated; nevertheless, it becomes more and more important, especially as the need to increase the repetition frequency of the trigger pulses becomes evident. Moreover, it is important to know something about the trigger sensitivity, by which is meant the minimum trigger-pulse amplitude that is necessary to obtain complete switching from one stable state into
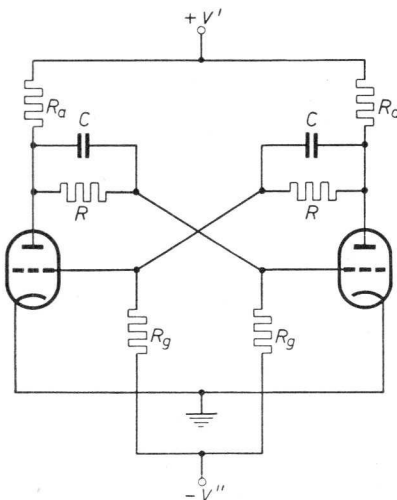
Fig. 1–3

[1]) J. T. Potter, "A Four-Tube Counter Stage", Electronics **17**, June 1944, p. 110.
   J. E. Grosdorf, "Electronic Counters", R.C.A. Review, Sept. 1946, p. 438.
   R. J. Blume, "Predetermined Counter", Electronics **21**, Feb. 1948, p. 88.
   G. J. Fergusson, G. H. Fraser, "The Design of Four-Tube Decade-Scalers", Review of Scientific Instruments **22**, Dec. 1951, p. 937.
   R. B. Mobsby, "A Decade Frequency Divider", Electronic Engineering **27**, July 1955, p. 295.
[2]) E. L. Kemp, "Gated Decade Counter requires no feedback", Electronics **26**, Feb. 1953, p. 145.
[3]) R. Weissmann, "Stable Ten-Light Decade Scaler", Electronics **22**, May 1949, p. 84.

the other. Using, with a certain safety margin, the smallest possible trigger pulse amplitude may result in less exacting demands on the pulse-generating device. Knowledge of the mechanism of the dynamic operation of the trigger circuit offers the possibility to investigate the influence of tube characteristics on the switching speed and trigger sensitivity. In general, high repetition frequencies will be advantageous for several reasons: in counting apparatus the resolution time will be small and consequently the efficiency of counting random pulses will be high; in electronic computers very complicated computing operations can be executed in a short time. Time measurements can be done more accurately the higher the clock pulse repetition frequency, as the accuracy depends chiefly on the counting or just missing of one pulse at the close of a time measurement operation.

Different names are used to designate the special circuit under consideration. We propose to adhere to the name bistable multivibrator, as it indicates the relation with two other circuits, viz. the monostable and the astable multivibrator. The latter is also called a free-running multivibrator, and is the only one that really is a "vibrator" or oscillator, as it spontaneously generates relaxation signals. It was first described by Abraham and Bloch (Comptes Rendus, Vol. 168, p. 1105, June 1919). The essential feature of the circuit is a strong capacitive feedback from the anode of the second tube of a two-tube amplifier to the grid of the first tube.

If the feedback capacitor is shunted by a suitable resistor, the astable multivibrator is changed into a monostable multivibrator, having one stable position from which it can temporarily be brought into another position by means of a trigger pulse. However, it will always return to its stable position within a time dependent on its inherent time constants.

If, moreover, the coupling capacitor between the anode of the first tube and the grid of the second tube is also shunted by a resistor of suitable value, and suitable grid bias voltages are applied, the monostable multivibrator is converted into a bistable multivibrator.

It will be clear that the main factors limiting the switching speed are to be found in the inherent time constants of the circuit, which are determined by coupling capacitances, tube capacitances, wiring and other stray capacitances and resistive components. As there is a practical limit to reducing the capacitances, the decrease in time constants will mainly have to be achieved by diminishing the resistances of the circuit. This implies an increase in power to be supplied by the D.C. voltage sources. The voltage drop across a small anode resistance, when a tube is switched

from cut-off to full conduction or vice versa, may become too small to be of any use for further application in a logic system. This could, of course, be prevented by using more powerful tubes that could supply high anode currents, but the expense and the inevitably higher inter-electrode capacitances of these tubes limit their application.

Apart from the above-mentioned limits to the switching speed, which originate from considerations of economy or construction, there is in some applications no sense in further efforts to increase the speed. If in a radiation counter, a resolution time is attained that gives an efficiency of counting random pulses of, say, 99%, then in most practical cases it will not be worth the trouble to increase the counting speed to 99.9% efficiency. In high-frequency measuring apparatus it may be more economical to bring down the frequency by superheterodyne methods – until it falls within the measuring range of the counter – than to try to extend the maximum frequency range that can be measured directly by the counter. It will also be clear that there is no use in increasing the speed of an electronic computing device if these computations take only a fraction of the time required for programming.

A high trigger sensitivity (small trigger voltage) will often be desirable, but a limit will be imposed by stability demands and possible influence of interfering signals.

Before proceeding to an exhaustive analysis of the operation of the bistable multivibrator, a survey will be given of the efforts made by others in this field so far as they have been published in recent literature.

Though most publications, as already mentioned, deal with the static condition, a few attempts have been made to get an insight into the dynamic operation of the bistable multivibrator.

2. SURVEY OF LITERATURE

A summary of the contents of articles dealing with the analysis of the bistable multivibrator is presented in chronological order.

B. E. Phelps: "Dual-Triode Trigger Circuits",
Electronics, July 1945, p. 110

In this paper an approximate explanation is given of the important and necessary function of the coupling capacitors between the anodes and grids of the tubes.

If these capacitors were not present, the grid voltages of both tubes, immediately the trigger pulse had cut off the conducting tube, would tend to the same final value, determined by the static condition of the circuit with both tubes cut off. Since the time constants in the two grid circuits are the same for a symmetrical multivibrator and the change in grid voltage of the originally non-conducting tube starts at a lower value than that of the other tube, the latter tube reaches its cut-off point sooner than the former and no triggering will occur. If, however, coupling capacitors are present between anode and grid of different tubes and the time constants of these coupling networks are much larger than those of the grid circuits, then it can be assumed that the voltages across the coupling capacitors are practically constant during the setting of the grid voltages to their final states (assuming both tubes to be kept non-conducting in some way). The voltage across the capacitor coupling the anode of the originally non-conducting tube to the grid of the other tube is much greater than the voltage across the other coupling capacitor. This causes the grid voltage of the originally non-conducting tube to tend to a much higher final value than that of the other tube and consequently it is able to reach its cut-off point sooner than the other grid voltage.

Moreover, the advantage of triggering with negative pulses at the anodes or grids as compared with positive pulses is pointed out. Positive trigger pulses at the grid of the tube which is cut off must make this tube conducting, but they are counteracted by negative pulses appearing at the anode of the conducting tube. This phenomenon is dealt with in section 7.1 of this book and illustrated by a practical case.

No explicit mathematical formulae for voltage changes at the anodes and grids are derived.

W. L. Buys: "Analysis of Scale Units",

Nucleonics, Vol. 3, November 1948, p. 49

Besides the static condition, the dynamic condition is discussed. The switching is assumed to be instantaneous, by way of sudden suppression and commencement of the anode current in the tubes. The sudden cessation of grid current flow in one tube is not taken into account in the calculation of the transient response of the circuit. In considering the positive-going grid voltage of the non-conducting tube, on the other hand, the influence of grid current is taken into account by assuming an internal grid resistance to be present between grid and cathode, as soon as the grid voltage reaches a value at which grid current starts to flow. This is assumed to coincide with the start of anode current flow, so no subdivision in three phases is made (see chapter 6 of this book). Only symmetrical circuits are considered.

M. Rubinoff: "Notes on the Design of Eccles-Jordan Flip-Flops", Communication and Electronics, Nr. 1, July 1952, p. 215

This paper is mainly devoted to stability considerations in the static condition; in particular the influence of tolerances in circuit components, tube characteristics and supply voltages is considered. A minor part of the paper is concerned with the dynamic condition of the circuit. The way of triggering is supposed to be such that the conducting tube is instantaneously cut off, giving rise to a sudden current step in the anode circuit. No grid current is taken into account. Only the grid-voltage change of the originally non-conducting tube is derived.

R. F. Johnston and A. G. Ratz: "A Graphical Method for Flip-Flop Design"

Communication and Electronics, Nr. 5, March 1953, p. 52

This paper only considers the stability in the static condition, more particularly the influence of tolerances in components, tube characteristics and supply voltages. Nothing is said about the dynamic condition.

R. Pressmann: "How to design Bistable Multivibrators"

Electronics, Vol. 26, April 1953, p. 164

Treats mainly D.C. stability, viz. the influence of component, supply-voltage and tube tolerances. The influence of the coupling capacitor on switching is considered in general.

D. K. Ritchie: "The Optimum D.C. Design of Flip-Flops"
Proc. I.R.E., Vol. 41, November 1953, p. 1614

Only D.C. design considerations are given, taking into account tolerances of components, supply voltages and tube characteristics. No treatment of the dynamic condition.

R. Piloty: "Die Dimensionierung der Eccles-Jordan-Schaltung"
Archiv der Elektrischen Übertragung, Bd. 7,
November 1953, p. 537

This is the most extensive analysis of the dynamic behaviour we have been able to find in the literature. Still, there are some assumptions that limit the general scope of this analysis. They are the following. Only symmetrical circuits are considered. The triggering is assumed to be initiated by a negative voltage step function at the grid of the conducting tube. This grid is assumed to be at zero potential with respect to the cathode in the static condition, no grid current being present. There is thus no automatic grid-current biasing, which implies that the voltage divider between the positive and negative HT supply sources has to contain such resistance values as to deliver exactly this zero potential at the grid mentioned. This is one of the most critical situations with respect to the sensitivity of the circuit to tolerances in components, tube characteristics and voltage supplies. In practice this kind of operation will generally be avoided. In this way, omitting grid current and neglecting finite rise time of the trigger pulse front, the only transient to be considered is the response of the circuit to the sudden ceasing of the anode-current flow in the conducting tube, when suddenly cut off. The influence of the commencement of anode-current flow in the initially non-conducting tube is not considered.

S. Higashi, I. Higashino, S. Kaneko and T. Oshio: "Flip-Flop Circuits",
Part I. Analysis.
Journal of the Institute of Polytechnics, Osaka City University, Vol. 4, series B, 1953, p. 7
Part II. Methods of Design.
Id. Vol. 5, series B, 1954, p. 37

The larger part of these articles is devoted to the monostable and the astable multivibrator.
The analysis of the bistable multivibrator is based on the assumption of a linear anode current/grid voltage characteristic of the tubes and a

graphical representation of the dependence of the grid voltages on one another, giving an insight into the possible stable and unstable conditions of the circuit. The differences between the grid voltages and the anode voltages of the conducting and the non-conducting tube are defined and illustrated graphically. In the same way the upper and lower limits of the trigger-pulse amplitude are determined. The influence of the coupling capacitances is not included.

W. RENWICK and M. PHISTER: "A DESIGN METHOD FOR DIRECT-COUPLED FLIP-FLOPS"

If, as limits of the grid voltages in the static condition, we take the values zero and cut-off voltage, it is possible to derive nominal values for the resistances of the circuit for which those limits will never be exceeded; for this we assume certain tolerances in resistances, voltage supplies and valve characteristics, and given nominal values of the supply voltages. Furthermore, on the assumption that the coupling network time-constant RC is equal to the grid-circuit time-constant $R_r C_i$ (see fig 6–1), an expression can be derived for the time-constant of the most important transient, which occurs during switching as Rubinoff showed (loc. cit.). By combining this expression with those derived for the resistances, it is possible to find a minimum value of this time-constant when varying the supply-voltages. No explicit analysis of the transients in general is given.

In conclusion, it can be stated that only a few accounts of the triggering mechanism of the bistable multivibrator have been published, and these have been based on rough approximations. In the following chapters it will be pointed out how it is possible to analyse the complete trigger cycle with fairly close approximation to practice, making use of two fundamental tools, viz. the operational calculus and a few theorems about sudden closing or opening of switches in networks.

3. INTRODUCTION TO THE PROBLEM

Before proceeding to a detailed analysis of the bistable multivibrator circuit it is necessary to define the starting conditions, the assumptions and the limitations which form the basis on which the analysis rests. The circuit to be analyzed will be that represented in fig. 1–3. The triggering is assumed to be performed by applying a negative-going voltage change via coupling capacitors C_c to both grids at the same time (see also fig. 3–1).
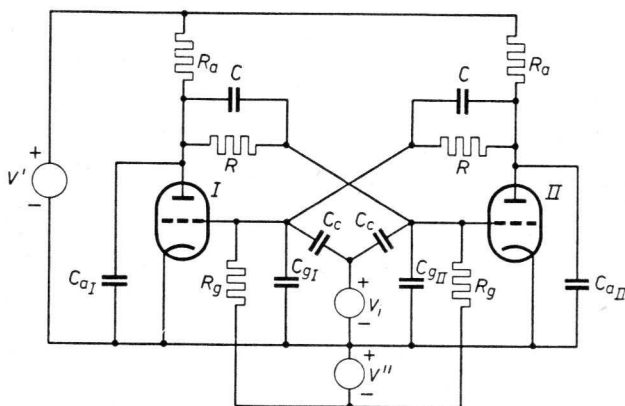
Fig. 3–1

The internal resistances of the trigger voltage supply as well as of the DC-supplies V' and V'' are assumed to be negligibly small. Inter-electrode and stray capacitances are taken into consideration as far as concerns parallel capacitances between the anodes and cathodes C_a and between the grids and cathodes C_g of the tubes. The influence of the anode-to-grid capacitance of each tube is difficult to determine exactly and will only be calculated approximatively. When an asymmetrical circuit is considered, the asymmetry will only consist of a different capacitive loading of the anodes, which is often met in practice, as the voltage changes in one of the anode circuits are generally used to operate further circuitry of which the multivibrator forms a part.
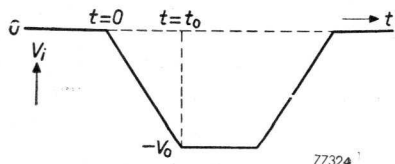
Fig. 3–2

The form of the trigger voltage V_i is represented in fig. 3–2. For $t \leq o$, $V_i = o$. For $o \leq t \leq t_o$, $V_i = -at$, where a is a positive constant. For $t \geq t_o$, V_i is supposed to be constant, at

a value $V_i = -V_o$. Thus the rise time is t_o and the slope of the trigger voltage

$$a = \frac{V_o}{t_o}. \tag{3-1}$$

In practice the trigger voltage will, after a certain time, fall back to zero. If the rear flank of this pulse-shaped trigger voltage is linear as well, the pulse will be trapezium shaped, which is a good approximation to many pulse forms in practice. The negative going front flank causes the multivibrator to trigger, which phenomenon will be analysed, whereas the positive-going rear flank has only a minor effect, mostly not able to disturb the triggering as will be pointed out later. This effect can also be calculated but this will not be done here.

At the instant $t = o$, when the trigger pulse starts, the circuit is assumed to be quiescent, all preceding transients having died out. In other words, for times $t < o$ the multivibrator is in a state that we referred to before as the static condition. At the instant $t = o$ a chain of transients starts and for $t > o$ the multivibrator is in a state which will be called the dynamic condition. This condition is to be regarded as consisting of three phases. The first phase starts at the instant $t = o$ when the trigger signal is applied, the amplitude and slope of which are supposed to be so high that within a time small with respect to the time t_o the conducting tube is cut off and the other tube is not yet conducting, which will generally be the case in practice. Both tubes are non-conducting and the circuit may thus be considered as a passive network during the first phase, which ends as soon as one of the tubes starts conducting again. For the multivibrator to operate in the desired way the originally non-conducting tube must reach its cut-off point first. The instant this occurs will be denoted $t = t_{II}$. Care must be taken that the resistance values of the voltage divider R_a, R, R_g are such that the final value to which the grid-to-cathode voltage of the tubes tends will be above the cut-off value.

At the instant $t = t_{II}$ the second phase of the dynamic condition starts, during which one of the tubes is drawing more and more anode current, its anode voltage consequently decreasing and, because of the coupling network R and C in parallel (see fig. 3–1), keeping the grid voltage of the other tube below the cut-off value. Should the final value of the grid voltage of the conducting tube, determined by the choice of the values of R_a, R and R_g, be below the voltage at which grid current starts to flow, then no other transients would occur and there would be no third phase of the dynamic condition, assuming as well that the final value of the grid

voltage of the other tube is below the cut-off point. However, the first mentioned condition is seldom chosen in practice as in that case the stabilizing influence of grid current is absent and tolerances in circuit components and supply voltages greatly influence the operation point of the conducting tube. This will be explained later, when dealing with the static condition.

Supposing that the final value of the grid voltage of the conducting tube is above the value at which grid current starts to flow, then at the instant the grid voltage reaches this special value new transients appear because of the commencement of grid current. At this instant $t = t_s$ the third phase of the dynamic condition starts and lasts until all transients have died out.

Recapitulating, tube I of fig. 3–1 is assumed to be conducting at $t < o$ and drawing grid current; it is then supposed that both the anode current and the grid current fall to zero in such a short time that it may be regarded as instantaneous. Both tubes are then non-conducting and the voltage changes at the anodes and the grids of the tubes can be calculated as the response of the as yet passive network to the trigger voltage, and to the suddenly disappearing anode and grid currents of tube I. The first phase ends at the instant $t = t_{II}$ when tube II becomes conductive. Then the response of the network to the increasing anode current of tube II must be calculated and superimposed on the transients resulting from the first phase. The second phase ends and the third commences at the instant $t = t_s$ when grid current starts to flow in tube II. This causes new transients to be superimposed on those resulting from preceding phases.

Before proceeding to the calculation of all the transients mentioned, it will be necessary to consider more closely the effect of the sudden opening or closing of switches in a network, as the transition of a tube from the conducting to the non-conducting state or vice versa can be reduced to an analogy with such switching phenomena.

4. OPENING OR CLOSING OF SWITCHES
IN A NETWORK

In fig. 4–1 the block N represents a linear, passive network, which may contain one or more voltage or current sources. Because of these sources a voltage $V(t)$ is present be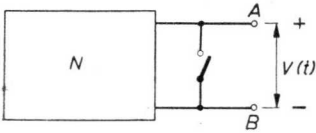tween points A and B. The effect of closing the switch at the instant $t = o$ can be derived in the following way. $V(t)$ is the voltage between points A and B if the switch remains open. If $V_1(t)$ represents the voltage between A and B when the switch is closed at the instant $t = o$, then $V_1(t) = V(t)$ for $t < o$ and $V_1(t) = o$ for $t > o$. This can be written $V_1(t) = \{1 - U(t)\} V(t)$, where $U(t)$ represents a unit step function. The application of a voltage source $V_1(t)$ thus has the same effect as the closing of the switch. This voltage source can be considered as the sum of two voltage sources $V(t)$ and $V_c(t)$, where $V_c(t) = -V(t) U(t)$. The currents and voltages in the network, therefore, are determined by the voltage or current sources contained in N, the voltage source $V(t)$ and the voltage source $V_c(t)$. The effect of the sources in N together with $V(t)$ is the same as that of the N-sources alone if the switch remains open. If this has been calculated, the effect of closing the switch can be found by calculating the effect of the voltage source $V_c(t) = -V(t) U(t)$ and superimposing it on the results calculated before. If, on the other hand, the switch is originally not open but closed, and it is opened at the instant $t = o$, the foregoing considerations remain valid, if the output voltage between points A and B is replaced by the output current flowing through the switch and in general voltages are replaced by currents, open-circuit by short-circuit, etc. This will be analysed with the aid of fig. 4–2.
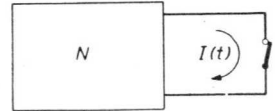
If the switch is not opened at all, a current $I(t)$ is supposed to flow at the output of the network N because of the voltage or current sources contained in N. In the case of opening the switch at the instant $t = o$, the current flowing through it will be called $I_1(t)$ and can be represented by $I_1(t) = \{1 - U(t)\} I(t)$. Thus, the application of a current source $I_1(t)$ has the same effect as the opening of the switch. This current source can be considered as the sum of two current sources $I(t)$ and $I_o(t)$, where $I_o(t) = -I(t) U(t)$. The currents and voltages in the network are now determined by the voltage or current sources contained in N, the current

Fig. 4–1

Fig. 4–2

source $I\,(t)$ and the current source $I_o\,(t)$. The effect of the sources in N together with $I\,(t)$ is the same as that of the internal N-sources only, if the switch remains closed.

The effect of opening the switch at $t = o$ then can be calculated by super-imposing on the former result the response of the network to the current source $I_o\,(t) = -I\,(t)\,U\,(t)$.

The foregoing procedure results in the replacement of switches by current or voltage sources containing discontinuities. Their effect on the network can be determined by application of the operational calculus. It can also be said that a variable network is transformed into a constant, linear network, containing discontinuous voltage or current sources. To a linear network the superposition theorem is applicable.

In the following analysis of the operation of the multivibrator, the first switching action, initiated by the trigger pulse, is assumed to be instan-taneous for the sake of simplicity and this will mostly be a good approxi-mation to practice, as care will be taken to make the slope of the trigger pulse as steep as possible. In that case the effect of suddenly cutting off the conducting tube can be taken into account by introducing between the anode and the cathode of this tube a current source of a strength $I_o\,(t) = -I_a\,(t)\,U\,(t)$, where $I_a\,(t)$ is the anode current flowing if no trigger pulse were applied. The response of the network to this current source must be superimposed on the undisturbed state of the multivibrator. If the tube is drawing grid current $I_g\,(t)$, a current source $-I_g\,(t)\,U\,(t)$ between the grid and the cathode must be applied as well.

At the end of the first phase the originally non-conducting tube starts conducting, because its grid-to-cathode voltage rises above the cut-off point. This tube now acts as a switch that is being closed. The time it takes the grid voltage to rise from the cut-off value to a value near zero is determined by the inherent time constants of the circuit and will usually not be negligibly small compared with the complete trigger cycle. Therefore, it will be necessary to consider in more detail the switching of a tube from cut-off to full conduction in a finite
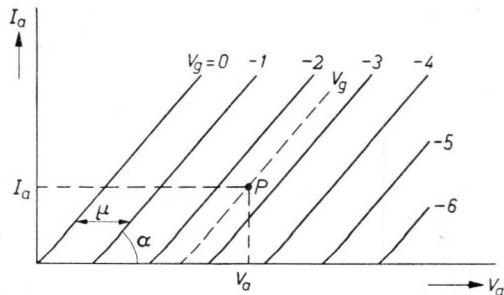

Fig. 4–3

time. To this purpose the anode-current against anode-voltage charac-teristics of a triode will be approximated by straight lines as represented

in fig. 4–3. The reciprocal slope of these lines is a measure for the internal resistance r_a of the tube ($r_a = \cot a$). The amplification factor μ is equal to the horizontal distance between the lines. The transconductance is given by the vertical distance between the lines. An arbitrary operating point P of the tube is defined by the anode voltage V_a and the grid voltage V_g in such a way that

$$I_a = (V_a - V_{a_1}) \tan a \quad \text{or} \quad I_a = \frac{V_a - V_{a_1}}{r_a}.$$

Where, $V_{a_1} = -\mu V_g$, thus

$$I_a = \frac{V_a + \mu V_g}{r_a}. \tag{4-1}$$

Generally, the anode of a tube is fed from a voltage source $V(t)$ via an impedance Z_a (see fig. 4–4). $V(t)$ will mostly be a constant voltage, but need not be so.
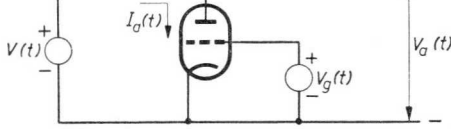
Fig. 4–4

A second relation between I_a and V_a can then be derived:

$$V(t) - V_a(t) = Z_a I_a(t) \tag{4-2}$$

From equations (4–1) and (4–2) it follows that:

$$V_a(t) = \frac{r_a}{r_a + Z_a} V(t) - \frac{Z_a}{r_a + Z_a} \mu V_g(t) \tag{4-3}$$

This expression is valid only as long as $V_a(t) + \mu V_g(t) \geq o$, as eq. (4–1) shows that $I_a = o$ for $V_a(t) + \mu V_g(t) = o$ or

$$V_g(t) = -\frac{V_a(t)}{\mu} \tag{4-4}$$

This value of V_g is the cut-off grid voltage corresponding to the particular value of the anode voltage.

If $V_g(t) < -\frac{V_a(t)}{\mu}$ the tube draws no anode current.

It will be assumed now that at times $t < t_a$ the tube is cut off, or in formula $V_g(t) < -\frac{V(t)}{\mu}$. At the instant $t = t_a$, the grid voltage reaches the cut-off value, in other words eq. (4–4) is valid

$$V_g(t_a) = -\frac{V(t_a)}{\mu} \tag{4-5}$$

If the time functions $V_g(t)$ and $V(t)$ are known, the value of t_a can be calculated from condition (4–5).

The effect of the tube becoming conductive at the instant $t = t_a$ can be interpreted with the aid of fig. 4–5.

If the voltage source $V_1(t)$ is given the following value: $V_1(t) = V(t) - \{V(t) + \mu V_g(t)\} U(t-t_a)$, then for $t < t_a$, $V_a(t) = V(t)$ the tube is non-conducting, and for $t \geq t_a$

$$V_a(t) = \frac{r_a}{r_a + Z_a} V(t) + \frac{Z_a}{r_a + Z_a} V_1(t) = \frac{r_a}{r_a + Z_a} V(t) - \frac{Z_a}{r_a + Z_a} \mu V_g(t)$$

which corresponds to equation (4–3).

The expression for $V_a(t)$, valid in the non-conducting condition for $t < t_a$ as well as in the conducting condition for $t \geq t_a$ is the following:

$$V_a(t) = V(t) - \frac{Z_a}{r_a + Z_a} [V(t) + \mu V_g(t)] U(t-t_a) \qquad (4-6)$$

In most bistable multivibrator circuits the grid voltage of the tube will rise beyond the point where grid current starts to flow. It will be assumed that this point is reached at a value zero of the grid voltage and that the internal grid resistance is so small that the grid and cathode can be considered to become short-circuited as soon as $V_g = o$. At the instant $t = t_s$, when V_g becomes zero, the second phase of the dynamic condition ends and the third commences. On the voltages and currents caused by transients during the preceding phases must be super-
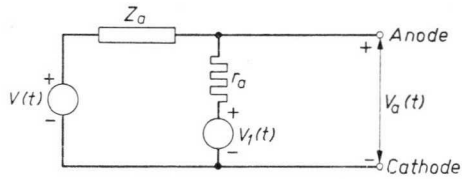
Fig. 4–5

imposed the response of the network to the sudden short-circuiting of the grid and cathode of the conducting tube. This response can be calculated by assuming a voltage source $V_c(t)$ to be present between grid and cathode, where $V_c(t) = -V_g(t) U(t-t_s)$.

After the preliminary observations made in this chapter about switching in networks, it is possible to deal with a systematical analysis of the operation of the multivibrator. First the static condition will be examined, which in the time scale used above exists during the time $t \leq o$. Any possible transients of preceding trigger cycles are supposed to have completely faded out. This static condition is the initial state, to which the transients have to be added when the dynamic condition starts at the instant $t = o$, with the application of the trigger pulse.

5. THE STATIC CONDITION OF THE BISTABLE MULTIVIBRATOR

In the static condition only constant voltage sources are present in the circuit, hence all capacitances can be left out of consideration, and in this case the circuit of fig. 3–1 can be simplified to that of fig. 5–1.
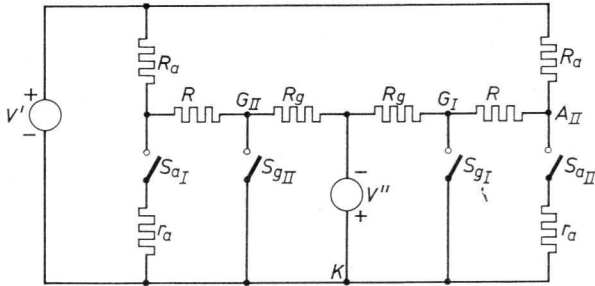
Fig. 5–1

In this figure all indices I refer to tube I and all indices II to tube II. A_I and A_{II} are the anodes of the tubes, G_I and G_{II} the grids, K is cathode. It is supposed that tube I is conducting and tube II is cut off. Thus, switches S_{aI} and S_{gI} are closed and S_{aII} and S_{gII} are open. The circuit can be separated into two independent parts, which are represented in figs 5–2 and 5–3.

In fig. 5–3 the more general case of a finite internal grid resistance r_g is represented.

In the circuit of fig. 5–2 an anode current I_{ao} flows through tube I and if two other currents I_1 and I_2 are introduced, the following relations exist:
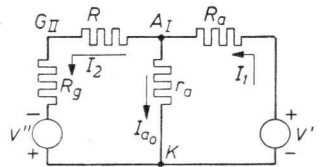
Fig. 5–2

$$I_1 = I_{ao} + I_2 \tag{5–1}$$

$$V' + V'' = I_1 R_a + I_2 (R + R_g) \tag{5–2}$$
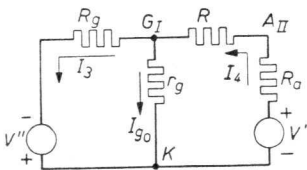
Fig. 5–3

Introducing $\varepsilon_a = \dfrac{R_a}{R_g + R + R_a}$ $\tag{5–3}$

it follows from expressions (5–1) and (5–2) that

$$I_2 = -\varepsilon_a I_{ao} + \frac{V' + V''}{R_g + R + R_a} \tag{5–4}$$

and
$$I_1 = (1 - \varepsilon_a) I_{ao} + \frac{V' + V''}{R_g + R + R_a} \tag{5-5}$$

From fig. 5–2 it can easily be seen that the voltage between G_{II} and cathode is

$$V_{gIIo} = -V'' + I_2 R_g = -V'' + \frac{R_g}{R_g + R + R_a} (V' + V'') - R_g \varepsilon_a I_{ao}$$

Introducing

$$\varepsilon_g = \frac{R_g}{R_g + R + R_a} \tag{5-6}$$

it can be written

$$V_{gIIo} = \varepsilon_g (V' - R_a I_{ao}) - (1 - \varepsilon_g) V'' \tag{5-7}$$

since
$$\varepsilon_a R_g = \varepsilon_g R_a$$

This value of Vg_{IIo} has to be below the cut-off voltage, as tube II must be non-conducting.

The voltage between A_I and cathode is

$$V_{aIo} = V' - I_1 R_a = V' - \varepsilon_a (V' + V'') - (1 - \varepsilon_a) R_a I_{ao}$$

or

$$V_{aIo} = (1 - \varepsilon_a)(V' - R_a I_{ao}) - \varepsilon_a V'' \tag{5-8}$$

Since $V_{aIo} = r_a I_{ao}$ as well, a relation between I_{ao} and r_a can be derived

$$I_{ao} = \frac{(1 - \varepsilon_a) V' - \varepsilon_a V''}{(1 - \varepsilon_a) R_a + r_a} \tag{5-9}$$

The internal anode resistance r_a can be evaluated from the tube characteristics (see fig. 4–3, where $r_a = \cot a$).
From fig. 5–3 it can be seen that

$$I_3 + I_{go} = I_4 \tag{5-10}$$

$$V' + V'' = I_3 R_g + I_4 (R_a + R) \tag{5-11}$$

From (5–10) and (5–11) it follows that

$$I_3 = \frac{V' + V''}{R_g + R + R_a} - (1 - \varepsilon_g) I_{go} \; ; I_4 = \frac{V' + V''}{R_g + R + R_a} + \varepsilon_g I_{go}$$

Thus

$$V_{gIo} = \varepsilon_g V' - (1 - \varepsilon_g) (V'' + R_g I_{go}) \tag{5-12}$$

and

$$V_{aIIo} = (1 - \varepsilon_a) V' - \varepsilon_a (V'' + R_g I_{go}) \tag{5-13}$$

The grid current I_{go} can be evaluated for the case that the internal grid resistance r_g is assumed to be zero. Then $V_{gIo} = o$ or

$$I_{go} = \frac{\varepsilon_g V' - (1 - \varepsilon_g) V''}{(1 - \varepsilon_g) R_g} \qquad (5\text{-}14)$$

Introducing this value of I_{go} into eq (5–13) gives

$$V_{aIIo} = \frac{R}{R + R_a} V' \qquad (5\text{-}15)$$

This result could have been read directly from fig. 5–3 for $r_g = o$, as it shows that in that case the voltage at A_{II} is determined by the voltage divider R, R_a across the supply source V'. However, the expression (5–13) will be of advantage in later calculations, and has therefore been derived first.

It will now be pointed out why it is advantageous to operate the conducting tube in the grid-current region. If the internal grid resistance is not zero, but has a finite value, determined by a grid current/grid voltage characteristic as represented in fig. 5–4, then the grid voltage V_{gIo} and the grid current I_{go} are defined on the one hand by this characteristic, on the other hand by the relation (5–12). This relation is represented by the straight line l_2 in fig. 5–4. The voltage $V_o = \varepsilon_g V' - (1-\varepsilon_g) V''$ and the reciprocal slope of l_2 is equal to $(1-\varepsilon_g) R_g$. The point of intersection of l_2 and the characteristic determines I_{go} and V_{gIo} ($= V_{g2}$ in fig. 5–4). If it is assumed that the supply voltages V' and V'' vary to such a value that $V_o = o$, then the line l_2 changes to l_1 and the resulting grid-voltage change would be only from V_{g2} to V_{g1}. If V_o, however, had been situated to the left of the grid-current cut-off point, then the grid voltage change would have been equal to the change of V_o. The steeper the characteristic rises, the more the grid voltage will be stabilized. In the ideal case that has been considered previously, the characteristic was assumed to coincide with the vertical axis.
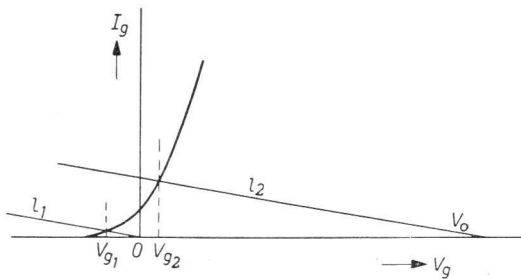
Fig. 5–4

The influence of tolerances in the resistances will also be minimized, though it is more difficult to calculate, as both V_o and the slope of l_2 depend on the values of these resistances.

Changes in V_{gIo} greatly influence the value of I_{ao} and therefore at the same time the total voltage change at the anodes of the tubes when the multivibrator is triggered. This voltage change ΔV_a is given by the difference between V_{aIIo} and V_{aIo}. From eqs (5–13) and (5–8) it follows

$$\Delta V_a = (1 - \varepsilon_a) R_a I_{ao} - \varepsilon_a R_g I_{go} \tag{5-16}$$

It must be noted that the presence of grid current reduces the value of this voltage change, but I_{go} is mostly so small compared with I_{ao} that the second term of the right-hand part of eq. (5–16) is only a small fraction of the other term. This disadvantage is more than counterbalanced by the advantage of the stabilizing effect of the grid current.

The anode and grid voltages of both tubes in the static condition have now been derived. They are the initial conditions for the transient phenomena which occur when a trigger pulse is applied to both grids. These transients must be superimposed on the static voltages and currents. There is no need to take into account the DC-supply voltages for calculating the transients, the influence of these voltages being included in the static conditions. The voltages V′ and V″ are therefore omitted in the circuits which are used for determining the dynamic condition.

6. THE DYNAMIC CONDITION

6.1 INTRODUCTION

The dynamic condition starts at the instant $t = o$ when the input voltage V_i remains no longer zero but falls linearly with a slope α to a value $-V_o$ (see fig. 3–2), which is reached at the instant $t = t_o$. From this instant onwards V_i remains constant at the value $-V_o$.

For $o \leq t \leq t_o$

$$V_i = -\alpha t \,, \tag{6-1}$$

where

$$\alpha = \frac{V_o}{t_o} \tag{6-2}$$

The voltage source V_i in series with the coupling capacitors C_c will be replaced by a current source I_i in parallel with C_c, where

$$I_i = C_c \frac{d V_i}{dt} \tag{6-3}$$

For
$$t \leq o : I_i = o \tag{6-4}$$

For
$$o \leq t \leq t_o : I_i = -\alpha C_c \tag{6-5}$$

For
$$t \geq t_o : I_i = o \tag{6-6}$$

Thus, I_i is a rectangular, negative-going pulse with a duration of t_o and an amplitude αC_c, or the superposition of a negative-going current step $-\alpha C_c$ at the instant $t = o$, and a positive-going current step $+ \alpha C_c$ at the instant $t = t_o$. This can be denoted by

$$I_i = -\alpha C_c \{U(t) - U(t - t_o)\} \tag{6-7}$$

The coupling capacitance C_c in parallel with the capacitance C_g (see fig. 3–1) gives a total grid-to-cathode capacitance

$$C_i = C_c + C_g \tag{6-8}$$

As assumed previously the input voltage instantaneously cuts off tube I and therefore current sources I_{ao} and I_{go} have to be introduced between the anode and cathode, and between the grid and cathode respectively of tube I.

6.2 FIRST PHASE

The resulting circuits of the bistable multivibrator during the first phase of the dynamic condition can be represented by the diagram of fig. 6–1. By neglecting the influence of the anode-to-grid capacitances C_{ag}, the

circuit can be considered to consist of two separate parts as represented
in figs. 6–2 and 6–3.

The response of the network to three current sources has to be deter-
mined. All current sources are step functions:

I_i is given by expression (6–7)

$$I_a = I_{ao}\, U\,(t) \tag{6–9}$$

$$I_g = I_{go}\, U\,(t) \tag{6–10}$$

The calculation of the voltages between the grids and earth (or cathode)
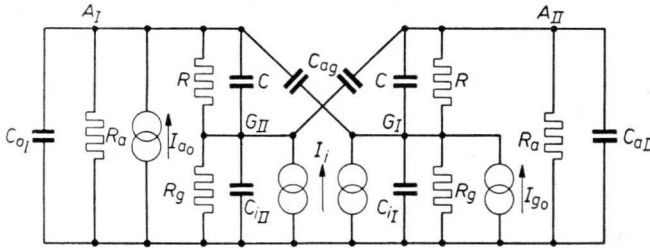
Fig. 6–1

and between the anodes and earth will be possible if the following impe-
dances are known.

(a) The impedances between the grids and earth.

Fig. 6–2

(b) The transfer impedances
giving the ratio of the
voltages between the
anodes and earth to the
currents applied between
the grids and earth.

(c) The transfer impedances
giving the ratio of the
voltages between the grids and earth to the currents applied between
the anodes and earth.

(d) The impedances between the
anodes and earth.

The derivation of these impedances
and subsequent calculation of the
voltages is fully given in appendix I.
In order not to get lost in details,
only the results will be presented
here. The voltage between G_{II} and earth is:
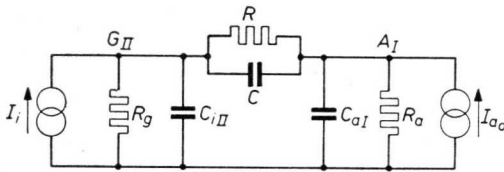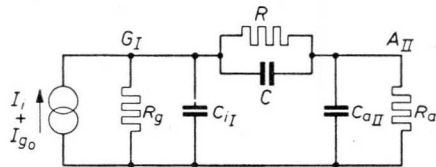
Fig. 6–3

$$V_{gII} \left(t_o \le t \le t_{II}\right) = V_1 + V_2\, e^{p_1 t} + V_3\, e^{p_2 t} \qquad \text{6-11)}$$

See appendix I, expression (I–36)

The voltage between A_I and earth is:

$$V_{aI} \left(t_o \le t \le t_{II}\right) = V_7 + V_8\, e^{p_1 t} + V_9\, e^{p_2 t} \qquad \text{(6–12)}$$

See appendix I, expression (1–40)

The voltage between G_I and earth is:

$$V_{gI} \left(t_o \le t \le t_{II}\right) = V_{10} + V_{11}\, e^{p_1' t} + V_{12}\, e^{p_2' t} \qquad \text{(6–13)}$$

See appendix I, expression (I–42)

The voltage between A_{II} and earth is:

$$V_{aII} \left(t_o \le t \le t_{II}\right) = V_4 + V_5\, e^{p_1' t} + V_6\, e^{p_2' t} \qquad \text{(6–14)}$$

See appendix I, expression (1–44)

Where

$$V_1 = V_{gIIo} + I_{ao}\, \varepsilon_a\, R_g = \varepsilon_g\, V' - \left(1 - \varepsilon_g\right) V'' \qquad \text{(6–15)}$$

$$V_2 = \tfrac{1}{2}\, a\, C_c \left(1 - \varepsilon_g\right) R_g \left(1 - K\right) \left(1 - e^{-p_1 t_o}\right) - \tfrac{1}{2}\, I_{ao}\, \varepsilon_a\, R_g \left(1 - P\right) \quad \text{(6–16)}$$

$$V_3 = \tfrac{1}{2}\, a C_c \left(1 - \varepsilon_g\right) R_g \left(1 + K\right) \left(1 - e^{-p_2 t_o}\right) - \tfrac{1}{2}\, I_{ao}\, \varepsilon_a\, R_g \left(1 + P\right) \quad \text{(6–17)}$$

$$V_4 = V_{aIIo} + I_{go}\, \varepsilon_a\, R_g = \left(1 - \varepsilon_a\right) V' - \varepsilon_a\, V'' \qquad \text{(6–18)}$$

$$V_5 = \tfrac{1}{2}\, a\, C_c\, \varepsilon_a\, R_g \left(1 - P'\right) \left(1 - e^{-p_1' t_o}\right) - \tfrac{1}{2}\, I_{go}\, \varepsilon_a\, R_g \left(1 - P'\right) \qquad \text{(6–19)}$$

$$V_6 = \tfrac{1}{2}\, a\, C_c\, \varepsilon_a\, R_g \left(1 + P'\right) \left(1 - e^{-p_2' t_o}\right) - \tfrac{1}{2}\, I_{go}\, \varepsilon_a\, R_g \left(1 + P'\right) \qquad \text{(6–20)}$$

$$V_7 = V_{aIo} + I_{ao} \left(1 - \varepsilon_a\right) R_a = \left(1 - \varepsilon_a\right) V' - \varepsilon_a\, V'' \qquad \text{(6–21)}$$

$$V_8 = \tfrac{1}{2}\, a C_c\, \varepsilon_a\, R_g \left(1 - P\right) \left(1 - e^{-p_1 t_o}\right) - \tfrac{1}{2}\, I_{ao} \left(1 - \varepsilon_a\right) R_a \left(1 - L\right) \quad \text{(6–22)}$$

$$V_9 = \tfrac{1}{2}\, a\, C_c\, \varepsilon_a\, R_g \left(1 + P\right) \left(1 - e^{-p_2 t_o}\right) - \tfrac{1}{2}\, I_{ao} \left(1 - \varepsilon_a\right) R_a \left(1 + L\right) \quad \text{(6–23)}$$

$$V_{10} = I_{go} \left(1 - \varepsilon_g\right) R_g = \varepsilon_g\, V' - \left(1 - \varepsilon_g\right) V'' \qquad \text{(6–24)}$$

$$V_{11} = \tfrac{1}{2}\, a\, C_c \left(1 - \varepsilon_g\right) R_g \left(1 - K'\right) \left(1 - e^{-p_1' t_o}\right) - \tfrac{1}{2}\, I_{go} \left(1 - \varepsilon_g\right) R_g \left(1 - K'\right)$$
$$\text{(6–25)}$$

$$V_{12} = \tfrac{1}{2}\, a\, C_c \left(1 - \varepsilon_g\right) R_g \left(1 + K'\right) \left(1 - e^{-p_2' t_o}\right) - \tfrac{1}{2}\, I_{go} \left(1 - \varepsilon_g\right) R_g \left(1 + K'\right)$$
$$\text{(6–26)}$$

$$K = \frac{2A - B}{B\sqrt{1 - 4E/B^2}}$$

$$P = \frac{2T - B}{B\sqrt{1 - 4E/B^2}}$$

$$L = \frac{2D - B}{B\sqrt{1 - 4E/B^2}}$$

See appendix I expr. (I–31), (I–34) and (I–39)

K', P', L' follow from K, P, L respectively by interchanging the indices I and II in A, B, E and D.

If the bistable multivibrator is symmetrical, i.e. if in fig. 6–1

$C_{iI} = C_{iII}$ and $C_{aI} = C_{aII}$, then $K = K'$, $P = P'$, $p_1 = p_1'$ and $p_2 = p_2'$.

6.3 SECOND PHASE

During the first phase of the dynamic condition both tubes are cut off. Their grid voltages tend to the following final values (at $t = \infty$):

$V_{gI}(\infty) = I_{go}(1 - \varepsilon_g)R_g$, as can easily be seen from expression (6–13) and $V_{gII}(\infty) = V_{gIIo} + I_{ao}\varepsilon_a R_g$. (see expression (6–11)). Introducing expressions (5–14) and (5–7) results in

$$V_{gI}(\infty) = V_{gII}(\infty) = \varepsilon_g V' - (1 - \varepsilon_g) V'' \tag{6–27}$$

This is simply the voltage at the mid-point of the voltage divider R_g, $(R + R_a)$ between the supply sources $-V''$ and $+V'$. It must be assumed that this voltage is above the cut-off voltage of the tubes, otherwise the bistable multivibrator would not function at all. Furthermore it will be assumed that the originally non-conducting tube II reaches its cut-off point earlier than tube I, as this is the condition for correct functioning of the multivibrator circuit. The limit of this correct operation is reached when the tubes attain their cut-off points simultaneously. When determining the sensitivity of the multivibrator, this condition will be investigated more thoroughly.

Tube II reaches its cut-off point at the instant $t = t_{II}$, this instant marks the end of the first phase and the start of the second phase of the dynamic condition. According to chapter 4 this instant t_{II} can be determined from the condition

$$V_{gII}(t_{II}) = -\frac{V_{aII}(t_{II})}{\mu} \tag{6–28}$$

New transients occur from this instant onwards, but only in the anode voltage V_{aII} and consequently in the grid voltage V_{gI} as well. The voltages V_{aI} and V_{gII} are represented by the same expressions that hold for the first phase ((6–12) and (6–11), respectively).

According to expression (4–6) the anode voltage of the second tube during the second phase is given by

$$V_{aII}(t) = V_{aII}(t)_1 - \frac{Z_{iaII}}{Z_{iaII} + r_a} \{V_{aII}(t)_1 + \mu V_{gII}(t)\} U(t - t_{II}) \qquad (6\text{–}29)$$

where $V_{aII}(t)_1$ and $V_{gII}(t)$ are given by the expressions for the first phase, (6–14) and (6–11), respectively. Z_{iaII} corresponds to Z_a of expression (4–6) and can be derived from expression (I–19) by interchanging indices I and II. As $V_{gII}(t)$ is valid for the first as well as for the second phase, no index 1 is used here.

The evaluation of this voltage V_{aII} is presented in appendix II.

$$V_{aII}(t) = V_{aII}(t)_1 - \frac{(1 - \varepsilon_a) R_a}{\{(1 - \varepsilon_a) R_a + r_a\} G'} \overset{p_j = p_1, p_2, p_1', p_2'}{\underset{j}{\Sigma}} V_j \, p_j \, e^{p_j t_{II}}$$

$$\left[\frac{X_{1j}}{-p_3}\{1 - e^{p_3(t - t_0)}\} + \frac{X_{2j}}{-p_4}\{1 - e^{p_4(t - t_{II})}\} + \frac{X_{3j}}{-p_j}\{1 - e^{p_j(t - t_{II})}\}\right] \times$$

$$\times U(t - t_{II}) \qquad (6\text{–}30)$$

This is expression (II–21) of appendix II. $Va_{II}(t)_1$ is given by expression (6–14), p_j is p_1, p_2, p_1', p_2', respectively. For a symmetrical multivibrator $p_1 = p_1'$ and $p_2 = p_2'$. V_j is given by expressions (II–22) to (II–25) inclusive. p_3 and p_4 are represented by expressions (II–14) and (II–15). For G' and F' see expressions (II–3) and (II–2). The X-quantities are given by expressions (II–16), (II–17) and (II–18).

For a symmetrical multivibrator the still rather cumbersome expression is represented in full by (II–28) of appendix II.

The voltage at the grid of tube I during the second phase is derived in appendix III. This voltage is given by expressions (III–8) and (III–12) of this appendix, viz.

$$V_{gI}(t) = V_{gI}(t)_1 - \frac{R_g (1 - \varepsilon_a) R_a}{(R + R_g) \{(1 - \varepsilon_a) R_a + r_a\} G'} \overset{p_j = p_1 \cdots p_2'}{\underset{j}{\Sigma}} V_j \, p_j \, e^{p_j t_{II}}$$

$$\left[\frac{Y_{1j}}{-p_3}\{1 - e^{p_3(t - t_{II})}\} + \frac{Y_{2j}}{-p_4}\{1 - e^{p_4(t - t_{II})}\} + \frac{Y_{3j}}{-p_j}\{1 - e^{p_j(t - t_{II})}\}\right] \times$$

$$\times U(t - t_{II}) \qquad (6\text{–}31)$$

Recapitulating, the grid and anode voltages of tubes I and II have been determined as functions of time during the first and second phases of the dynamic condition of the multivibrator circuit, where

Vg_I is given by expressions (6–13) and (6–31),

Va_I by expression (6–12),

Vg_{II} by expression (6–11) and

Va_{II} by expressions (6–14) and (6–30).

6.4 THIRD PHASE

As already assumed in chapter 4, the grid voltage of the second tube will rise until the point where grid current starts to flow, i.e. at $V_{gII} = o$ where grid G_{II} and cathode are suddenly short-circuited. This can be taken into account by introducing between grid G_{II} and cathode a voltage source

$$V_c(t) = Vg_{II}(t) \, U(t - t_s) \tag{6–32}$$

where $Vg_{II}(t)$ is given by expression (6–11), valid during the first and second phases and t_s is the instant at which Vg_{II} becomes zero. This value t_s is to be determined from expression (6–11) by putting $V_{gII}(t_s) = 0$. This new voltage source $V_c(t)$ causes new terms in the voltages at A_{II}, at A_I and at G_I.

The new transient at A_{II} is:

$$V_{aII}^{**}(t) = \frac{Z_{iaII}}{Z_{iaII} + r_a} \mu V_{gII}(t) \, U(t - t_s) \tag{6–33}$$

The new transient at G_I is:

$$V_{gI}^{**}(t) = \frac{Z_{gI} \, Z_{aII}}{(Z + Z_{gI}) \, Z_{aII} + r_a \, (Z + Z_{gI} + Z_{aII})} \mu V_{gII}(t) \, U(t - t_s) \tag{6–34}$$

[compare expression (III-5)].

The new transient at A_I is:

$$V_{aI}^{**}(t) = -\frac{Z_{aI}}{Z + Z_{aI}} V_{gI}(t) \, U(t - t_s) \tag{6–35}$$

These transients are evaluated in Appendix IV and are given by expressions (IV–4), (IV–5) and (IV–13).

The total voltage at A_{II} during the three phases of the dynamic condition is the sum of expressions (6–30) and (IV–4).

$$V_{aII}(t) = V_{aII}(t)_1 - \frac{(1 - \varepsilon_a) R_a}{\{(1 - \varepsilon_a) R_a + r_a\} G'} \left[\overset{p_j = p_1 \cdots p_2'}{\underset{j}{\Sigma}} V_j\, p_j\, e^{p_j t_{II}} \right.$$

$$\left\{ \frac{X_{1j}}{-p_3} \{1 - e^{p_3(t - t_{II})}\} + \frac{X_{2j}}{-p_4} \{1 - e^{p_4(t - t_{II})}\} + \frac{X_{3j}}{-p_j} \{1 - e^{p_j(t - t_{II})}\} \right\}$$

$$U(t - t_{II}) - \overset{p_j = p_1, p_2}{\underset{j}{\Sigma}} V_j\, p_j\, e^{p_j t_s} \left\{ \frac{X_{1j}}{-p_3} \{1 - e^{p_3(t - t_s)}\} + \frac{X_{2j}}{-p_4} \{1 - e^{p_4(t - t_s)}\} + \right.$$

$$\left. \left. + \frac{X_{3j}}{-p_j} \{1 - e^{p_j(t - t_s)}\} \right\} U(t - t_s) \right] \tag{6-36}$$

where $V a_{II}(t)_1$ is given by expression (6–14).
The total voltage at G_I during the three phases is the sum of expressions (6–31) and (IV–5):

$$V_{gI}(t) = V_{gI}(t)_1 - \frac{R_g(1 - \varepsilon_a) R_a}{(R + R_g)\{(1 - \varepsilon_a) R_a + r_a\} G'} \left[\overset{p_j = p_1 \cdots p_2'}{\underset{j}{\Sigma}} V_j\, p_j\, e^{p_j t_{II}} \right.$$

$$\left\{ \frac{Y_{1j}}{-p_3} \{1 - e^{p_3(t - t_{II})}\} + \frac{Y_{2j}}{-p_4} \{1 - e^{p_4(t - t_{II})}\} + \frac{Y_{3j}}{-p_j} \{1 - e^{p_j(t - t_{II})}\} \right\}$$

$$U(t - t_{II}) - \overset{p_j = p_1, p_2}{\underset{j}{\Sigma}} V_j\, p_j\, e^{p_j t_s} \left\{ \frac{Y_{1j}}{-p_3} \{1 - e^{p_3(t - t_s)}\} + \right.$$

$$\left. \left. + \frac{Y_{2j}}{-p_4} \{1 - e^{p_4(t - t_s)}\} + \frac{Y_{3j}}{-p_j} \{1 - e^{p_j(t - t_s)}\} \right\} U(t - t_s) \right] \tag{6-37}$$

where $V_{gI}(t)_1$ is given by expression (6–13).
The total voltage at A_I during the three phases is the sum of expressions (6–12) and (IV–13):

$$V_{aI}(t) = V_{aI}(t)_{1,2} + \frac{R_a}{(R + R_a)} p_n \left[p_1\, V_2\, e^{p_1 t_s} \left\{ \frac{1 + Tp_n}{-p_n(p_n - p_1)} \right. \right.$$

$$\{1 - e^{p_n(t - t_s)}\} + \frac{1 + Tp_1}{p_1(p_n - p_1)} \{1 - e^{p_1(t - t_s)}\} \right\} + p_2\, V_3\, e^{p_2 t_s} \left\{ \frac{1 + Tp_n}{-p_n(p_n - p_2)} \right.$$

$$\left. \left. \{1 - e^{p_n(t - t_s)}\} + \frac{1 + Tp_2}{p_2(p_n - p_2)} \{1 - e^{p_2(t - t_s)}\} \right\} \right] U(t - t_s) \tag{6-38}$$

where $V_{aI}(t)_{1,2}$ is given by expression 6–12.
The anode and grid voltages of tubes I and II have now been calculated as functions of time during the whole trigger-cycle. V_{aII} is represented by expression (6–36), V_{gI} by expression (6–37) and V_{aI} by expression (6–38), whilst V_{gII} can be represented by the following expression:

$$V_{gII}(t) = V_{gII}(t)_{1,2}\{1 - U(t-t_s)\} \qquad (6\text{--}39)$$

Where $V_{gII}(t)_{12}$ is given by expression (6–11), valid during the second phase as well.

Note: A check on the calculation of the expressions for the voltage changes at the anodes and grids is to compare the final values (at $t = \infty$) with the initial values (at $t \leq 0$) of the other tube. The following relations hold:

The grid voltage V_{gIo} must be equal to V_{gII} at $t = \infty$, and V_{gIIo} must be the same as V_{gI} at $t = \infty$. The same applies to the anode voltages, which also change rôles when the multivibrator is triggered. These relations have been verified and confirmed.

7. THE COMPLETE TRIGGER CYCLE

The time functions for the anode and grid voltages during the complete trigger cycle have been calculated for a numerical example and are graphically represented in figs. 7–1, 2, 3, 4. The calculations were simplified as it turned out that the transient components of V_{aII} from the first phase have practically disappeared at the instant $t = t_{II}$, which means that $V_{aII} = V_4 = $ constant (expr. (6–14)). The circuit and other data are the following (see fig. 3–1 and 3–2): $V' = 150\ V$, $V'' = 100\ V$, $R_a = 20\ k\Omega$, $R = R_g = 200\ k\Omega$, $C = 100\ pF$, $C_c = 40\ pF$, $C_g = 10\ pF$, $t_o = 0.2\ \mu$ sec., $V_o = 25\ V$, $\mu = 35$, $r_a = 8\ k\Omega$.

The curves marked a apply to a symmetrical multivibrator of which $C_{aI} = C_{aII} = 5\ pF$, whilst the curves marked b and c apply to an asymmetrical multivibrator with $C_{aI} = 110\ pF$ and $C_{aII} = 5\ pF$. The calculated curves are represented by the fully-drawn lines. No account has been taken of the influence of C_{ag} or of the rear flank of the trigger pulse. It is possible to account for the influence of C_{ag}, but this involves such complicated calculations (fourth-order equations to be solved for determining the normal modes of the circuit) that they become very impracticable to handle. The influence of C_{ag} on the waveforms may be considered to be such that their slopes and amplitudes are reduced to some extent, but calculations in which C_{ag} is ignored will nevertheless give a good idea of the general aspect of the waveforms. Differences of a few volts in amplitude may, however, considerably influence the values of the times t_I and t_{II} at which the tubes should reach their cut-off points. Therefore, in calculating the trigger sensitivity the influence of C_{ag} has not been neglected and fortunately this does not lead to excessively complicated formulae.

For the sake of comparison with practice, the curves displayed by an oscilloscope have also been plotted in the figures (broken lines). It should be recognized that the time scale on the screen of the oscilloscope was only about one tenth of that used for the graphs, so that some inaccuracy was introduced in drawing the steep fronts.

7.1. DISCUSSION OF THE WAVEFORMS

From fig. 7–1, which represents the waveform of V_{gII}, it can be clearly seen that V_{gII} reaches the cut-off value (approximately -4 V) in a much shorter time ($t = t_{II}$) in case a ($C_{aI} = 5\ pF$) than in case b (capacitive load, $C_{aI} = 110\ pF$), in other words the capacitive load considerably increases the duration of the first phase.
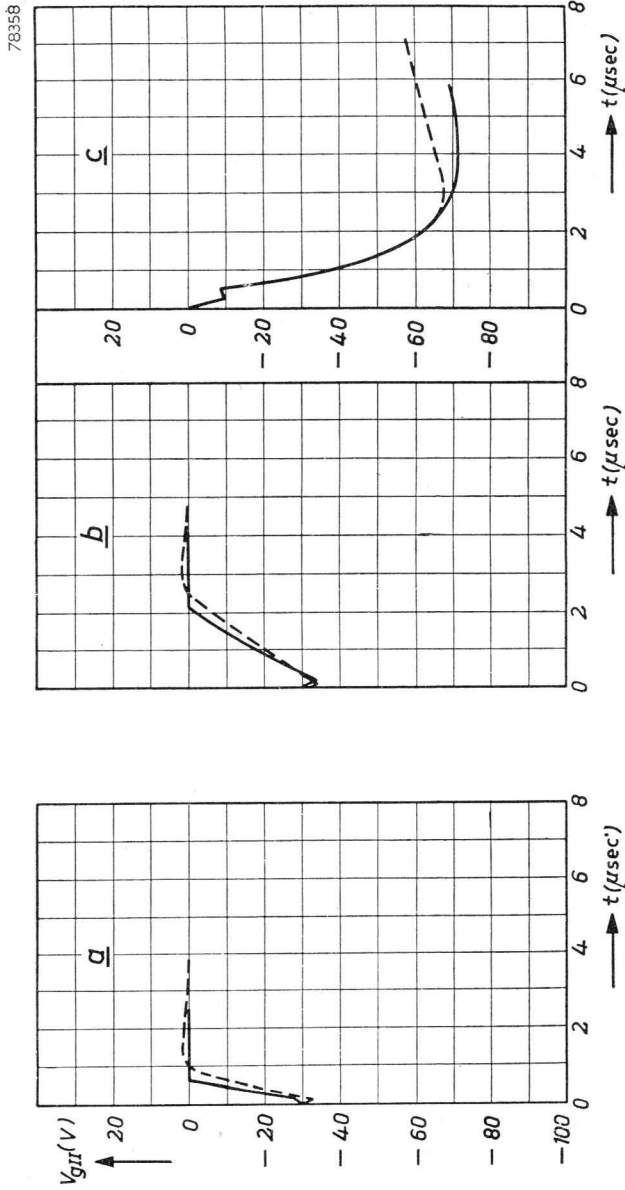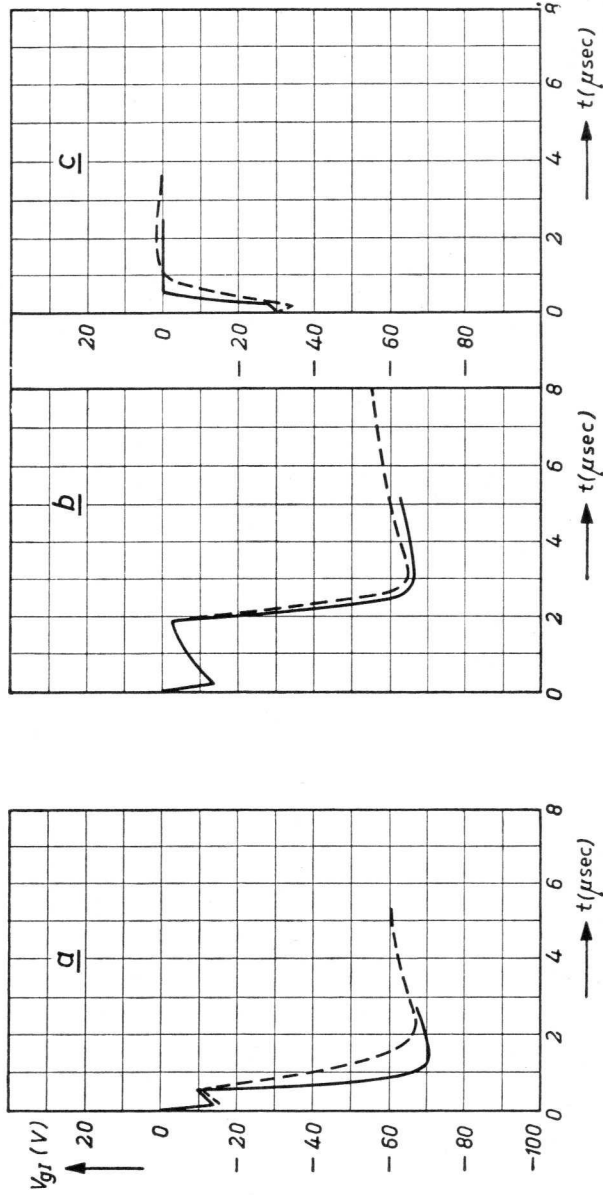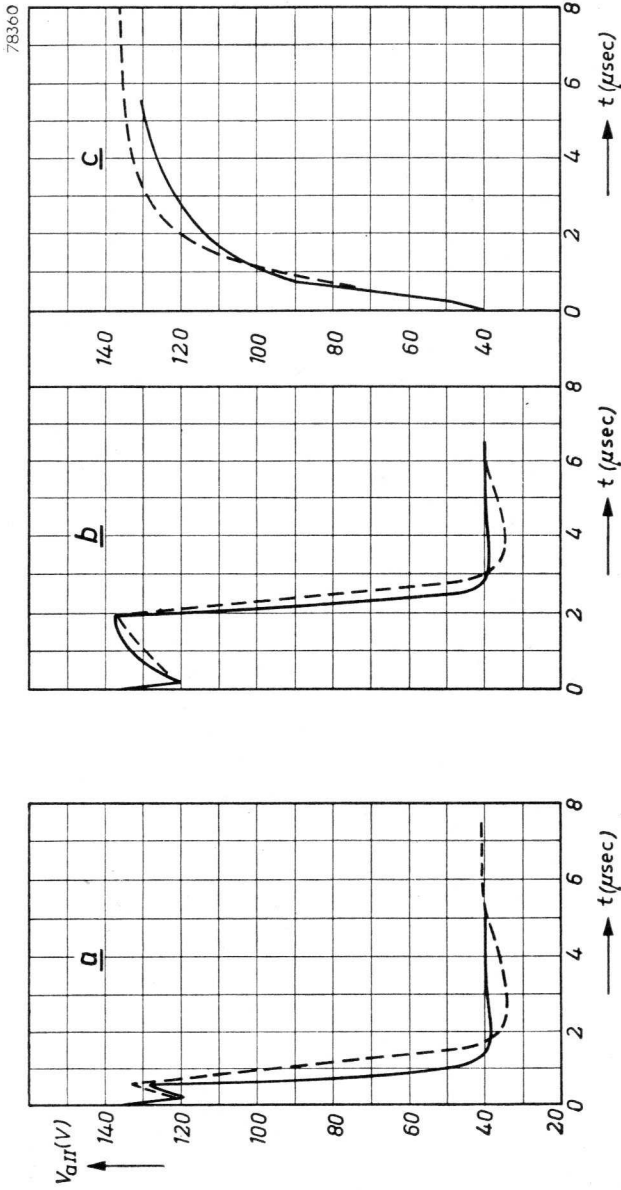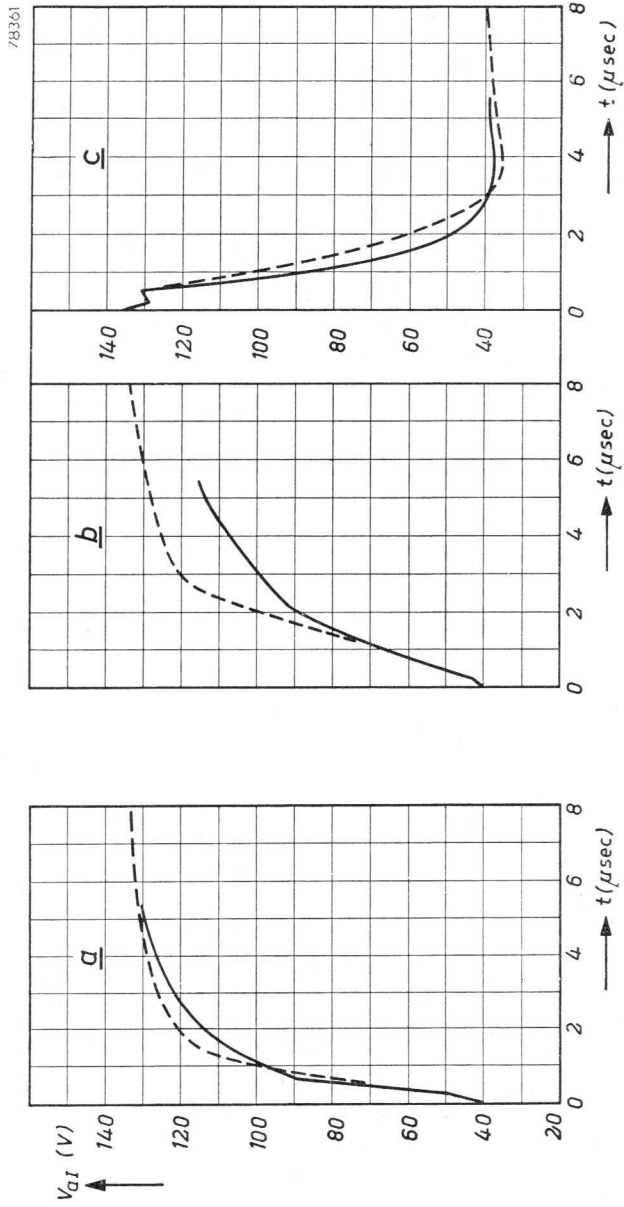
Fig. 7-1

Fig. 7-2

Fig. 7-3

Fig. 7-4

At the instant $t = t_{II}$ the grid voltage of tube I, represented in fig. 7–2, has reached a value $-10\ V$ and $-4\ V$ in case a and case b respectively. This shows that the triggering is much more certain in the unloaded than in the loaded condition. It is only because the anode voltage of tube I (see fig. 7–4b, about 85 V) is much smaller than the anode voltage of tube II (see fig. 7–3b, about 138 V) at the instant t_{II}, that the cut-off voltage of tube I is not yet reached at $V_{gI} = -4\ V$.

At the instant $t = t_{II}$ the second phase of the trigger cycle commences. Curves a and b of fig. 7–3 reveal that the anode voltage V_{aII} greatly decreases from this instant onwards, and consequently the grid voltage V_{gI} (see fig. 7–2) also decreases. The multivibrator is finally triggered. Fig. 7–1 shows that V_{gII} reaches the value zero shortly after the instant $t = t_{II}$; owing to the flow of grid current, V_{gII} is then kept constant at this value. In practice there is some overshoot, which should be attributed to the fact that the grid resistance is not zero as was assumed in the calculations. The influence of the discontinuity will therefore be smaller than calculated.

The fully-drawn curves plotted in fig. 7–4 show the calculated effects of this discontinuity (at approximately 0.7 μ sec for curve a and at approximately 2 μ sec for curve b) on the anode voltage V_{aI}. This effect could not be clearly discerned on the oscillograms. The oscillograms shown in figs. 7–6 and 7–9, which apply to other trigger circuits, do show these discontinuities.

The oscillograms of figs. 7–5 and 7–6 refer to a symmetrical unloaded multivibrator having the same data as the previously mentioned circuit. Triggering was, however, achieved by means of square-wave pulses with a period of 15 μ sec. Fig. 7–5 shows the grid voltage variation of one of the tubes; that of the other tube is obviously identical. Fig. 7–6 displays the anode-voltage variation of both tubes. The discontinuity which can be clearly seen in the ascending part of the oscillogram is due to the start of grid current flow in the other tube.

Figs. 7–7, 8, 9, 10 show the oscillograms of the grid and anode voltages of an asymmetrical multivibrator, triggered by negative-going pulses having a width of 40 μ sec, a period of 60 μ sec and an amplitude of 35 V. The circuit data are once again identical to those of the previous circuits; C_{aI} and C_{aII} were 110 pF and $5pF$, respectively.

The variation of V_{gII} is displayed by the oscillogram shown in fig. 7–7; the negative-going front should be compared with curve c of fig. 7–1 and the positive-going front with curve b of this figure.

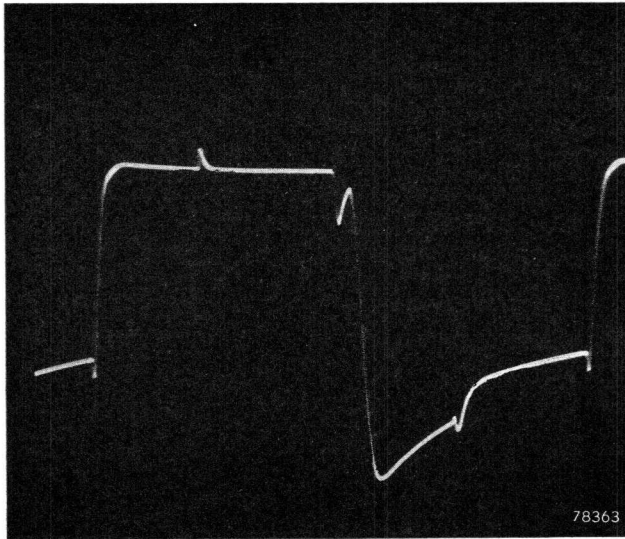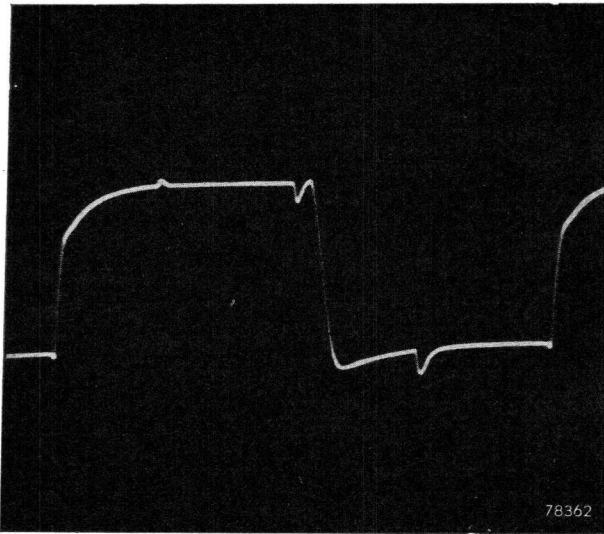Fig. 7–8 shows the variation of V_{gI}; this should be compared with curves b and c of fig. 7–2.
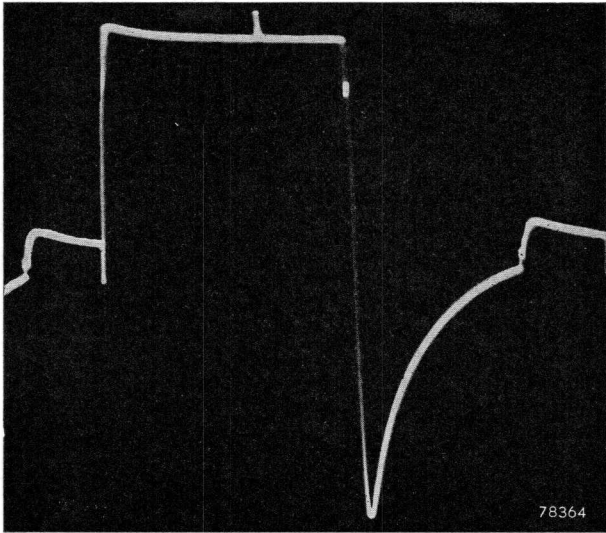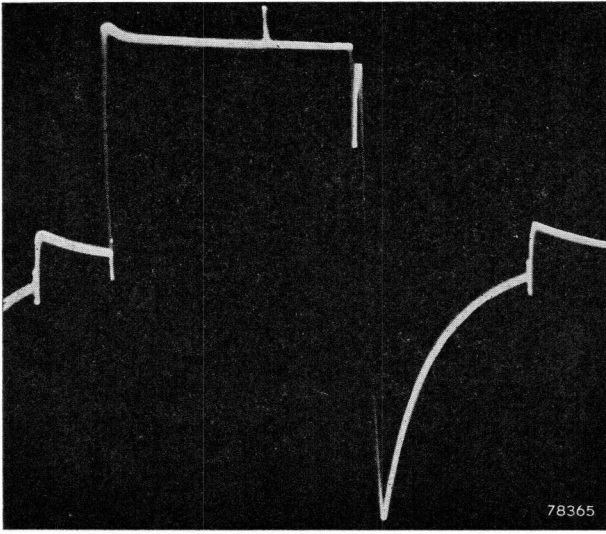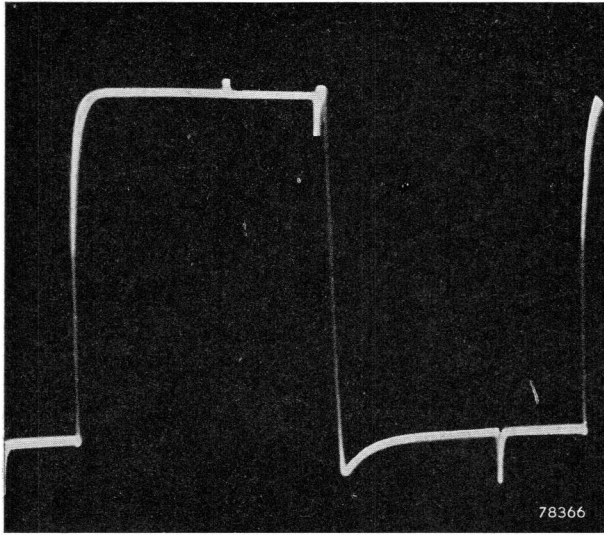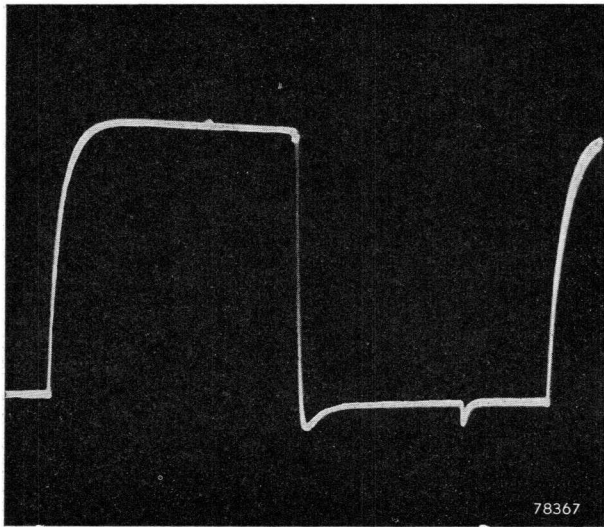
Fig. 7–5

Fig. 7–6

Fig. 7–7

Fig. 7–8

Fig. 7–9

Fig. 7–10

Fig. 7–9 gives the oscillogram of V_{aII} and should be compared with curves b and c of fig. 7–3.

Finally, the oscillogram of fig. 7–10 shows the variation of V_{aI} and should be compared with curves b and c of fig. 7–4.

In the curves representing the calculated time functions the influence of the positive-going rear flanks of the trigger pulses has been disregarded. In practice care should be taken that these positive-going flanks do not disturb the normal triggering. These pulses should not, for example, drive the grid voltage of the non-conducting tube (i.e. the initially conducting tube I) above its cut-off point. Curves a and b of fig. 7–2 reveal the considerable overshoot of V_{gI} in the negative direction, its final value being —30 V. It would therefore be advantageous to choose the width of the trigger pulse in such a way that the positive-going rear flank coincides with this overshoot region. This will not be possible, however, when a multivibrator is triggered by a preceding one, because the pulses produced thereby are always roughly square-wave shaped and the positive-going flank will always occur just between two negative-going flanks. However, the negative anode-voltage pulse, caused by the positive-going flank at the grid of the conducting tube, has a compensating effect on the positive-going flank at the grid of the non-conducting tube. This effect is clearly shown by the oscillogram of fig. 7–5 half way along the gradually increasing part of the voltage curve. Initially, the voltage tends to rise, but the slightly delayed negative pulse at the anode of the conducting tube is passed to the grid of the non-conducting tube via the coupling capacitor C and even overcompensates the positive-going input pulse, so that a negative pulse results.

The final static conditions for the curves a and b of figs. 7–1, 2, 3, 4 are: $V_{gI} = $ —30 V, $V_{aI} = 136\ V$, $V_{gII} = 0\ V$ and $V_{aII} = 40\ V$. The functions are now reversed, tube I being cut off and tube II being conducting. The next negative-going flank of V_i will trigger the multivibrator once again. In the case of a symmetrical circuit ($C_{aI} = C_{aII} = 5\ pF$) the waveforms during this new trigger action follow from the theoretical results, by changing the indices I and II in all formulae, the waveform of V_{gII} thus being identical to that of V_{gI} during the preceding trigger action. The new waveforms corresponding to figs. 7–1a, 2a, 3a, 4a have therefore not been given separately, as the new fig. 7–2a corresponds to 7–1a and the new fig. 7–4a to 7–3a, and vice versa.

In the case of an asymmetrically loaded multivibrator the situation is less simple, but the waveforms can nevertheless also be calculated; the results are shown by curves c.

Notwithstanding the presence of the load capacitance $C_{aI} = 110\ pF$ the switching time, or the duration of the first trigger phase, is now much shorter than in the first case b. This is due to the fact that the switching time is now defined by the waveform of V_{gI}, which is independent of C_{aI}. The switching time is about 0.6 μ sec, whereas it was about 2 μ sec in the first case.

It can, moreover, be seen that the trigger sensitivity will be better in the second case. In the first case the grid voltage of the initially conducting tube, V_{gI}, has almost reached its cut-off value at the instant in which tube II starts to draw anode current (at $t \approx 2\ \mu$ sec; see curve b fig. 7–2). In the second case, however, the grid voltage of the initially conducting tube, V_{gII} (curve c, fig. 7–1), rises at a much slower rate owing to the influence of $C_{aI} = 110\ pF$. At the instant at which tube I starts to draw current the (negative) value of V_{gII} will still be almost three times that of V_{gI} in the first case. In other words, V_{gI} rises much faster than V_{gII} during the same periods of time.

The sensitivity of an asymmetrical multivibrator is thus not the same for the two stable conditions, and is smallest for the initial condition in which the capacitively loaded tube is conducting. In practice this smallest sensitivity defines the usefulness of the circuit.

It can also be seen that the sensitivity of an asymmetrically loaded multivibrator is improved by loading the multivibrator symmetrically (for example $C_{aI} = C_{aII} = 110\ pF$). In that case the grid voltage V_{gI} (curve b, fig. 7–2) will rise more slowly and reach the cut-off point later, so that it will be easier for the grid voltage of the other tube to reach its cut-off value first.

This fact has been confirmed experimentally. By way of example the average value of V_{cr}, the minimum input voltage amplitude wanted to trigger the multivibrator, measured on a series of some 40 experimental samples of double triodes, will be given. For symmetrical, unloaded multivibrator circuits the critical trigger amplitude had an average value of 17 V. For an asymmetrical circuit (150 pF load in one of the anode circuits) this average value was 38 V. By connecting the load of 150 pF to both anode circuits the sensitivity of the multivibrator was increased, the average value of V_{cr} then being 31.5 V.

8. THE TRIGGER SENSITIVITY

In chapter 6 explicit expressions have been derived for the anode and grid voltages as functions of time during the complete trigger cycle. With the aid of these expressions various properties of the circuit can be investigated, including in particular the trigger sensitivity; in fact, the need to know the influence of tube characteristics on the sensitivity was the reason for starting the investigation and analysis given here. In section 6–2 it has already been mentioned that the limit of correct triggering operation is reached if both tubes attain their cut-off grid voltages simultaneously. The times t_I and t_{II} that elapse before tube I and tube II reach their respective cut-off points after the application of the trigger voltage V_i, when the feedback was temporarily inactive, can be calculated from the relations

$$V_{gI}(t_I) = \frac{-V_{aI}(t_I)}{\mu} \tag{8–1}$$

and

$$V_{gII}(t_{II}) = \frac{-V_{aII}(t_{II})}{\mu} \tag{8–2}$$

The time functions representing the anode and grid voltages are given by expressions (6–11, 12, 13, 14). One of the variables defining these functions is the amplitude V_o of the trigger voltage V_i (see fig. 3–2). Varying V_o will result in varying the values of t_I and t_{II}. Practical experience shows that at too low a value of V_o no switch-over of the multivibrator occurs. It is evident that in this case $t_I < t_{II}$. At a certain value, $V_o = V_{cr}$, the values of t_I and t_{II} will be equal and this will be a limit for correct triggering. Therefore V_{cr} will be called the critical trigger voltage amplitude, and is a measure for the trigger sensitivity. The lower V_{cr}, the higher the sensitivity of the multivibrator circuit.

Up till now, the influence of the capacitance C_{ag} between the anode and grid of each tube has not been allowed for in the calculations, as it considerably complicates the problem. However, practical experience showed evidence that the anode-to-grid capacitance of the tubes had a considerable influence on the trigger sensitivity. Therefore it is desirable to take into account this influence of C_{ag}.

For a non-conducting tube the effect of C_{ag} will nearly be equivalent to the presence of a capacitive voltage divider between anode and grid, and will influence signals with a steep slope. A fraction of the anode voltage variation is transmitted to the grid of the same tube due to the anode-to-

grid capacitance of the tube. For tube I this can be taken into account by the factor

$$b_I = \frac{C_{agI}}{C_{agI} + C_c + C_{gI} + \dfrac{C\,C_{aII}}{C + C_{aII}}} \tag{8-3}$$

and for tube II by the factor

$$b_{II} = \frac{C_{agII}}{C_{agII} + C_c + C_{gII} + \dfrac{C\,C_{aI}}{C + C_{aI}}} \tag{8-4}$$

For a more elaborate discussion of the influence of C_{ag} see Appendix V. The anode-voltage variation is the difference between the total anode voltage during the first phase of the dynamic condition and the static-condition voltage. With this correction the expressions (8–1) and (8–2) become:

$$V_{gI}(t_I) + b_I\{V_{aI}(t_I) - V_{aI_o}\} = -\frac{1}{\mu} V_{aI}(t_I) \tag{8-5}$$

$$V_{gII}(t_{II}) + b_{II}\{V_{aII}(t_{II}) - V_{aIIo}\} = -\frac{1}{\mu} V_{aII}(t_{II}) \tag{8-6}$$

Introducing expressions (6–11, 12, 13, 14) into these equations gives

$$\left(b_I + \frac{1}{\mu}\right) V_8\, e^{p_1 t_I} + \left(b_I + \frac{1}{\mu}\right) V_9\, e^{p_2 t_I} + V_{11}\, e^{p_1' t_I} + V_{12}\, e^{p_2' t_I} + V_{10} +$$

$$+ \left(b_I + \frac{1}{\mu}\right) V_7 - b_I V_{aIo} = 0 \tag{8-7}$$

$$V_2\, e^{p_1 t_{II}} + V_3\, e^{p_2 t_{II}} + \left(b_{II} + \frac{1}{\mu}\right) V_5\, e^{p_1' t_{II}} + \left(b_{II} + \frac{1}{\mu}\right) V_6\, e^{p_2' t_{II}} + V_1 +$$

$$+ \left(b_{II} + \frac{1}{\mu}\right) V_4 - b_{II} V_{aIIo} = 0 \tag{8-8}$$

To solve these equations for t_I and t_{II}, one can only try, by substituting several values of V_o, to find a value V_{cr} for which $t_I = t_{II}$. For the symmetrical multivibrator, however, a more elegant method can be derived. In that case $p_1 = p_1'$, $p_2 = p_2'$ and $b_I = b_{II} = b$. The equations take the following form:

$$\left\{\left(b + \frac{1}{\mu}\right) V_8 + V_{11}\right\} e^{p_1 t_I} + \left\{\left(b + \frac{1}{\mu}\right) V_9 + V_{12}\right\} e^{p_2 t_I} + V_{10} +$$

$$+ \left(b + \frac{1}{\mu}\right) V_7 - b V_{aIo} = 0 \tag{8-9}$$

$$\left\{\left(b+\frac{1}{\mu}\right) V_5 + V_2\right\} e^{p_1 t_{II}} + \left\{\left(b+\frac{1}{\mu}\right) V_6 + V_3\right\} e^{p_2 t_{II}} + V_1 +$$

$$\left(b+\frac{1}{\mu}\right) V_4 - b V_{aIIo} = 0 \qquad (8\text{--}10)$$

The following notations will be used:

$$e^{p_1 t_I} = x_I \qquad (8\text{--}11)$$

$$e^{p_1 t_{II}} = x_{II} \qquad (8\text{--}12)$$

$$\frac{p_2}{p_1} = \gamma \qquad (8\text{--}13)$$

Then equations (8–9) and (8–10) become:

$$\left\{\left(b+\frac{1}{\mu}\right) V_8 + V_{11}\right\} x_I + \left\{\left(b+\frac{1}{\mu}\right) V_9 + V_{12}\right\} x_I^\gamma + V_{10} +$$

$$+ \left(b+\frac{1}{\mu}\right) V_7 - b V_{aIo} = 0 \qquad (8\text{--}14)$$

$$\left\{\left(b+\frac{1}{\mu}\right) V_5 + V_2\right\} x_{II} + \left\{\left(b+\frac{1}{\mu}\right) V_6 + V_3\right\} x_{II}^\gamma + V_1 +$$

$$+ \left(b+\frac{1}{\mu}\right) V_4 - b V_{aIIo} = 0 \qquad (8\text{--}15)$$

When $V_o = V_{cr}$ then $t_I = t_{II}$, or $x_I = x_{II} = x$. Substituting these values in eqs (8–14) and (8–15) and subtracting these equations gives:

$$A_2 x^\gamma + A_1 x + A_0 = 0 \qquad (8\text{--}16)$$

Where

$$A_2 = -\tfrac{1}{2}\left(b+\frac{1}{\mu}\right)\{I_{ao}\left(1-\varepsilon_a\right) R_a\left(1+L\right) - I_{go}\varepsilon_a R_g \left(1+P\right)\} -$$

$$- \tfrac{1}{2} I_{go}\left(1-\varepsilon_g\right) R_g\left(1+K\right) + \tfrac{1}{2} I_{ao}\varepsilon_a R_g\left(1+P\right) \qquad (8\text{--}17)$$

$$A_1 = -\tfrac{1}{2}\left(b+\frac{1}{\mu}\right)\{I_{ao}\left(1-\varepsilon_a\right) R_a\left(1-L\right) - I_{go}\varepsilon_a R_g\left(1-P\right)\}$$

$$- \tfrac{1}{2} I_{go}\left(1-\varepsilon_g\right) R_g\left(1-K\right) + \tfrac{1}{2} I_{ao}\varepsilon_a R_g\left(1-P\right) \qquad (8\text{--}18)$$

$$A_0 = b\left(V_{aIIo} - V_{aIo}\right) = b\{(1-\varepsilon_a) R_a I_{ao} - \varepsilon_a R_g I_{go}\} \qquad (8\text{--}19)$$

Equation (8–16) is independent of V_{cr} and therefore, if x is determined by solving the equation, then V_{cr} can be calculated from either eq. (8–14) or (8–15). However, in general, eq. (8–16) will not be easily solved by conventional methods, as γ is normally a rather high power and not even a whole number. Therefore, a graphical method is to be applied.

If in one graph the functions $F_1(x) = x^\gamma$ and $F_2(x) = -\dfrac{A_1}{A_2}x - \dfrac{A_o}{A_2}$ are plotted, then the point of intersection of the graphical representations gives the value of x to be determined.

8.1. INFLUENCE OF TUBE CHARACTERISTICS AND CAPACITIVE ANODE LOAD

An example of calculating the influence of tube characteristics and of a capacitive load in both anode circuits on the sensitivity will be given. The circuit to be investigated is assumed to have the following characteristic data (compare figs. (3–1) and (3–2)). $V' = 150\ V$, $V'' = 100\ V$, $R_a = 20\ k\Omega$, $R = R_g = 200\ k\Omega$, $C = 100\ pF$, $C_c = 40\ pF$, $t_o = 0.2\ \mu\ sec$. The grid-to-cathode capacitance of each tube is assumed to be $C_g = 10\ pF$. This gives $C_i = C_c + C_g = 50$ pF (see expr. (6–8)). The anode-to-cathode capacitance C_a will be chosen as a parameter, taking values of $5\ pF$, $50\ pF$ and $150\ pF$.

If the amplification factor of the tubes is $\mu = 50$, and the internal anode resistance $r_a = 7k\Omega$, then the critical trigger-voltage amplitude V_{cr} depends, according to the calculations, on the value of the anode-to-grid capacitance C_{ag} in the way indicated in table I.

Table I

C_{ag} (pF)	A_2	A_1	A_0	x	V_{cr} (V)	
2.5	60.63	—34.84	1.92	0.970	9.2	$C_a = 5\ pF$
4.5	57.68	—34.90	5.32	0.967	13.4	$\gamma = 21.2$
6.8	54.19	—35.01	8.78	0.964	18.0	
2.5	62.80	—35.66	0.79	0.935	13.0	$C_a = 50\ pF$
4.5	60.75	—35.72	2.90	0.931	17.2	$\gamma = 9.7$
6.8	58.36		5.31	0.927	21.6	
2.5	62.82	—35.23	0	0.852	20.8	$C_a = 150\ pF$
4.5	60.96	—35.25	2.12	0.850	26.0	$\gamma = 4.75$
6.8	59.46	—35.28	3.69	0.848	29.5	

These results are graphically represented in figs 8–1 and 8–2. It can be seen from these figures that the critical trigger-voltage amplitude is an approximately linear function of the capacitive load in the anode circuits, with a mean slope $\dfrac{dV_{cr}}{dC_a} = 0.082\,\dfrac{V}{pF}$, and that it is also an approximately
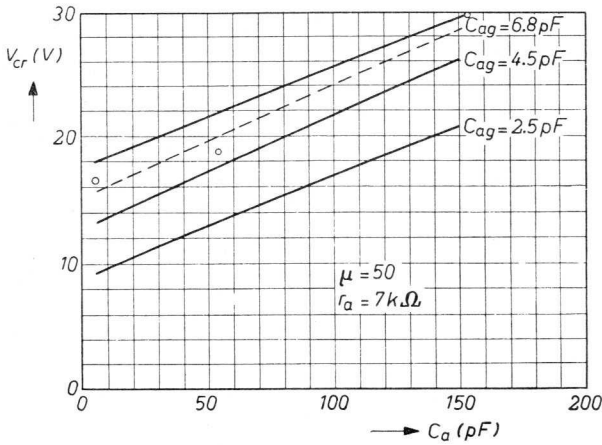
Fig. 8–1

linear function of the anode-to-grid capacitance of the tubes, having a mean slope $\dfrac{dV_{cr}}{dC_{ag}} = 2\,\dfrac{V}{pF}$.

The influence of the amplification factor μ is calculated, assuming that $C_a = 50\ pF$, $C_{ag} = 4.5\ pF$ and $r_a = 7\ k\Omega$.

The result is presented in table II and graphically in fig. 8–3 (curve I).

Table II

μ	A_2	A_1	A_0	x	V_{cr} (V)	
25	58.79	—35.69	2.90	0.933	20.6	
35	59.51	—35.69	2.90	0.933	18.8	$\gamma = 9.7$
50	60.75	—35.70	2.90	0.931	17.2	

The influence of the internal anode resistance r_a at values $C_a = 50\ pF$, $C_{ag} = 4.5\ pF$, $\mu = 50$ is also calculated, and the result is given in table III and fig. 8–4 (curve I).

The critical trigger-voltage amplitude decreases with increasing amplification factor and constant internal anode resistance and increases with increasing internal anode resistance and constant amplification factor.

Table III

r_a $k\Omega$	A_2	A_1	A_0	x	V_{cr} (V)	
5.4	64.9	—36.91	0	0.936	16.3	
7.0	60.75	—35.70	2.90	0.931	17.2	$\gamma = 9.7$
9.0	56.62	—34.22	6.21	0.923	18.6	

As the amplification factor μ and the internal anode resistance r_a are related to the transconductance g_m by the following expression

$$\frac{\mu}{r_a} = g_m \qquad (8\text{–}20)$$

it must be expected that, for constant transconductance, their influence on the critical trigger-voltage amplitude will be small, at least in the cal-

Fig. 8–2

Fig. 8–3

culated region. This has been investigated by varying μ and r_a in such a way that their ratio remains constant, starting from the values $\m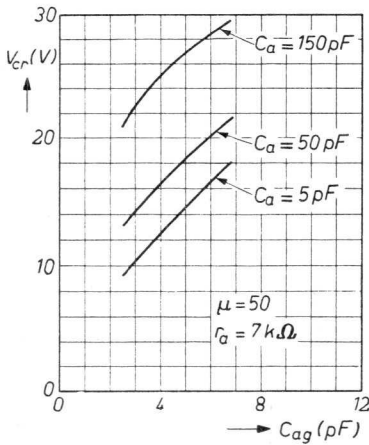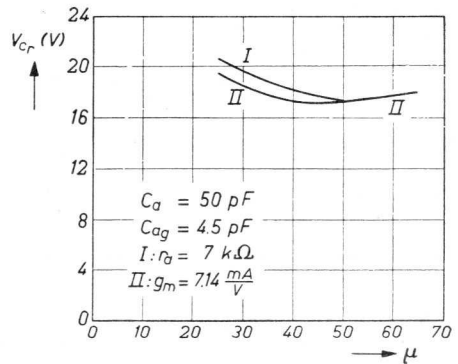u = 50$ and $r_a = 7\ k\Omega$, corresponding to $g_m = 7.14\ \frac{mA}{V}$. For these values the critical trigger voltage V_{cr} has already been calculated and amounts to 17.2

volts. The results of these additional calculations are represented in table IV and in the graphs of figs. 8–3 and 8–4 (curves II).

Table IV

μ	r_a $(k\Omega)$	A_2	A_1	A_0	x	V_{cr} (V)	
64.3	9.0	56.92	—34.44	5.92	0.922	17.8	$C_{ag} = 4.5\ pF$
50	7.0	60.75	—35.70	2.90	0.931	17.2	$C_a = 50\ pF$
40	5.6	63.64	—37.11	-0.504	0.938	17.1	$\gamma = 9.7$
32	4.5	66.18	—37.57	1.72	0.942	18.2	$g_m = 7.14$
25	3.5	68.20	—38.57	3.60	0.938	19.5	

As can be seen, there is a certain minimum value of V_{cr}, in other words for a given value of the transconductance there are optimum values of r_a and μ.

It must be borne in mind that all conclusions drawn from the foregoing calculations are not of a general character, but apply to the specific data treated.

The results of calculations can be compared with experimental investigations.

The trigger sensitivity of a double triode type E92CC has been measured under similar conditions as were assumed to exist in the foregoing calculations. The amplification factor of this tube is $\mu=50$, its internal anode resistance being 7 $k\Omega$. This internal resistance is
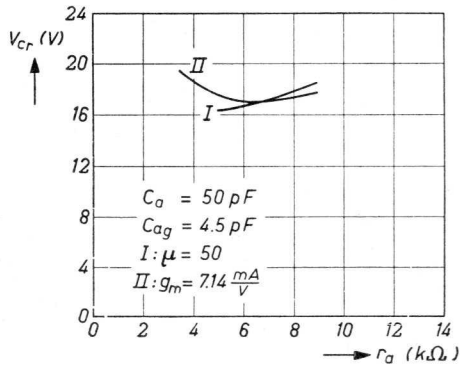
Fig. 8–4

taken as the reciprocal value of the slope of the I_a-V_a characteristic at $V_g = 0$. The capacitances in the anode circuit have been put equal to 5 pF, which is based on experimental experience. The trigger sensitivity is measured to be 16.5 V, when no extra capacitive load is applied to the anodes, whereas it is 18.7 V with 47 pF applied between the anode and cathode of each tube, and 29.6 V with 150 pF anode load applied. These measuring data are represented by the small circles in fig. 8–1. A mean straight line, drawn through these measuring points is represented by the

broken line in fig. 8–1. The conclusion to be drawn from these measuring data is that an effective anode-to-grid capacitance of about 6 pF should be assumed to exist. The C_{ag} of an E92CC is 2.5 pF. The wiring capacitance of the circuit between anode and grid was measured and found to be 4.6 pF. Thus, the total capacitance between anode and grid of the tubes was 7.1 pF. The conclusion is that these experimental data are in quite good agreement with those derived from the calculations.

One more check on the theory was carried out.

Assuming C_{ag} to be 6 pF, the trigger sensitivity with asymmetrical capacitive anode load was calculated. If one anode is loaded with 47 pF and the other tube has no externally applied capacitive load, then $C_{aI} = 52 \; pF$ and $C_{aII} = 5 \; pF$. With these capacitance values the trigger sensitivity is calculated to be 23 V, whereas it is actually measured to be 21 V, which is also quite a good agreement.

In chapter 10 some considerations on the influence of the coupling capacitors C and C_c have been included.

9. THE TRIGGERING SPEED

In the calculations of the transient behaviour of the bistable multivibrator the assumption was made that before the instant of application of an input trigger voltage the circuit was in its static condition, i.e. all the previous triggering effects had died out by this instant. Theoretically there would be an infinitely long time before all transients of the dynamic condition have completely died away. In practice, however, a subsequent triggering will occur at a definite time after the first trigger pulse has been applied. An important question is, what will be the lower limit in the time interval between two trigger pulses at which the multivibrator is still operating satisfactorily. It is difficult to define this limit explicitly, at any rate not as plainly as could be done with respect to the trigger sensitivity.

What are the operations to be performed by the multivibrator circuit? When triggering at both grids simultaneously the aim is, as has been formulated previously, to get one output pulse at every two input pulses, i.e. essentially a frequency division. As soon as this ratio 2 : 1 is lost because of too high a repetition frequency of the input pulses, one can say that the maximum triggering speed is attained. In another way of operation, negative trigger pulses are fed to the grid of the tube that is momentarily conducting or alternatively positive pulses to the grid of the non-conducting tube. In this application the aim is to change the potential of the anodes or grids as rapidly as is necessary in the given circumstances. A certain minimum change of potential level will be wanted, and as soon as the next trigger pulse occurs so rapidly after the previous pulse that this change is not obtained, the maximum trigger speed is reached. It is not possible from the foregoing analysis to derive the speed limits mentioned for the two cases, as this analysis assumes that the system is at rest before it is triggered, and this would by no means be satisfied at the speed limit. A new way of approach would have to be introduced, a quasi-stationary condition being assumed to exist.

Nevertheless, the results of calculations presented in the foregoing chapters may give an idea of the triggering speed to be attained by a given circuit, and of means to improve it.

There is one absolute upper limit of triggering speed to be defined, viz. the time t_{II}, during the first phase of the dynamic condition, when both tubes are cut off. Within this time no new input pulse will be able to produce further triggering. The time t_{II} depends on the time constants of the circuit, given by the negative reciprocal values of p_1 and p_2 (expressions (I–25) and (I–26). From section 8 it can be seen that t_{II} also

depends on the amplitude of the trigger pulse. At the critical amplitude V_{cr} it can be calculated from the value of x as given in tables I, II, III, IV. According to expression (8–12):

$$x = e^{p_1 t_{II}} \tag{9-1}$$

or

$$t_{II} = \frac{ln\ x}{p_1} \tag{9-2}$$

To give an idea of the value of t_{II} at the critical trigger voltage amplitude for the circuit, for which table I is calculated, expression (9–2) will be evaluated with the aid of the values of x from table I and of p_1 from the following table V

Table V

$Ca\ (pF)$	$p_1\ (\mu\ sec^{-1})$
5	—0.0661
50	—0.0663
150	—0.0665

The results are given in table VI

Table VI

$Ca\ (pF)$	$t_{II}\ (\mu\ sec)$	
5	0.45	
50	1.01	$C_{ag} = 2.5\ pF$
150	2.42	
5	0.56	
50	1.14	$C_{ag} = 6.8\ pF$
150	2.49	

The influence of the anode-to-grid capacitance is not very great but that of the anode capacitance is.

As can be concluded from the values of x in tables II, III and IV, the influence of μ and r_a is not marked (p_1 does not depend on μ and r_a).

Next it can be stated that the sooner the circuit approaches its final static state, after having been triggered, the smaller the time interval between

two subsequent triggerpulses may be. This implies that the time constants of the circuit should be small. These time constants are:

$$T_1 = -\frac{1}{p_1}, \; T_2 = -\frac{1}{p_2}, \; T_1' = -\frac{1}{p_1'}, \; T_2' = -\frac{1}{p_2'}, \; T_3 = -\frac{1}{p_3},$$

$$T_4 = -\frac{1}{p_4} \text{ and } T_n = -\frac{1}{p_n}.$$

(see chapter 6).

It can be shown that a decrease in any resistance or capacitance of a circuit composed of resistances and capacitances only results in a decrease in all the time constants. This will be derived for the multivibrator circuit considering first the circuit arrangement during the first phase of the dynamic condition. It then holds that the driving-point impedances of the circuit are of the following general form, apart from a constant multiplication factor:

$$Z(p) = \frac{p + b_1}{p^2 + a_1 p + a_2} \tag{9-3}$$

as can be seen from expressions (I–7), and (I–19). The zeros and poles of this impedance function are defined by the roots of equations

$$p + b_1 = 0 \tag{9-4}$$

and

$$p^2 + a_1 p + a_2 = 0 \tag{9-5}$$

respectively.

There will be one zero, viz, at $p = -b_1$ and two poles, viz. at $p = p_1$ and $p = p_2$ (see expressions (I–25) and (I–26)). These values of p determine the normal modes of the circuit.

From general network theory it is known that for a network, consisting of R's and C's only, the quantities a_1, a_2 end b_1 are positive, real; further that the normal modes are always negative, real; finally that

$$p_2 < -b_1 < p_1 < o \tag{9-6}$$

(Reference is made to p. 211 of vol. II of "Communication Networks", by E. A. Guillemin, Wiley & Sons, 1935).

With this knowledge it is possible to sketch the impedance function $Z(p)$ as it depends on p. In fig. 9–1 the curves I, II and III represent the general form of $Z(p)$ as a function of p given by expression (9–3).

It will now be assumed that a resistance R is shunted across the imped-

ance $Z(p)$. In that case the normal modes are tobe determined from the condition

$$Z(p) = -R \qquad (9\text{–}7)$$

In fig. 9–1 these normal modes are determined by the intersection points of curves II, III and the dotted curve VI. It can be seen that the values of p corresponding to these points of intersection will always be more negative than p_1 and p_2 respectively.

Thus, inserting a resistance across one of the resistances of the circuit, or decreasing one of the circuit resistances, which amounts to the same-thing, will always result in a decrease of the characteristic time constants of the circuit. From this general statement it can be concluded that the time constants during the second phase of the dynamic condition, T_3 and T_4, are always smaller than the corresponding values, T_1' and T_2' respectively, from the first phase. For during the second phase one of the anode resistances of the multivibrator circuit is shunted by the internal anode resistance of the conducting tube. In the third phase one of the grid resistances is shunted by the internal grid resistance of the conducting tube, which will result in a still smaller time constant in this phase. The influence of a change in one of the capacitances of the circuit on the characteristic time constants can be derived in a similar way to the method used for a change in resistances. Assuming a capacitance C to be shunted across $Z(p)$, the new characteristic frequencies have to be determined from the condition
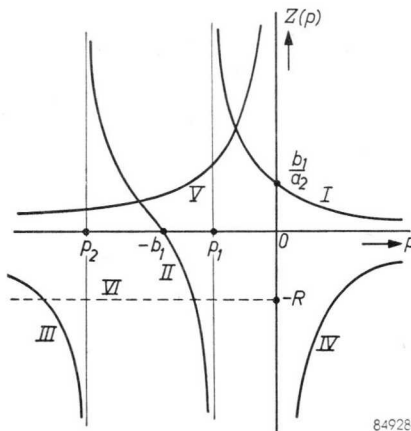
Fig. 9–1

$$-\frac{1}{Cp} = Z(p) \qquad (9\text{–}8)$$

The function $-\dfrac{1}{Cp}$ is represented in fig. 9–1 by the curves IV and V, and the roots of equation (9–8) are given by the points of intersection of curve V and curves I and II. To these points correspond values of p that are always less negative than p_1 and p_2, respectively. In other words,

the new time constants will be larger than T_1 and T_2 as a result of the increase of one of the capacitances of the circuit.

When aiming at a high triggering speed it is thus advantageous to reduce the value of all resistances and capacitances as much as possible. There are limits, of course, to this reduction. The resistances, for instance, greatly determine the values of the voltages and currents of the circuit in the static condition. Considerations of supply power available and tolerable, and the anode voltage change wanted when triggering the multivibrator, will fix the minimum values of resistances to be applied. Tubes with a low internal anode resistance (low μ high g_m) will be advantageous for obtaining small time constants during the second phase of the complete cycle. How far can the capacitances be reduced? The anode-to-cathode capacitances C_a are determined by the tube capacitances and the wiring capacitances. Both have to be reduced to the utmost. The same holds for the input capacitances between grid and cathode of the tubes and the wiring capacitances, which together form C_g. However, the sum $C_i = C_g + C_c$ determines the grid circuit constant T_g, where C_c is the coupling capacitance between the trigger-voltage source and the grids. Therefore, C_c should be reduced as much as possible. Here of course, there is also a limit. Too small a value of C_c reduces the current pulse $I_i = -aC_c$ (see expression (6–7)) to such an extent that the tube will no longer be safely triggered at a given input voltage amplitude V_o.

Finally, the coupling capacitors C between the anodes and grids of the tubes must be reduced. A limit is presented here by the fact that the steep voltage rise at the anode of the tube that is suddenly cut off must be passed by this capacitance C to such a degree that the grid voltage of the non-conducting tube increases rapidly enough to reach its cut-off point earlier than the other tube. In other words, too small a value of C will prevent the proper triggering of the circuit.

Some practical experience will be dealt with in chapter 10, together with some details about the influence of C_c and C both on the trigger sensitivity and the triggering speed.

10. DESIGN CONSIDERATIONS

When designing a bistable multivibrator several aspects will have to be kept in mind. The bistable circuit should if possible have a high triggering speed, a high trigger sensitivity, a low power consumption, a good stability and a low sensitivity to interferences. All these demands, however, cannot be satisfied at the same time, as an improvement of one or more of the properties mentioned mostly results in a deterioration of others. This has been mentioned already at the end of Chapter 1.

Therefore, general rules for designing a bistable multivibrator are difficult to formulate. Each case will have to be considered separately. For example, if a scaler or any other device containing only a few multivibrator circuits has to be built, then the power consumption will not be restricted to such an extent as it would be when a large number of those circuits have to be incorporated in a high-capacity electronic computer, say. One of the reasons to aim at as low a power consumption as possible in that case would be that the heat dissipation has to be kept within certain bounds.

The choice of component values will generally be greater than the choice of available tube types. Therefore, the first thing to do will be to choose a type of tube that is the best to fulfil the demands in the special case considered. A low internal anode resistance and low capacitances will be advantageous for attaining a high speed; a high amplification factor and particularly a low anode-to-grid capacitance may increase the trigger sensitivity. Furthermore maximum allowed values of anode and grid currents of the tube are published by the manufacturer and it is advisable to choose values within as small a safety margin below these maxima as is possible. A large anode current allows for a small anode load resistance, which is advantageous with respect to the speed to be attained. A large grid current has a large stabilizing effect (see Chapters 3 and 5).

Once the value of the anode current I_{ao} of the conducting tube is chosen, the value of its anode voltage is defined from the I_a-V_a characteristic at zero grid voltage ($V_{aIo} = r_a I_{ao}$).

Usually, the required anode-voltage change, when triggering the multivibrator will be known. It may, for example, be defined by the further use to be made of this voltage change, or occasionally by the kind of indication of the position of the multivribrator. Gas discharge tubes are usually used for this purpose and then a certain minimum voltage change is wanted to ignite these tubes. If the anode-voltage change is

fixed the anode voltage of the non-conducting tube V_{aIIo} is known from V_{aIo} and the anode-voltage change.

Next, the voltage at the grid of the non-conducting tube, V_{gIIo}, can be fixed to a value safely below the cut-off point to prevent the influence of interfering signals.

According to the foregoing remarks it can be considered a rather general case to take as known quantities I_{ao}, I_{go}, V_{aIo}, $\triangle V_a (= V_{aIIo} - V_{aIo})$, V_{gIIo}.

From the expressions derived for the static condition in chapter 5 four independent equations can be extracted, which are conveniently chosen as follows:

$$V_{gIIo} = \varepsilon_g V' - (1 - \varepsilon_g) V'' - \varepsilon_g R_a I_{ao} \tag{5-7}$$

$$V_{aIIo} - V_{aIo} = (1 - \varepsilon_a) R_a I_{ao} - \varepsilon_a R_g I_{go} \tag{5-16}$$

$$(1 - \varepsilon_a) R_a I_{ao} = (1 - \varepsilon_a) V' - \varepsilon_a V'' - V_{aIo} \tag{5-9}$$

$$(1 - \varepsilon_g) R_g I_{go} = \varepsilon_g V' - (1 - \varepsilon_g) V'' \tag{5-14}$$

The unknown quantities in these equations are ε_a, ε_g, V', V'', R_a and R_g. However, a relation exists between some of them:

$$R_a = \varepsilon_a (R_g + R + R_a) \tag{10-1}$$

$$R_g = \varepsilon_g (R_g + R + R_a) \tag{10-2}$$

or: $\varepsilon_g R_a = \varepsilon_a R_g$ \hfill (10-3)

This reduces the number of unknown quantities to five. Thus, one of them still has to be chosen before the others can be determined.

One of them may conveniently be the value of the positive HT supply voltage V', as this must be at any rate higher than the anode voltage of the non-conducting tube V_{aIIo}, say by an amount of some ten volts. As the output voltages of conventional HT supply apparatus generally have more or less standardized values, one of these values that best fits the foregoing demand may be chosen.

It is then possible to find from equations (5-7), (5-16), (5-9) and (5-14) explicit expressions for ε_a, ε_g, R_a, R_g and V'' as functions of the known quantities.

Elimination of R_a, R_g and I_{go} from the four equations is possible in the following way. From equations (5-9) and (5-14) $R_a I_{ao}$ and $R_g I_{go}$ can be expressed in terms of ε_g and ε_a and then substituted in equations

(5–7) and (5–16). These equations are then reduced to the following simple forms:

$$\varepsilon_g = (1 - \varepsilon_a)\, (V_{gII_o} + V'') \,/\, (V_{aI_o} + V'') \tag{10–4}$$

$$\varepsilon_a = (1 - \varepsilon_g)\, (V' - V_{aII_o}) \,/\, V' \tag{10–5}$$

From these equations it follows that:

$$\varepsilon_g = V_{aII_o}\,(V_{gII_o} + V'') \,/\, \{ V'\,(V_{aI_o} - V_{gII_o}) + V_{aII_o}\,(V_{gII_o} + V'') \} \tag{10–6}$$

$$\varepsilon_a = (V' - V_{aII_o})\,(V_{aI_o} - V_{gII_o}) \,/\, \{ V'\,(V_{aI_o} - V_{gII_o}) +$$
$$+ V_{aII_o}\,(V_{gII_o} + V'') \} \tag{10–7}$$

As both ε_g and ε_a are ratios of resistances, their values must be positive. This condition leads to another condition with respect to the value of V''. The denominator of both expressions is positive, which can be seen by re-arranging it in the following form: $V'V_{aI_o} + V''V_{aII_o} - V_{gII_o}\,(V' - V_{aII_o})$.

The first two terms are positive; the last one also, because $-V_{gII_o}$ is positive as well as $V' - V_{aII_o}$. The denominator being always positive, it can directly be seen that ε_a is positive, as its numerator is also positive. For ε_g to be positive it is necessary that $V_{gII_o} + V'' > 0$ or $V'' > - V_{gII_o}$. The third ratio of resistances, viz. ε must also be positive. This gives the condition $1 - \varepsilon_a - \varepsilon_g > 0$. Substitution of (10–6) and (10–7) leads to $V_{aII_o}(V_{aI_o} - V_{gII_o}) > 0$, which condition is indeed always fulfilled. From the fact that ε_g, ε_a and ε are all positive it can be concluded that all resistances must have the same sign.

Next R_a can be solved from equation (5–7):

$$R_a = \{ V'\,(V_{aII_o} - V_{aI_o}) - V_{gII_o}\,(V_{aII_o} - V') \} \,/\, I_{ao}\, V_{aII_o} \tag{10–8}$$

From equation (10–3):

$$R_g = R_a \varepsilon_g / \varepsilon_a = (V_{gII_o} + V'')\, \{ V'\,(V_{aII_o} - V_{aI_o}) - V_{gII_o}\,(V_{aII_o} - V') \}/$$
$$/ I_{ao}\,(V' - V_{aII_o})\,(V_{aI_o} - V_{gII_o}) \tag{10–9}$$

As in practice $V' > - V_{gII_o}$ and $V_{aII_o} - V_{aI_o} > V' - V_{aII_o}$, the expressions for R_a and R_g are positive. The value of R can be determined from expr. (10–1) or (10–2), and will be positive, because R_a and R_g are. Finally I_{go} is found from equation (5–14):

$$I_{go} = (V' - V_{aIIo}) \{V_{aIIo} V_{gIIo} + V'' (V_{aIIo} - V_{aIo} + V_{gIIo})\} I_{ao} /$$
$$/ (V_{gIIo} + V'') \{V_{aIIo} (V' - V_{gIIo}) - V' (V_{aIo} - V_{gIIo})\}.$$

From this equation V'' can be expressed in known quantities:

$$V'' = [V_{gIIo} V_{aIIo} (V' - V_{aIIo}) I_{ao} - V_{gIIo} \{V' (V_{aIIo} - V_{aIo}) -$$
$$V_{gIIo} (V_{aIIo} - V')\} I_{go}] / (-(V' - V_{aIIo}) (V_{aIIo} - V_{aIo} + V_{gIIo}) I_{ao} +$$
$$+ \{V' (V_{aIIo} - V_{aIo}) - V_{gIIo} (V_{aIIo} - V')\} I_{go}] \qquad (10\text{--}10)$$

In practice, when designing a multivibrator circuit, one will first have to calculate the value of V'' from expression (10–10). Then check whether V'' is larger than $-V_{gIIo}$, which is necessary for a positive value of ε_g, as shown before. Once V'' is determined the other unknown quantities can be calculated.

A numerical example will be given. Starting from the following given quantities: $V' = 200$ V, $V_{aIo} = 50$ V, $V_{aIIo} = 150$ V, $V_{gIIo} = -20$ V, $I_{ao} = 5$ mA, $I_{go} = 0{,}8$ mA the calculations give the following results:

$V'' = 93$ V, $R_a = 25$ kΩ, $R = 73.5$ kΩ, $R_g = 80$ kΩ.

With the above procedure the static condition is determined and here the capacitances do not come into play. For the dynamic condition, however, the values of the coupling capacitances between anodes and grids and between the trigger-pulse source and grids are of importance. Both trigger sensitivity and speed are influenced by them. At first it would seem to be rather difficult to find a method for straight-forward determination of the optimum values of the coupling capacitors which were termed C and C_c respectively in previous chapters. However, the following reasoning may show that it is possible to derive a certain relation between C and C_c that must be fulfilled to obtain optimum speed and sensitivity. This relation is the following:

$$RC = R_g C_i \qquad (10\text{--}11)$$
or $\qquad T = T_g \qquad (10\text{--}12)$

(see expressions (I–1) and (I–2)) where $Ci = C_c + C_g$, C_g being the total capacitance between grid and cathode. Or in words, the time constant of the coupling circuit between anodes and grids must equal the time constant in the grid circuit. If this relation exists, then the quantities X derived in appendix II will be equal to the quantities Y derived in appendix III, because $D' = T$ according to expression (I–20). In that

case the transient voltage V_{gI}* at the grid of tube I (expr. (III–8)) will be a true copy of the transient anode voltage of tube II (expr. (II–21)), only decreased by a factor $R_g/(R + R_g)$, the transients at A_{II} and G_I from the first phase being of minor importance, because tube II is not yet conducting.

If $T > T_g$ then the shape of V_{gI} will be such that it falls rapidly to a high negative value and then gradually rises to its final value ("over-shoot"; see for example the oscillograms of figs. 7.5 and 7.7, where T was twice the value of T_g). If the next trigger pulse appears at an instant when the grid voltage V_{gI} has not risen sufficiently, then the corresponding tube I may not be brought into the conducting state before tube II has reached this state and then the triggering fails.

In the opposite case, $T < T_g$, (to be called "undershoot") the grid voltage V_{gI} falls to a rather small negative value and then continues to fall with a much smaller slope to its final value. This may seem advantageous for high speed triggering, but the positive-going voltage at grid G_{II} may not reach the cut-off point rapidly enough to achieve proper triggering.

Therefore it is to be expected that the case $T = T_g$ is the most favourable condition for attaining a high triggering speed at a reasonable sensitivity. With these considerations in mind the following procedure for deter-mining the values of the coupling capacitances is recommended. Choose a value of C_c, next a value of C in accordance with condition (10–11) and then calculate the trigger sensitivity as indicated in chapter 8. Should the required minimum trigger pulse amplitude be too high with respect to the available amplitude then C_c and C have to be chosen larger, their ratio remaining unchanged, until the sensitivity is in accordance with the available trigger pulse amplitude. Then one is sure to have the maximum speed obtainable with that sensitivity.

The above statements about the influence of the coupling capacitors on speed and sensitivity have been confirmed by measurements on the circuit mentioned and defined at the beginning of section 8–1. The values of C and C_c in this circuit have been varied. For a large number of combina-tions of these values the trigger sensitivity and the maximum speed have been determined. The results are represented in table VII. The sensitivity is measured at an input pulse repetition frequency of 10 kc/s, well below the lowest maximum speed that ever occurred. It is expressed by the minimum trigger pulse amplitude V_{cr} at that frequency. The speed is expressed in kc/s, being the maximum frequency f_m at which the multi-vibrator still operated correctly as a binary frequency divider when trig-gered at both grids simultaneously by pulses of an amplitude of 30 V.

The maximum pulse frequency available was 200 kc/s; the maximum pulse amplitude 37 V.

Table VII

C_c (pF)	C 30 (pF)		40		50		60		100		120	150
	V_{cr}	f_m	V_{cr}	f_m	V_{cr}	f_m	V_{cr}	f_m	V_{cr}	f_m	V_{cr} f_m	V_{cr} f_m
20	33.5	—	32.5	—	30.0	—	28.0	52	25.5	40		
30	29.5	>200	27.5	>200	24.5	140	23.0	110	20.5	72		
40	29.5	>200	24.5	>200	21.3	>200	20.0	195	17.7	112		
50	>37		25.5	>200	20.5	>200	19.0	>200	16.5	150		
60			>37		20.5	>200	18.5	>200	15.5	175		
70					22.0	>200	18.5	>200				
80					>37	—	18.5	>200				
90							20.0					
100							31.0		11.5	>200		
120									11.5		10,3 192	
150									12.1			9.2 158

From table VII it can be seen that at a fixed value of C the trigger sensitivity shows a maximum at that value of C_c which equals C. Because the values of R and R_g are also the same (200 kΩ), this means that the time constants T and T_g are equal if $C = C_c$.

At a fixed value of C_c the sensitivity increases with increasing value of C, on the other hand the speed decreases.

At a fixed value of C the speed increases with increasing C_c.

At equal values of C and C_c ($T = T_g$) the trigger sensitivity increases with increasing capacitances, whereas the speed decreases. However, the speed will be higher than at $C_c < C$.

Note: The equations governing the static condition allow for the determination of the influence of component and tube tolerances on the stability of this condition. This is not dealt with here, because it has been the subject of several articles, mentioned in chapter 2.

11. VARIATIONS OF THE FUNDAMENTAL CIRCUIT AND WAY OF TRIGGERING

11.1 AUTOMATIC GRID BIAS

Instead of incorporating the separate negative grid bias supply $-V''$ in the multivibrator circuit as shown in fig. 3–1, automatic negative grid bias may be applied by inserting a by-passed cathode resistor in the circuit (see fig. 11–1).

If the time constant of the cathode circuit is sufficiently large, the voltage drop thus produced may be considered as a constant voltage source, at least during the triggering action. This voltage drop depends, however, on the value of the anode current in the static condition. The foregoing considerations and formulae derived from them may be used in analysing the circuit of fig. 11–1 as long as it is kept in mind that
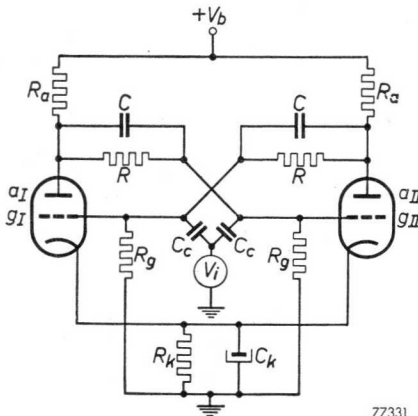

Fig. 11–1

$$V'' = R_k I_{ao} \qquad (11\text{–}1)$$

and

$$V' = V_b - R_k I_{ao} \qquad (11\text{–}2)$$

In these expressions the influence of the grid current I_{go}, that also flows through R_k, has been neglected with respect to the anode current I_{ao}.

In the static condition the voltages at the grids and anodes must be taken with respect to the cathode. Their values with respect to earth will be larger by an amount $R_k I_{ao}$.

For the transient voltages it does not matter whether they refer to cathode or to earth as it is assumed that the value of the by-pass capacitor is such that it represents a short-circuit for these transients.

11.2 TRIGGER PULSES APPLIED TO ONE GRID ONLY

As already mentioned in the introduction, the triggering may be produced either by applying pulses to the grids of both tubes simultaneously, or by applying pulses to the grids of tube I and tube II alternately.

The first method is used for instance in frequency-division circuits: one multivibrator circuit will halve the input pulse frequency. The second method is used for instance in those circuits that are used to open or close

gates. When negative pulses are only applied to the grid of the conducting tube, the circuit operation can be analysed in an analogous way to the methods of the previous chapters.

If, for instance, in the circuit of fig. 3–1 only a negative-going voltage is applied to the grid of tube I, that is assumed to be conducting, then it will be clear that in fig. 6–2 the current source I_i must be omitted. Consequently, during the first phase of the dynamic condition the voltage at grid G_{II} will be represented by the following expression instead of by expression (I–36):

$$V_{gII}(t) = V_{gIIo} + I_{ao}\,\varepsilon_a\,R_g\,\{1 - \tfrac{1}{2}(1 - P)\,e^{p_1 t} - \tfrac{1}{2}(1 + P)\,e^{p_2 t}\}\,U(t)$$

$$(11\text{–}3)$$

and the voltage at A_I by

$$V_{aI}(t) = V_{aIo} + I_{ao}(1 - \varepsilon_a)\,R_a\,\{1 - \tfrac{1}{2}(1 - L)\,e^{p_1 t} - \tfrac{1}{2}(1 + L)\,e^{p_2 t}\}\,U(t)$$

$$(11\text{–}4)$$

instead of by expression (I–40).

The voltages at G_I and A_{II} remain the same as those represented by expressions (I–42) and (I–44), respectively.

Referring to expressions (6–15) to (6–26) inclusive, the changes can also be indicated in the following way:

$V_1, V_4, V_5, V_6, V_7, V_{10}, V_{11}, V_{12}$ remain unchanged

$$V_2 = -\tfrac{1}{2}\,I_{ao}\varepsilon_a\,R_g\,(1 - P) \tag{11–5}$$

$$V_3 = -\tfrac{1}{2}\,I_{ao}\,\varepsilon_a\,R_g\,(1 + P) \tag{11–6}$$

$$V_8 = -\tfrac{1}{2}\,I_{ao}\,(1 - \varepsilon_a)\,R_a\,(1 - L) \tag{11–7}$$

$$V_9 = -\tfrac{1}{2}\,I_{ao}\,(1 - \varepsilon_a)\,R_a\,(1 + L) \tag{11–8}$$

When introducing these values in the formulae given in chapter 6, the grid and anode voltages during the complete dynamic condition can be evaluated.

One of the results of this single-grid triggering will be that the trigger sensitivity is increased, since the positive-going voltage at grid II originating from the rising voltage at anode I is no longer counteracted by the negative input-voltage pulse at grid II, as in the case of double-grid triggering. Thus, the cut-off grid voltage of tube II will be attained sooner.

12. SOME ACTUAL BISTABLE MULTIVIBRATOR CIRCUITS

In this chapter a few actual bistable multivibrator circuits are presented, ranging from the simplest type to a complicated one which enables high-speed operation up to 20 Mc/s.

12.1. BISTABLE MULTIVIBRATOR FOR MAXIMUM TRIGGER PULSE FREQUENCY OF 200 Kc/s

This multivibrator is equipped with the double-triode type E 90 CC and is basically equivalent to the circuit of fig. 3–1, only the negative supply voltage source V'' is replaced by an automatic grid-bias source as represented in fig. 12–1. The circuit diagram in fig. 12–1 shows a cascade of four stages. The special method of coupling between the different stages results in a decimal counter, which is shown schematically in fig. 12–2. Decimal indication of the position of the counter is by means of ten neon lamps (0 to 9) and a resistance network R_9, R_{10}.
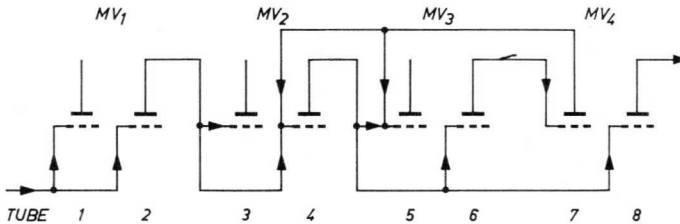
Fig. 12–2

The counter can be reset manually to the zero position by pressing push-button R (at bottom right in fig. 12–1).

Because the operation of neon lamps necessitates rather high voltage swings at the anodes of the tubes, high values of anode resistances had to be used so restricting the maximum operating speed to 200 kc/s.

Specification

> Tubes: E90CC   Neon lamps: Philips Z8
> Voltages:

supply voltage	200	V D.C. at 46 mA
anodes of conducting tubes	67	V
grids of conducting tubes	36	V
anodes of non-conducting tubes	161	V
grids of non-conducting tubes	16	V
cathodes	36	V
heater supply		6.3 V A.C. at 1.6 A
voltage across R_8 with reset-button pressed		approx. 25 V

Fig. 12-1

Output voltage approx. 50 V:

negative with rise time of approx. 1.5 μsec at count of zero,
positive with rise time of approx. 4 μsec at count of four.

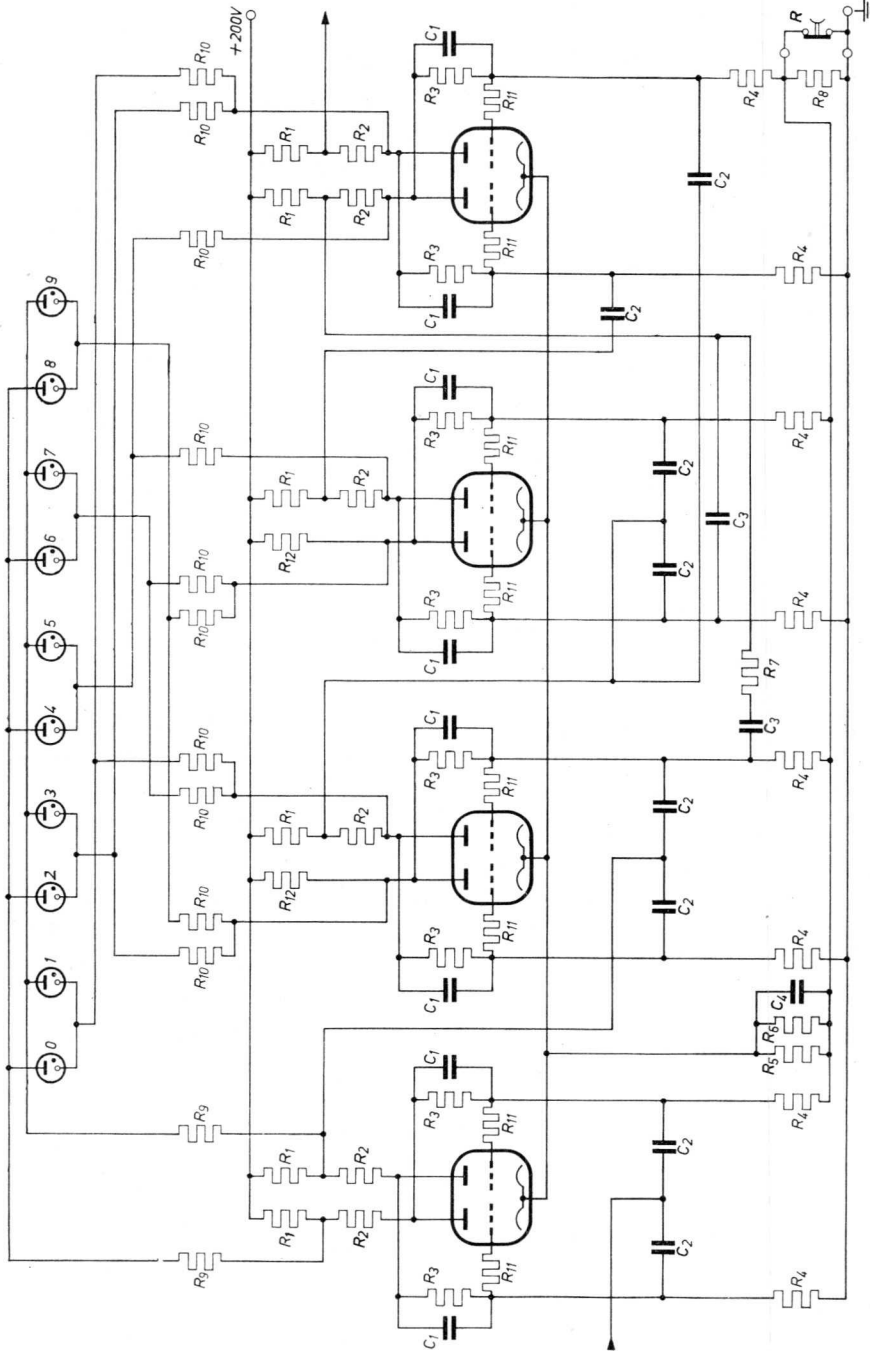Input signal requirements: the decade responds to negative-going voltage excursions of at least 35 V with a rise time of less than 1.5 μsec. In order to ensure that the decade does not respond to positive-going voltage excursions the amplitude of the input signal should be less than 70 V. Max. input repetition frequency: 200 kc/s.

Component values:

R_1	8.2 kΩ	2%	1 W	R_9	220 kΩ	5%	$\frac{1}{2}$ W
R_2	6.8 kΩ	2%	1 W	R_{10}	470 kΩ	5%	$\frac{1}{2}$ W
R_3	47 kΩ	1%	$\frac{1}{2}$ W	R_{11}	1 kΩ	10%	$\frac{1}{2}$ W
R_4	15 kΩ	1%	$\frac{1}{8}$ W	C_1	82 pF	5%	
R_5	1.2 kΩ	2%	2 W	C_2	33 pF	5%	
R_6	22 kΩ	10%	$\frac{1}{2}$ W	C_3	68 pF	5%	
R_7	10 kΩ	10%	$\frac{1}{2}$ W	C_4	0.01 μF	10%	
R_8	680 kΩ	10%	1 W				

12.2. BISTABLE MULTIVIBRATOR FOR INPUT PULSE FREQUENCY UP TO 1 Mc/s

Replacing the input coupling capacitances (C_2 of fig. 12–1) by diodes increases the speed of a bistable multivibrator. This is because the time-constant in the grid circuit is lowered so allowing a lower coupling network time constant (CR in fig. 11–1). A reduction in any time constant in the circuit results in a higher trigger speed as is shown in chapter 9. Moreover, the input coupling diodes result in better discrimination between possitive and negative input trigger pulses and have a steering effect in that they bring the negative-going pulse exactly to the grid of the conducting tube and keep it far from the grid of the cut off tube. This improves the trigger sensitivity of the multivibrator as suggested in section 2 of Chapter 11.

This circuit also uses E90CC tubes, but because of the changes mentioned it attains a maximum triggering speed of 1 Mc/s. Its circuit diagram can be taken from fig. 12–3, which represents a decade counter containing neon lamp position indicators.

One germanium diode is used in the first stage. Its purpose is to cut off the positive pulses that would result after differentiation of the incoming signal. Because of this diode the sensitivity remains practically constant up to 1 Mc/s.

Point R in the circuit of fig. 12.3 is normally connected to earth via an external push-button switch. The decade can be reset to the zero position by momentarily disconnecting point R from earth. In this way all the right-hand sections of the double triodes become conducting.

Specification

Tubes: E90CC and EB91.
Neon lamps: Philips Z8.
Germanium diode: OA73.

Voltages:

supply voltage	200	V D.C. at 68 mA
anodes of conducting tubes	84	V
grids of conducting tubes	30	V
anodes of non-conducting tubes	183	V
grids of non-conducting tubes	15	V
cathodes	30	V
heater supply		6.3 V A.C. at 3.1 A
voltage across R_8 with reset-button pressed	approx. 25 V	

Output voltage approx. 45 V:

negative with rise time of approx. 1 μsec at count of zero,
positive with rise time of approx. 2 μsec at count of four.

Input signal requirements: the decade responds to negative-going voltage excursions of at least 25 V with a rise time of less than 0.2 μsec. Max. input repetition frequency: 1 Mc/s.

Component values:

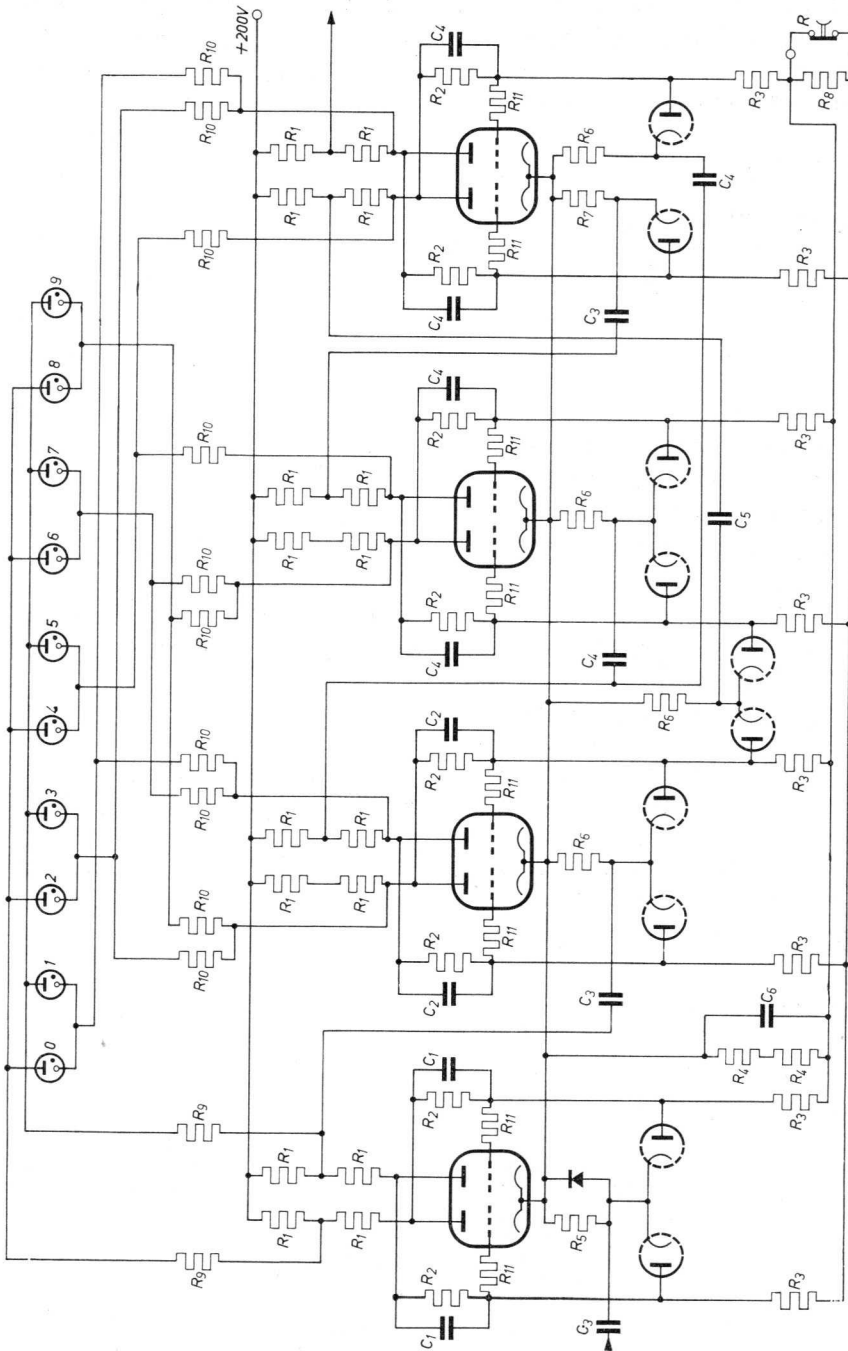|								
R_1	3.9 kΩ	2%	2 W		R_{10}	470 kΩ	5%	$\frac{1}{2}$ W
R_2	68 kΩ	1%	$\frac{1}{2}$ W		R_{11}	1 kΩ	10%	$\frac{1}{2}$ W
R_3	15 kΩ	1%	$\frac{1}{8}$ W		C_1	15 pF	5%	
R_4	270 Ω	2%	2 W		C_2	18 pF	5%	
R_5	3.3 kΩ	10%	$\frac{1}{2}$ W		C_3	22 pF	5%	
R_6	10 kΩ	10%	$\frac{1}{2}$ W		C_4	33 pF	5%	
R_7	33 kΩ	10%	$\frac{1}{2}$ W		C_5	68 pF	5%	
R_8	470 Ω	10%	$1\frac{1}{4}$ W		C_6	0.01 μF	10%	
R_9	220 kΩ	5%	$\frac{1}{2}$ W					

Fig. 12-3

It should be noted that the 200 kc/s decade described in the preceding section can be driven by this 1 Mc/s decade.

When several decades are combined in a counter their reset push buttons can be combined in one, the points R of each decade being connected to this switch.

In the above circuits, variations of $\pm$ 10% in the anode supply voltage and of $\pm$ 5% in the heater supply voltage are allowed.

12.3. Bistable multivibrator for 7 Mc/s maximum input pulse frequency

By making use of the special high-speed switching double-triode type E88CC and dispensing with the neon-lamp indicators a multivibrator with a higher switching speed can be obtained. Its circuit diagram can be taken from fig. 12–4.

This figure again represents a decade counter composed of four binary stages with the same type of coupling and feedback between various stages as used in the two counters in sections 12–1 and 12–2. The reset is slighty different from that of the preceding counters (see position of push-button R in fig. 12–4).

In addition, peaking coils L_1, L_2 and L_3 are incorporated in the anode circuits of stages one and two to give steeper flanks to the voltage swings at these anodes. The indication system makes use of a specially developed small cathode-ray tube, type DM 160, that gives a brilliant green fluorescent light when fully conducting and is dark as soon as only a few volts at negative potential are applied between grid and cathode.

The indication is now in a binary coded decimal form, in such a way that the sum of the numbers (indicated beside each indicator tube in fig. 12–4), of the glowing tubes represents the decimal number indicating the position of the counter. For instance, when tubes 1 and 4 are indicating, the counter is in position 5.

When four of these types of multivibrator are connected simply in cascade to give a counter of sixteen, the maximum input trigger-pulse repetition frequency at which the counter operates satisfactorily is 7 Mc/s. When combined with a decimal counter in the way indicated by fig. 12–4 this maximum frequency is reduced to 5 Mc/s because of the action of feedback.

Specification
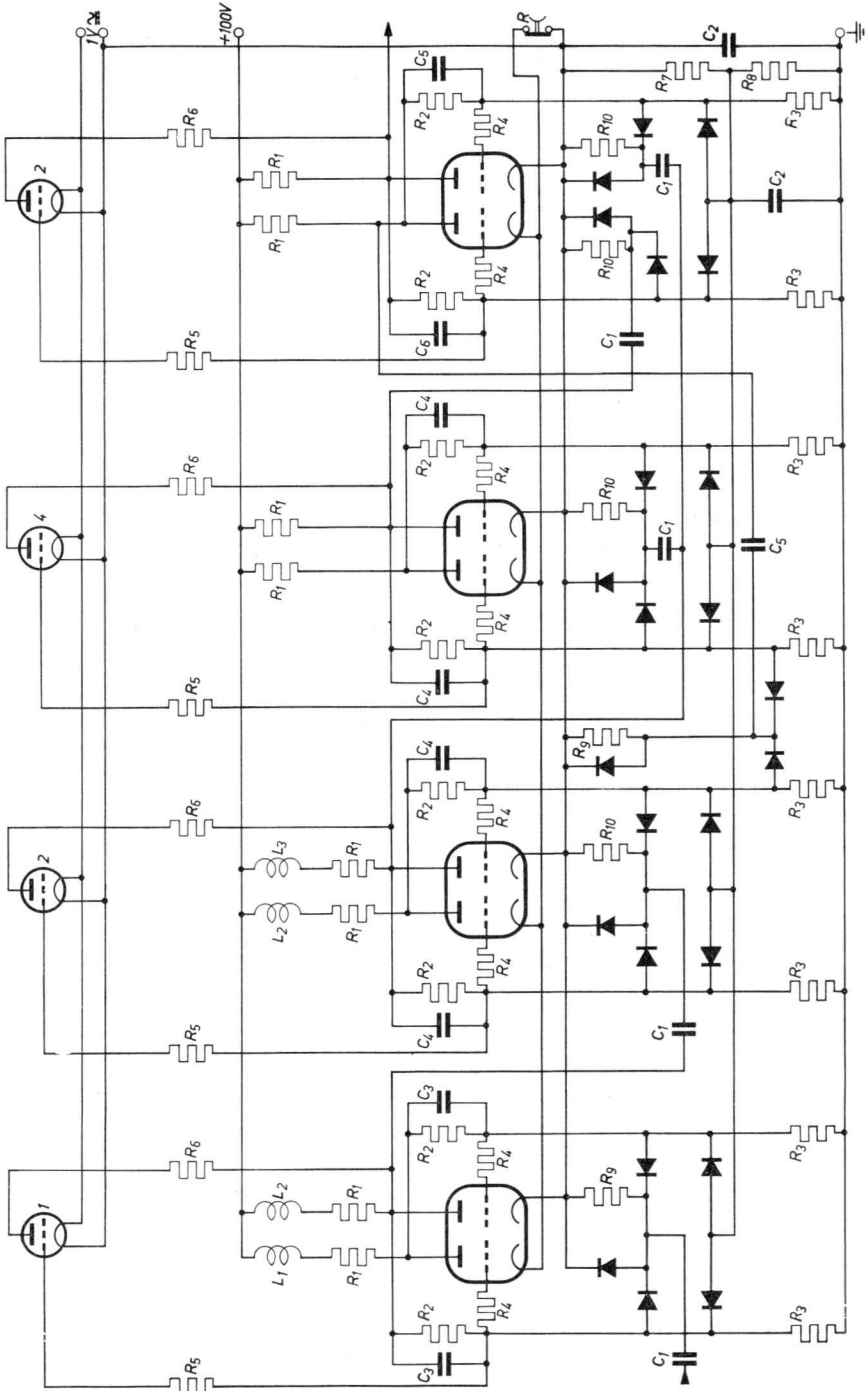
Tubes: E88CC and DM160.
Germanium diodes: OA71.

Fig. 12-4

Voltages:

supply voltage	100 V D.C. at 68 mA
anodes of conducting tubes	79 V
grids of conducting tubes	38 V
anodes of non-conducting tubes	96 V
grids of non-conducting tubes	32 V
cathodes	38 V
Heaters and filaments E88CC	6.3 V A.C. at 1.2 A
DM160	1 V A.C. or D.C. at 0.12 A

Output voltage approx. 17 V:

negative at count of zero with "rise-time" of approx. 0.3 μsec

positive at count of four with "rise-time" of approx. 0.5 μsec

The stage responds to negative-going input voltage excursions of about 12 V with a rise time of about 0.05 μsec.

The capacitive load at the output of the stages should not exceed 22 pF.

The supply voltage need not be stabilized.

Component values:

R_1	1.5 kΩ	2%	$\frac{1}{2}$ W	L_1	30 μH		
R_2	22 kΩ	1%	$\frac{1}{4}$ W	L_2	50 μH		
R_3	15 kΩ	1%	$\frac{1}{4}$ W	L_3	100 μH		
R_4	220 Ω	10%	$\frac{1}{2}$ W				
R_5	1 MΩ	10%	$\frac{1}{2}$ W	C_1	22 pF	5%	
R_6	100 kΩ	10%	$\frac{1}{2}$ W	C_2	0.01 μF	10%	
R_7	56 Ω	5%	1 W				
R_8	120 Ω	2%	$\frac{1}{2}$ W	C_3	27 pF	5%	
R_9	680 Ω	2%	3 W	C_4	47 pF	5%	
R_{10}	1 kΩ	10%	$\frac{1}{2}$ W	C_5	68 pF	5%	
R_{11}	2.2 kΩ	10%	$\frac{1}{2}$ W	C_6	100 pF	5%	

12.4. MULTIVIBRATOR WITH HIGH DC STABILITY AND HIGH SPEED

Another multivibrator circuit with the double-triode E88CC has been designed in which a high standard of DC stability has been imposed. At the same time a high trigger speed for a decimal counter composed of these multivibrators has been attained by using an extra amplifier stage between the first and the second multivibrators. The circuit diagram is represented in fig. 12–5.

The supply voltages amount to 85 V at 32.2 mA current drain for the anodes, and —65 V at 11.8 mA current drain for the grids; tolerances
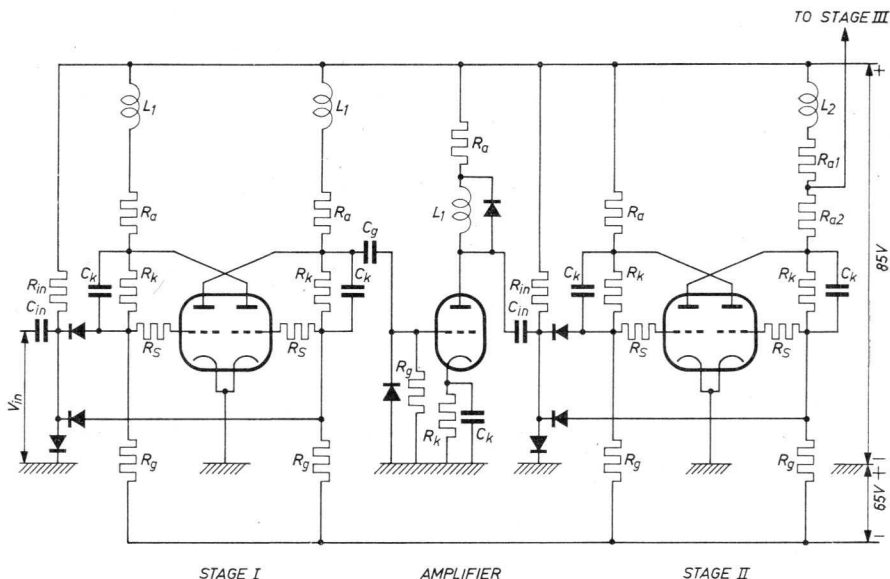
Fig. 12–5. Stages III and IV are identical to stage II exept that L_2 can be omitted.

Specification

Tubes: E88CC

Germanium diodes: OA85

Component values

First multivibrator

R_a	1.8 kΩ	$\pm$	2%	1 W
R_k	10 kΩ	$\pm$	2%	$\frac{1}{2}$ W
R_g	10 kΩ	$\pm$	2%	$\frac{1}{2}$ W
R_s	220 Ω	$\pm$	20%	$\frac{1}{4}$ W
R_{in}	39 kΩ	$\pm$	10%	$\frac{1}{4}$ W
C_k	15 pF	$\pm$	10%	
C_{in}	47 pF	$\pm$	10%	
L_1	25 μH	$\pm$	10%	

Amplifier

R_a	1.5 kΩ	$\pm$	10%	$\frac{1}{2}$ W
R_k	680 Ω	$\pm$	10%	$\frac{1}{2}$ W
R_g	100 kΩ	$\pm$	10%	$\frac{1}{4}$ W
C_k	330 pF	$\pm$	10%	
C_g	47 pF	$\pm$	10%	
L_1	50 μH	$\pm$	10%	

Second multivibrator

R_{a1}	1 kΩ	$\pm$	2%	1 W
R_{a2}	820 Ω	$\pm$	2%	$\frac{1}{2}$ W
R_k	10 kΩ	$\pm$	2%	$\frac{1}{2}$ W
R_g	10 kΩ	$\pm$	2%	$\frac{1}{2}$ W
R_s	220 Ω	$\pm$	20%	$\frac{1}{4}$ W
R_{in}	39 kΩ	$\pm$	10%	$\frac{1}{4}$ W
C_k	27 pF	$\pm$	10%	
C_{in}	56 pF	$\pm$	10%	
L_2	15 μH	$\pm$	10%	

Third and fourth multivibrator

R_{a1}	1 kΩ	$\pm$	2%	1 W
R_{a2}	820 Ω	$\pm$	2%	$\frac{1}{2}$ W
R_k	10 kΩ	$\pm$	2%	$\frac{1}{2}$ W
R_g	10 kΩ	$\pm$	2%	$\frac{1}{2}$ W
R_s	220 Ω	$\pm$	20%	$\frac{1}{4}$ W
R_{in}	39 kΩ	$\pm$	10%	$\frac{1}{4}$ W
C_k	27 pF	$\pm$	10%	
C_{in}	68 pF	$\pm$	10%	
L_2	15 μH	$\pm$	10%	

of $\pm$ 2 V are allowed in these voltages without upsetting the operation of the counter over the whole frequency range from zero up to 13 Mc/s. At the maximum input frequency of 13 Mc/s the tolerance in the input pulse is very tight, but at 11.5 Mc/s it allows up to 13 V to 16 V variation in amplitude.

The shape of the inputpulse should preferably be an almost perfect square-wave with flank rise-times of about 10 millimicroseconds, and an amplitude of 14.5 V. Tolerances in the components are indicated in the parts list.

The final (fourth) stage of the multivibrator chain can be loaded at the maximum trigger frequency with a resistive load of 1.5 kΩ between anode and the positive HT line, with a resistive load of 13 kΩ between anode and cathode and a capacitive load of 82 pF between anode and cathode.

12.5. 18 Mc/s BISTABLE MULTIVIBRATOR

The design of the bistable multivibrator described in this section aimed at attaining the highest possible speed of triggering. For this an auxiliary circuit is introduced, thus making the multivibrator depart considerably from the basic principle upon which it is normally based and which has been the object of the analysis given in this book.

The high speed has been attained by making use of an extra feedback between the anode of one tube and the grid of the other. This feedback is obtained by using a transformer as the coupling element. Its windings are in a closed pot-core, type 14/8, made of a ferrite material, called Ferroxplana, which has excellent high frequency properties (low losses). This greatly contributes to the speeding up of the switching processes.

The circuit diagram of the multivibrator is in fig. 12–6. This also shows that a cathode-follower stage is necessary to couple one stage to the next. This is mainly for the purpose of reducing the load on the output of the first stage ($T_1 \ldots T_6$ represent the Ferroxplana pot-core transformers). Clamping the grid potential to a certain negative voltage level $-$V also helps in improving the speed. The resistors in series with the speed-up capacitors improve the positive-going flank of the anode voltages.

The maximum trigger speed of a single multivibrator stage is slightly over 20 Mc/s, whilst the maximum frequency of several stages coupled together is between 18 and 19 Mc/s.

The trigger pulses at the input of the first stage are negative-going and
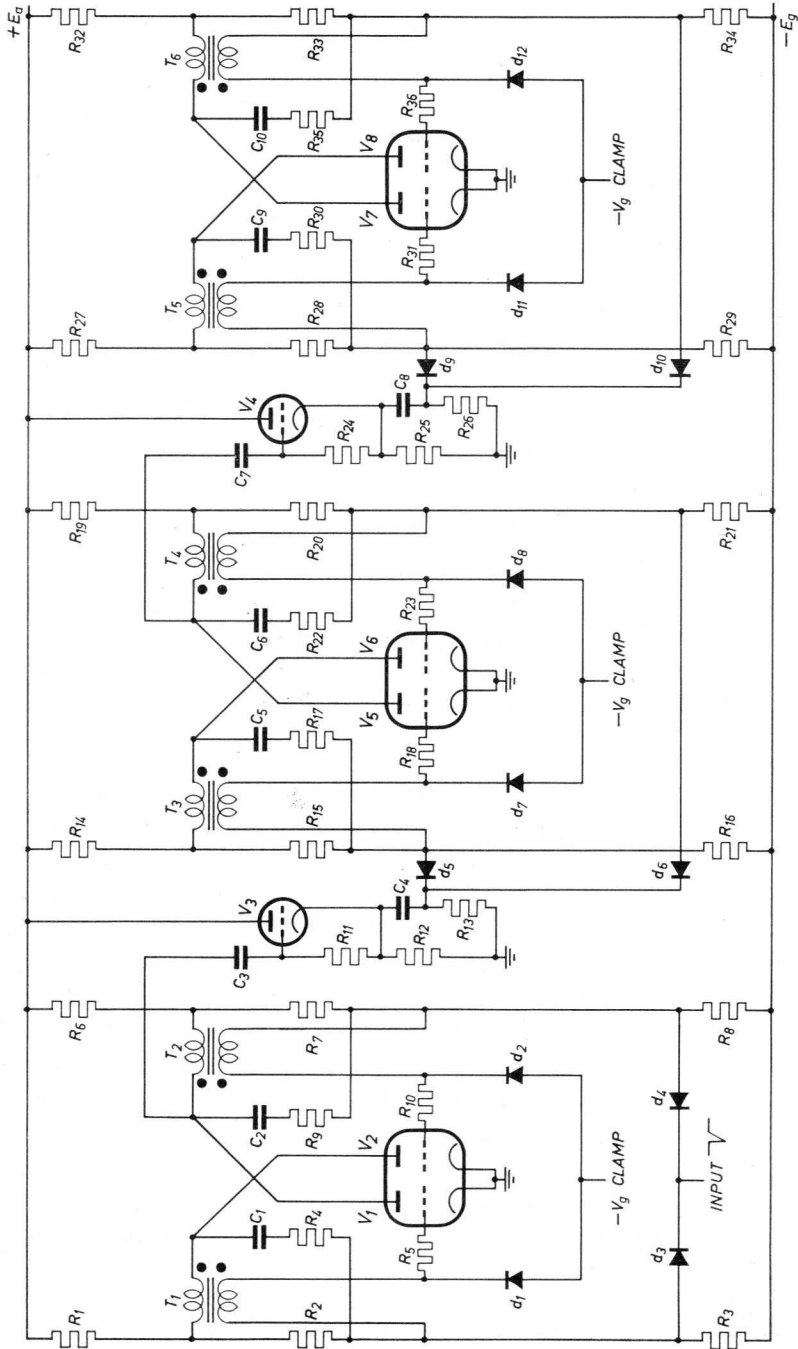
Fig. 12-6

nearly triangular shaped, with a base width of about 20 millimicroseconds and an amplitude of preferably 4 to 5 V.

Further details of the circuit can be found in the following specification.

Specification

Tubes E88CC

Germanium diodes OA9.

Component values.

R_1	820	Ω	1 W	10%	R_{19}	820	Ω	1 W	10%
R_2	47	kΩ	$\frac{1}{4}$ W	2%	R_{20}	47	kΩ	$\frac{1}{4}$ W	2%
R_3	47	kΩ	$\frac{1}{4}$ W	2%	R_{21}	47	kΩ	$\frac{1}{4}$ W	2%
R_4	4.7	kΩ	$\frac{1}{2}$ W	10%	R_{22}	4.7	kΩ	$\frac{1}{2}$ W	10%
R_5	470	Ω	$\frac{1}{2}$ W	10%	R_{23}	470	Ω	$\frac{1}{2}$ W	10%
R_6	820	Ω	1 W	10%	R_{24}	1	MΩ	$\frac{1}{2}$ W	10%
R_7	47	kΩ	$\frac{1}{4}$ W	2%	R_{25}	1.5	kΩ	1 W	10%
R_8	47	kΩ	$\frac{1}{4}$ W	2%	R_{26}	2.7	kΩ	1 W	10%
R_9	4.7	kΩ	$\frac{1}{2}$ W	10%	R_{27}	820	Ω	1 W	10%
R_{10}	470	Ω	$\frac{1}{2}$ W	10%	R_{28}	47	kΩ	$\frac{1}{4}$ W	2%
R_{11}	1	MΩ	$\frac{1}{2}$ W	10%	R_{29}	47	kΩ	$\frac{1}{4}$ W	2%
R_{12}	1.5	kΩ	1 W	10%	R_{30}	4.7	kΩ	$\frac{1}{2}$ W	10%
R_{13}	2.7	kΩ	1 W	10%	R_{31}	470	Ω	$\frac{1}{2}$ W	10%
R_{14}	820	Ω	1 W	10%	R_{32}	820	Ω	1 W	10%
R_{15}	47	kΩ	$\frac{1}{4}$ W	2%	R_{33}	47	kΩ	$\frac{1}{4}$ W	2%
R_{16}	47	kΩ	$\frac{1}{4}$ W	2%	R_{34}	47	kΩ	$\frac{1}{4}$ W	2%
R_{17}	4.7	kΩ	$\frac{1}{2}$ W	10%	R_{35}	4.7	kΩ	$\frac{1}{2}$ W	10%
R_{18}	470	Ω	$\frac{1}{2}$ W	10%	R_{36}	470	Ω	$\frac{1}{2}$ W	10%

C_1	18 pF	10%	cer.	C_6	18 pF	10%	cer.
C_2	18 pF	10%	cer.	C_7	100 pF	10%	cer.
C_3	100 pF	10%	cer.	C_8	27 pF	10%	cer.
C_4	27 pF	10%	cer.	C_9	18 pF	10%	cer.
C_5	18 pF	10%	cer.	C_{10}	18 pF	10%	cer.

$T_{1, 2, 3, 4, 5, 6}$ = Ferroxplana potcore 14/8

2×10 turns bifilar wound, 0.15 mm copper silk enamelled, no airgap

$+ E_a$ = 85 V

$- E_g$ = 77 V

$- V_{g\ clamp}$ = 6.2 V

I_a per triode while conducting 20 mA

I_{Ea} = 110 mA

I_{Eg} = 15 mA

13. CONCLUSION

It has been shown in the previous chapters that it is possible to analyse the operation of a bistable multivibrator. An attempt has been made to approach as nearly as possible practical circumstances. However, some assumptions are unavoidable in order to keep the results practicable. It will be good to summarize here the restrictions under which the results obtained are valid.

The shape of the trigger voltages, applied to the grids is taken to be trapezoidal, only the influence of the negative going front flank being considered (see fig. 3–2). The choice of this special shape is thought to be a reasonable approximation to practical pulse shapes and offers the advantage that the input voltage source is readily converted into an input current source, giving a rectangular current pulse, for which the response of the network is relatively easy to calculate. It is, however, quite possible to calculate the response to another kind of voltage function, for instance an exponential time function, but it would complicate the calculation without necessarily being a better approximation to practice. The influence of the positive going rear flank of the input voltage is not calculated, though it could also be done. In chapter 7 it is argued that the influence of this rear flank is not very important and in general does not endanger the correct operation of the trigger.

The amplitude V_o of the trigger voltage and the slope a of the negative going front flank are taken to be so large, that the time taken to cut off the conducting tube is negligibly small compared with the inherent time constants of the circuit, in other words this tube is assumed to be instantaneously cut off. Again this is thought to be a good approximation to general practice, but it is also possible to take into consideration a finite time for cutting off the conducting tube. This would of course considerably complicate the calculation.

The voltage between the grid and cathode of the conducting tube is taken to be zero, which is very nearly attained when this tube draws grid current. It means that at grid-to-cathode voltages of zero or positive values the internal grid resistance is very small. A better approximation to practice would be to take into account a finite internal resistance between grid and cathode, involving again more complicated calculations. Next, a few assumptions are introduced that make it possible to separate the multivibrator into two parts which do not influence one another. The first assumption made is that the internal resistances of the supply voltage and trigger voltage sources can be neglected. This is thought

to be admissible in most practical cases, especially for the supply voltage sources when these are stabilized. For the trigger voltage source it will usually be a necessary condition to have a low internal resistance as it is loaded with the low internal grid-to-cathode resistance of the conducting tube.

In the second place the influence of the capacitance between the anode and grid of each tube is not taken into account when calculating the waveforms of the voltage changes at the anodes and grids of the tubes. It is theoretically possible to include these capacitances in the circuit to be analysed, but impracticably complicated calculations would result. In the first phase of the dynamic condition, when both tubes are non-conducting, an approximative method of taking into account these capacitances is used in the calculation of the trigger sensitivity.

All other tube, wiring and stray capacitances can be included in the analysis.

With the foregoing assumptions and restrictions it is possible to analyse completely the static and transient conditions of a triggered bistable multivibrator. The waveforms of the voltage changes at the anodes and grids of the tubes can be determined when a trigger pulse applied to both grids simultaneously or to only one grid at a time causes the circuit to switch over from one static condition to the other. The dynamic condition can be divided in three successive phases with transients occurring at the commencement of each phase.

The analysis also enables the calculation of the trigger sensitivity and determination of the influence of tube characteristics, circuit components and trigger pulse shape on the sensitivity.

As the time constants determining the shape of the transient time functions are known from the analysis, an idea of the maximum triggering speed can be obtained. An actual calculation of this speed is not possible from the analysis, as one of the assumptions has been that the circuit is completely at rest at the instant a trigger pulse appears. At high pulse repetition frequencies this condition is not fulfilled.

Moreover, experiments reveal that the speed increases with the amplitude of the trigger pulse, which would make it still more difficult to give an exact definition of the speed.

Calculated waveforms and trigger sensitivity agree very well with measurements on practical circuits.

A chapter has been added in which the results of some actual multivibrator circuits are dealt with. In general a chain of multivibrators in cascade is formed from the fundamental circuit and used as a decimal counter

stage with the aid of suitable feedback. If the latter is not applied, a binary counter results. It will be clear that each separate multivibrator can be used, for instance, as a voltage level switch able to operate gates in logic circuits. These find many applications in data-handling systems, computers, control systems and the like.

Appendix I. Calculation of the anode- and grid voltages in the first phase

(a) The impedance between G_{II} and earth (see fig. 6–2).
Indicating the impedance of R_g and C_{iII} in parallel by Z_{gII}, the impedance of R and C in parallel by Z, the impedance of R_a and C_{aI} in parallel by Z_{aI}, and denoting the time constants by

$$R_g C_{iII} = T_{gII} \tag{I-1}$$

$$RC = T \tag{I-2}$$

$$R_a C_{aI} = T_{aI} \tag{I-3}$$

the expressions for the impedances become:

$$Z_{gII} = R_g \frac{1}{1 + T_{gII}\, p} \tag{I-4}$$

$$Z = R \frac{1}{1 + T\, p} \tag{I-5}$$

$$Z_{aI} = R_a \frac{1}{1 + T_{aI}\, p} \tag{I-6}$$

The impedance between G_{II} and earth will be:

$$Z_{igII} = \frac{Z_{gII}\, (Z + Z_{aI})}{Z_{gII} + Z + Z_{aI}} =$$

$$\frac{R_g \{R\, (1 + T_{aI}p) + R_a\, (1 + Tp)\}}{R_g\, (1 + Tp)\, (1 + T_{aI}p) + R\, (1 + T_{gII}p)\, (1 + T_{aI}p) + R_a\, (1 + Tp)\, (1 + T_{gII}p)}$$

The expression for Z_{igII} is of the form

$$Z_{igII} = (1 - \varepsilon_g)\, R_g \frac{1 + Ap}{1 + Bp + Ep^2}. \tag{I-7}$$

where ε_g is given by expression (5–6).

$$A = \frac{RT_{aI} + R_a T}{R + R_a} \tag{I-8}$$

$$B = \varepsilon_g\, (T + T_{aI}) + \varepsilon\, (T_{gII} + T_{aI}) + \varepsilon_a\, (T_{gII} + T) \tag{I-9}$$

where ε_a is given by expression (5–3)

$$\varepsilon = 1 - \varepsilon_g - \varepsilon_a = \frac{R}{R_g + R + R_a} \tag{I-10}$$

and

$$E = \varepsilon_g \, T \, T_{aI} + \varepsilon \, T_{gII} \, T_{aI} + \varepsilon_a \, T_{gII} \, T. \tag{I-11}$$

It will be clear that the expression for the impedance Z_{igI} between G_I and earth (see fig. 6–3) has a form similar to that of expression (I–7), in which only the indices I and II have to be interchanged and where

$$T_{gI} = R_g C_{iI} \tag{I-12}$$

$$T_{aII} = R_a C_{aII}. \tag{I-13}$$

(b) The transfer impedance Z_{aIgII} will be:

$$Z_{aIgII} = \frac{Z_{gII} Z_{aI}}{Z_{gII} + Z + Z_{aI}} \tag{I-14}$$

or

$$Z_{aIgII} = \varepsilon_a R_g \frac{1 + T p}{1 + B p + E p^2} \tag{I-15}$$

(c) The transfer impedance Z_{gIIaI} is equal to Z_{aIgII}:

$$Z_{gIIaI} = Z_{aIgII}. \tag{I-16}$$

In the same way it holds, for the circuit of fig. 6–3, that

$$Z_{gIaII} = Z_{aIIgI}. \tag{I-17}$$

(d) The impedance Z_{iaI} between A_I and earth is:

$$Z_{iaI} = \frac{Z_{aI} (Z + Z_{gII})}{Z_{gII} + Z + Z_{aI}} \tag{I-18}$$

$$Z_{iaI} = (1 - \varepsilon_a) \, R_a \frac{1 + D p}{1 + B p + E p^2}, \tag{I-19}$$

where

$$D = \frac{R \, T_{gII} + R_g \, T}{R + R_g}. \tag{I-20}$$

The voltages at the anodes and grids will now be calculated.

(1) The voltage between G_{II} and earth (fig. 6–2).
This voltage will be:

$$V_{gII} (t) = V_{gIIo} + Z_{igII} I_i + Z_{gIIaI} I_a \tag{I-21}$$

V_{gIIo} is given by expression (5–7):

$$Z_{igII} I_i = Z_{igII} [-a\, C_c \{U(t) - U(t - t_o)\}] \qquad (I\text{--}22)$$

$$\text{(see expression 6--7)}$$

$$Z_{gIIaI} I_a = Z_{gIIaI} I_{ao} U(t) \qquad (I\text{--}23)$$

The expression for Z_{igII} and Z_{gIIaI} can be split up into partial fractions.

$$Z_{igII} = \frac{(1 - \varepsilon_g)\, R_g}{E\,(p_1 - p_2)} \left[-\left(\frac{1}{p_1} + A\right)\frac{-p_1}{p - p_1} + \left(\frac{1}{p_2} + A\right)\frac{-p_2}{p - p_2} \right] \qquad (I\text{--}24)$$

Where

$$p_1 = -\frac{B}{2E}\left\{1 - \sqrt{1 - \frac{4E}{B^2}}\right\} \qquad (I\text{--}25)$$

$$p_2 = -\frac{B}{2E}\left\{1 + \sqrt{1 - \frac{4E}{B^2}}\right\}. \qquad (I\text{--}26)$$

p_1 and p_2 will both be negative, real quantities, as the network of fig. (6–2) contains only capacitances and resistances.
A unit current step applied to an impedance

$$Z(p) = \frac{a}{p + a} \qquad (I\text{--}27)$$

will cause a voltage across this impedance

$$V(t) = (1 - e^{-at})\, U(t) \qquad (I\text{--}28)$$

This will be expressed by the following notation:

$$Z(p)\, U(t) \equiv (1 - e^{-at})\, U(t) \qquad (I\text{--}29)$$

Applying this transformation to expression (I–24) gives

$$Z_{igII}\, U(t) \equiv \frac{(1 - \varepsilon_g)\, R_g}{E\,(p_1 - p_2)} \left[-\left(\frac{1}{p_1} + A\right)(1 - e^{p_1 t}) + \left(\frac{1}{p_2} + A\right)(1 - e^{p_2 t}) \right] U(t)$$

This can be rearranged and finally written:

$$Z_{igII}\, U(t) \equiv (1 - \varepsilon_g)\, R_g \left[1 - \tfrac{1}{2}(1 - K)\, e^{p_1 t} - \tfrac{1}{2}(1 + K)\, e^{p_2 t}\right] U(t), \quad (I\text{--}30)$$

where

$$K = \frac{2A - B}{B\sqrt{1 - 4E/B^2}} \qquad (I\text{--}31)$$

Now, expression (I–22) can be evaluated, remembering that the response to a unit-step function $U(t-t_o)$ is the same as that to a unit-step function $U(t)$, provided the time scale is shifted by replacing t by $t-t_o$. Thus:

$$Z_{igII} I_i = -a C_c (1-\varepsilon_g) R_g [\{1 - \tfrac{1}{2}(1-K) e^{p_1 t} - \tfrac{1}{2}(1+K) e^{p_2 t}\} U(t) -$$
$$- \{1 - \tfrac{1}{2}(1-K) e^{p_1(t-t_o)} - \tfrac{1}{2}(1+K) e^{p_2(t-t_o)}\} U(t-t_o) \qquad (I\text{–}32)$$

In the same way it can be deduced that the transformation of the impedance Z_{gIIaI} is

$$Z_{gIIaI} U(t) \equiv \varepsilon_a R_g \{1 - \tfrac{1}{2}(1-P) e^{p_1 t} - \tfrac{1}{2}(1+P) e^{p_2 t}\} U(t). \qquad (I\text{–}33)$$

where

$$P = \frac{2T-B}{B\sqrt{1-4E/B^2}}. \qquad (I\text{–}34)$$

Then, expression (I–23) will be:

$$Z_{gIIaI} I_a = \varepsilon_a R_g I_{ao} \{1 - \tfrac{1}{2}(1-P) e^{p_1 t} - \tfrac{1}{2}(1+P) e^{p_2 t}\} U(t) \qquad (I\text{–}35)$$

The total voltage between G_{II} and earth during the first phase of the dynamic condition, as given by expression (I–21), will be the following time-function:

$$V_{gII}(t) = V_{gIIo} - a C_c (1-\varepsilon_g) R_g [\{1 - \tfrac{1}{2}(1-K) e^{p_1 t} - \tfrac{1}{2}(1+K) e^{p_2 t}\}$$
$$U(t) - \{1 - \tfrac{1}{2}(1-K) e^{p_1(t-t_o)} - \tfrac{1}{2}(1+K) e^{p_2(t-t_o)}\} U(t-t_o)] + \varepsilon_a R_g I_{ao}$$
$$\{1 - \tfrac{1}{2}(1-P) e^{p_1 t} - \tfrac{1}{2}(1+P) e^{p_2 t}\} U(t) \qquad (I\text{–}36)$$

(2) The voltage between A_I and earth (fig. 6–2)
This voltage will be:

$$V_{aI}(t) = V_{aIo} + Z_{iaI} I_a + Z_{aIgII} I_i. \qquad (I\text{–}37)$$

The transformation of the impedance Z_{iaI} into a time function is:

$$Z_{iaI} U(t) \equiv (1-\varepsilon_a) R_a \{1 - \tfrac{1}{2}(1-L) e^{p_1 t} - \tfrac{1}{2}(1+L) e^{p_2 t}\} U(t) \qquad (I\text{–}38)$$

where

$$L = \frac{2D-B}{B\sqrt{1-4E/B^2}} \qquad (I\text{–}39)$$

Expression (I–37), therefore, will be

$$V_{aI}(t) = V_{aIo} + (1-\varepsilon_a) R_a I_{ao} \{1 - \tfrac{1}{2}(1-L) e^{p_1 t} - \tfrac{1}{2}(1+L) e^{p_2 t}\} U(t) -$$
$$- a C_c \varepsilon_a R_g \{1 - \tfrac{1}{2}(1-P) e^{p_1 t} - \tfrac{1}{2}(1+P) e^{p_2 t}\} U(t) -$$
$$- \{1 - \tfrac{1}{2}(1-P) e^{p_1(t-t_o)} - \tfrac{1}{2}(1+P) e^{p_2(t-t_o)}\} U(t-t_o)]. \qquad (I\text{–}40)$$

(3) The voltage between G_I and earth (fig. 6–3)

$$V_{gI}(t) = V_{goI} + Z_{igI}(I_i + I_g),\qquad (\text{I–41})$$

where

$$I_i + I_g = (-a\,C_c + I_{go})\,U(t) + a\,C_c\,U(t - t_o)$$

and

$$V_{gIo} = o.$$

Thus:

$$V_{gI}(t) = (-a\,C_c + I_{go})\,(1 - \varepsilon_g)\,R_g\,\{1 - \tfrac{1}{2}\,(1 - K')\,e^{p_1't} - $$
$$- \tfrac{1}{2}\,(1 + K')\,e^{p_2't}\}\,U(t) + a\,C_c\,(1 - \varepsilon_g)\,R_g\,\{1 - \tfrac{1}{2}\,(1 - K')\,e^{p_1'(t - t_o)} - $$
$$- \tfrac{1}{2}\,(1 + K')\,e^{p_2'(t - t_o)}\}\,U(t - t_o)\qquad (\text{I–42})$$

(4) The voltage between A_{II} and earth (fig. 6–3)

$$V_{aII}(t) = V_{aIIo} + Z_{aIIgI}(I_i + I_g)\qquad (\text{I–43})$$

$$V_{aII}(t) = V_{aIIo} + (-a\,C_c + I_{go})\,\varepsilon_a\,R_g\,\{1 - \tfrac{1}{2}\,(1 - P')\,e^{p_1't} - $$
$$- \tfrac{1}{2}\,(1 + P')\,e^{p_2't}\}\,U(t) + a\,C_c\,\varepsilon_a\,R_g\,\{1 - \tfrac{1}{2}\,(1 - P')\,e^{p_1'(t - t_o)} - $$
$$- \tfrac{1}{2}\,(1 + P')\,e^{p_2'(t - t_o)}\}\,U(t - t_o)\qquad (\text{I–44})$$

K' is found from K by substituting p_1', p_2' and A' for p_1, p_2 and A resp., where A is given by expression (I–8) and A' is derived from A by substituting T_{aII} for T_{aI}. (see expressions (I–3) and (I–13)).
p_1' and p_2' are derived from p_1 and p_2 by replacing T_{aI} by T_{aII}, T_{gII} by T_{gI} (see expressions (I–1) and (I–12)).
P' is derived from P by replacing Index I by II and vice versa.

Appendix II. Calculation of V_{aII} in the second phase

Expression (6–29) can be evaluated if the expression $\dfrac{Z_{iaII}}{Z_{iaII} + r_a}$ and the time function $V_{aII}(t)_1 + \mu V_{gII}(t)$ are known. The first expression results from (I–19) by interchanging the indices I and II:

$$\frac{Z_{iaII}}{Z_{iaII} + r_a} = \frac{(1 - \varepsilon_a)\, R_a\, (1 + D'p)}{(1 - \varepsilon_a)\, R_a\, (1 + D'p) + r_a\, (1 + B'p + E'p^2)} \quad \text{(II–1)}$$

Calling

$$\frac{(1 - \varepsilon_a)\, R_a}{(1 - \varepsilon_a)\, R_a + r_a}\, D' + \frac{r_a}{(1 - \varepsilon_a)\, R_a + r_a}\, B' = F' \quad \text{(II–2)}$$

and

$$\frac{r_a}{(1 - \varepsilon_a)\, R_a + r_a}\, E' = G', \quad \text{(II–3)}$$

expression (II–1) can be written

$$\frac{Z_{iaII}}{Z_{iaII} + r_a} = \frac{(1 - \varepsilon_a)\, R_a}{(1 - \varepsilon_a)\, R_a + r_a}\, \frac{1 + D'p}{1 + F'p + G'p^2}. \quad \text{(II–4)}$$

The time function $V_{aII}(t)_1 + \mu\, V_{gII}(t)$ can be found from expressions (6–14) and (6–11). It is the sum of a constant term V_o and a time function $V(t)$

$$V_{aII}(t)_1 + \mu\, V_{gII}(t) = V_o + V(t). \quad \text{(II–5)}$$

From expression (6–28) it follows that

$$V_{aII}(t_{II})_1 + \mu\, V_{gII}(t_{II}) = 0. \quad \text{(II–6)}$$

or:

$$V_o + V(t_{II}) = 0. \quad \text{(II–7)}$$

Subtracting (II–7) from (II–5) gives

$$V_{aII}(t)_1 + \mu\, V_{gII}(t) = V(t) - V(t_{II}). \quad \text{(II–8)}$$

$V(t)$ is a sum of exponential functions

$$V(t) = \Sigma j\, V_j e^{p_j t} = V_5 e^{p_1't} + V_6 e^{p_2't} + \mu\, V_2 e^{p_1 t} + \mu\, V_3 e^{p_2 t} \quad \text{(II–9)}$$

V_5, V_6, V_2 and V_3 are given in chapter 6.

Thus:

$$V(t) - V(t_{II}) = \Sigma j\, V_j\, (e^{p_j t} - e^{p_j t_{II}}),$$

or: $\qquad V_{aII}(t)_1 + \mu\, V_{gII}(t) = \Sigma j\,[-V_j\, e^{p_j t_{II}}\{1 - e^{p_j(t-t_{II})}\}].$ (II–10)

Transformed into a p-function, this becomes:

$$\{V_{aII}(t)_1 + \mu\, V_{gII}(t)\}\, U(t-t_{II}) \equiv \Sigma j\left\{-V_j\, e^{p_j t_{II}}\frac{-p_j}{p-p_j}\, U(t-t_{II})\right\}.\ \text{(II–11)}$$

The evaluation of expression (6–29) is now reduced to the calculation of time functions, corresponding to an operational expression of the following form:

$$f_j(t-t_{II}) \equiv \frac{1+D'p}{1+F'p+G'p^2}\,\frac{-p_j}{p-p_j}\, U(t-t_{II})\qquad \text{(II–12)}$$

Expression (II–12) can be split up into partial fractions, the result being:

$$f_j(t-t_{II}) \equiv -\frac{p_j}{G'}\frac{X_{1j}}{p-p_3}+\frac{X_{2j}}{p-p_4}+\frac{X_{3j}}{p-p_j}\, U(t-t_{II}).\ \text{(II–13)}$$

where

$$p_3 = -\frac{F'}{2G'}\left\{1-\sqrt{1-\frac{4G'}{F'^2}}\right\}\qquad \text{(II–14)}$$

$$p_4 = -\frac{F'}{2G'}\left\{1+\sqrt{1-\frac{4G'}{F'^2}}\right\}\qquad \text{(II–15)}$$

p_3 and p_4 are negative, real quantities.

$$X_{1j} = \frac{1+D'p_3}{(p_3-p_4)(p_3-p_j)}\qquad \text{(II–16)}$$

$$X_{2j} = \frac{1+D'p_4}{(p_4-p_3)(p_4-p_j)}\qquad \text{(II–17)}$$

$$X_{3j} = \frac{1+D'p_j}{(p_j-p_3)(p_j-p_4)}\qquad \text{(II–18)}$$

The time functions, corresponding to the p-functions in expression (II–13) are well-known exponential functions, thus:

$$f_j(t-t_{II}) = -\frac{p_j}{G'}\left[\frac{X_{1j}}{-p_3}\{1-e^{p_3(t-t_{II})}\}+\frac{X_{2j}}{-p_4}\{1-e^{p_4(t-t_{II})}\}+\right.$$

$$\left.+\frac{X_{3j}}{-p_j}\{1-e^{p_j(t-t_{II})}\}\right]U(t-t_{II}).\qquad \text{(II–19)}$$

Substituting expressions (II–4), (II–11) and (II–12) in (6–29) gives:

$$V_{aII}(t) = V_{aII}(t)_1 - \left[\frac{(1-\varepsilon_a)\,R_a}{(1-\varepsilon_a)\,R_a + r_a} \Sigma j \left\{ -V_j\, e^{p_j t_{II}} f_j\,(t-t_{II}) \right\} \right] U\,(t-t_{II})$$

$$(II\text{--}20)$$

Finally, expression (II–19) must be substituted, giving:

$$V_{aII}(t) = V_{aII}(t)_1 - \frac{(1-\varepsilon_a)\,R_a}{(1-\varepsilon_a)\,R_a + r_a} \Sigma j\, \frac{V_j\,p_j}{G'}\, e^{p_j t_{II}} \left| \frac{X_{1j}}{-p_3} \{1 - e^{p_3(t-t_{II})}\} + \right.$$

$$\left. + \frac{X_{2j}}{-p_4} \{1 - e^{p_4(t-t_{II})}\} + \frac{X_{3j}}{-p_j} \{1 - e^{p_j(t-t_{II})}\} \right] U\,(t-t_{II}). \quad (II\text{--}21)$$

For the asymmetrical multivibrator there are four terms, constituting the sum in expression (II–21), because there are four reciprocal time constants p_j, viz. p_1, p_2, p_1', p_2'.
To p_1 corresponds:

$$V_j = \mu\,V_2 = \mu\,\{\tfrac{1}{2}\,a\,C_c\,(1-\varepsilon_g)\,R_g\,(1-K)\,(1-e^{-p_1 t_o}) -$$

$$- \tfrac{1}{2}\,I_{ao}\,\varepsilon_a\,R_g\,(1-P)\} \quad (II\text{--}22)$$

To p_2 corresponds:

$$V_j = \mu\,V_3 = \mu\,\{\tfrac{1}{2}\,a\,C_c\,(1-\varepsilon_g)\,R_g\,(1+K)\,(1-e^{-p_2 t_o}) -$$

$$- \tfrac{1}{2}\,I_{ao}\,\varepsilon_a\,R_g\,(1+P)\}. \quad (II\text{--}23)$$

To p_1' corresponds:

$$V_j = V_5 = \tfrac{1}{2}\,a\,C_c\,\varepsilon_a\,R_g\,(1-P')\,(1-e^{-p_1' t_o}) - \tfrac{1}{2}\,I_{go}\,\varepsilon_a\,R_g\,(1-P').$$

$$(II\text{--}24)$$

To p_2' corresponds:

$$V_j = V_6 = \tfrac{1}{2}\,a\,C_c\,\varepsilon_a\,R_g\,(1+P')\,(1-e^{-p_2' t_o}) - \tfrac{1}{2}\,I_{go}\,\varepsilon_a\,R_g\,(1+P').$$

$$(II\text{--}25)$$

For the symmetrical multivibrator there are only two terms in the sum of expression (II–21) corresponding to p_1 and p_2, respectively.

$$V_j = \mu\,V_2 + V_5 = \{\tfrac{1}{2}\,\mu\,a\,C_c\,(1-\varepsilon_g)\,R_g\,(1-K) + \tfrac{1}{2}\,a\,C_c\,\varepsilon_a\,R_g\,(1-P)\}$$

$$(1-e^{-p_1 t_o}) - (\mu\,I_{ao} + I_{go})\,\varepsilon_a\,R_g\,(1-P) \quad (II\text{--}26)$$

$$V_j = \mu\,V_3 + V_6 = \{\tfrac{1}{2}\,\mu a\,C_c\,(1-\varepsilon_g)\,R_g\,(1+K) + \tfrac{1}{2}\,a\,C_c\,\varepsilon_a\,R_g\,(1+P)\}$$

$$(1-e^{-p_2 t_o}) - \tfrac{1}{2}\,(\mu\,I_{ao} + I_{go})\,\varepsilon_a\,R_g\,(1+P) \quad (II\text{--}27)$$

For this case, the complete expression for V_{aII} will be given, expressions (II–26) and (II–27) being substituted into expression (II–21):

$$V_{aII}(t) = V_{aII}(t)_1 - \frac{(1-\varepsilon_a)\,R_a}{(1-\varepsilon_a)\,R_a + r_a}\left[\frac{p_1}{G'}\,e^{p_1 t_{II}}\right.$$

$$\left\{\left\{\tfrac{1}{2}\,\mu a C_c\,(1-\varepsilon_g)\,R_g\,(1-K) + \tfrac{1}{2}\,a C_c \varepsilon_a\,R_g\,(1-P)\right\}(1-e^{-p_1 t_0}) - \right.$$

$$\left. - \tfrac{1}{2}\,(\mu\,I_{ao} + I_{go})\,\varepsilon_a\,R_g\,(1-P)\right\}\left\{\frac{1+Dp_3}{-p_3\,(p_3-p_4)\,(p_3-p_1)}(1-e^{p_3(t-t_{II})}) + \right.$$

$$\frac{1+Dp_4}{-p_4\,(p_4-p_3)\,(p_4-p_1)}(1-e^{p_4(t-t_{II})}) + \frac{1+Dp_1}{-p_1\,(p_1-p_3)\,(p_1-p_4)}$$

$$\left.(1-e^{p_1(t-t_{II})})\right\} + \frac{p_2}{G'}\,e^{p_2 t_{II}}\left\{\left\{\tfrac{1}{2}\,\mu a C_c\,(1-\varepsilon_g)\,R_g\,(1+K) + \tfrac{1}{2}\,a C_c\,\varepsilon_a\,R_g\right.\right.$$

$$\left.(1+P)\right\}(1-e^{-p_2 t_0}) - \tfrac{1}{2}\,(\mu\,I_{ao} + I_{go})\,\varepsilon_a\,R_g\,(1+P)\right\}$$

$$\left\{\frac{1+Dp_3}{-p_3\,(p_3-p_4)\,(p_3-p_2)}(1-e^{p_3(t-t_{II})}) + \frac{1+Dp_4}{-p_4\,(p_4-p_3)\,(p_4-p_2)}\right.$$

$$\left.\left.(1-e^{p_4(t-t_{II})}) + \frac{1+Dp_2}{-p_2\,(p_2-p_3)\,(p_2-p_4)}(1-e^{p_2(t-t_{II})})\right\}\right]\,U\,(t-t_{II})\quad\text{(II–28)}$$

Appendix III. Calculation of V_{gI} in the second phase

The voltage between G_I and cathode during the second phase of the dynamic condition will be the sum of the value derived for the first phase and a component produced by the response of the network of fig. III–1 to the voltage source:

$$V_c(t) = - [V_{aII}(t)_1 + \mu V_{gII}(t)]\, U(t - t_{II}) \equiv$$

$$\equiv \Sigma_j V_j\, e^{p_j t_{II}} \frac{-p_j}{p - p_j}\, U(t - t_{II}). \qquad (\text{III–1})$$

according to expression (II–11).
Comparison of fig. III–1 with fig. 6–3 will make clear that
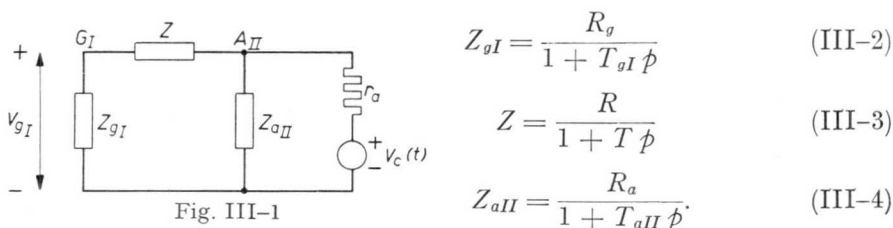

Fig. III–1

$$Z_{gI} = \frac{R_g}{1 + T_{gI}\, p} \qquad (\text{III–2})$$

$$Z = \frac{R}{1 + T\, p} \qquad (\text{III–3})$$

$$Z_{aII} = \frac{R_a}{1 + T_{aII}\, p}. \qquad (\text{III–4})$$

Now it can be deduced by simple application of Kirchhoff's laws that the response to $V_c(t)$ causes a component:

$$V_{gI}^*(t) = \frac{Z_{gI}\, Z_{aII}}{(Z + Z_{gI})\, Z_{aII} + r_a(Z + Z_{gI} + Z_{aII})}\, V_c(t). \qquad (\text{III–5})$$

After introducing expressions (III–2), (III–3) and (III–4), this gives finally:

$$V_{gI}^*(t) = \frac{R_g(1 - \varepsilon_a)\, R_a(1 + T\, p)}{(R + R_g)\{(1 - \varepsilon_a)\, R_a + r_a\}(1 + F'p + G'p^2)}\, V_c(t), \qquad (\text{III–6})$$

where F' and G' correspond to the values given in appendix II by expressions (II–2) and (II–3) resp. Introducing expression (III–1) gives:

$$V_{gI}^*(t) = \frac{R_g(1 - \varepsilon_a)\, R_a}{(R + R_g)\{(1 - \varepsilon_a)\, R_a + r_a\}\, G'}\, \Sigma_j - V_j\, e^{p_j t_{II}}\, p_j$$

$$\frac{1 + T\, p}{(p - p_j)(p - p_3)(p - p_4)}\, U(t - t_{II}). \qquad (\text{III–7})$$

where p_3 and p_4 are given by expressions (II–14) and (II–15).
In an analogous way to the method of appendix II, by splitting the p-function into partial fractions, the sum can be written:

$$\Sigma j - V_j \, e^{p_j t_{II}} \, p_j \left(\frac{Y_{1j}}{p - p_3} + \frac{Y_{2j}}{p - p_4} + \frac{Y_{3j}}{p - p_j} \right) U \, (t - t_{II}).$$

which gives for V^*_{gI} as a function of time:

$$V^*_{gI} \, (t) = - \frac{R_g \, (1 - \varepsilon_a) \, R_a}{(R + R_g) \, \{(1 - \varepsilon_a) \, R_a + r_a\} \, G'} \, \Sigma_j \, V_j \, p_j \, e^{p_j t_{II}} \left[\frac{Y_{1j}}{-p_3} \right.$$

$$\left. \{1 - e^{p_3(t - t_{II})}\} + \frac{Y_{2j}}{-p_4} \{1 - e^{p_4(t - t_{II})}\} + \frac{Y_{3j}}{-p_j} \{1 - e^{p_j(t - t_{II})}\} \right] U \, (t - t_{II})$$

$$\text{(III–8)}$$

The Y-functions have the following form:

$$Y_{1j} = \frac{1 + T \, p_3}{(p_3 - p_4) \, (p_3 - p_j)} \qquad \text{(III–9)}$$

$$Y_{2j} = \frac{1 + T \, p_4}{(p_4 - p_3) \, (p_4 - p_j)} \qquad \text{(III–10)}$$

$$Y_{3j} = \frac{1 + T \, p_j}{(p_j - p_3) \, (p_j - p_4)}. \qquad \text{(III–11)}$$

The total voltage at G_I in the second phase will be:

$$V_{gI} \, (t) = V_{gI} \, (t)_1 + V_{gI}{}^* \, (t). \qquad \text{(III–12)}$$

Appendix IV. Calculation of the transients at A_{II}, G_I and A_I in the third phase

Expression (6–33) is of the same kind as the second right-hand term of expression (6–29), and consequently can be evaluated by the same procedure as was applied in Appendix II. By analogy with expression (II–10), we can write:

$$\mu\, V_{gII}\,(t) = -\Sigma j\, V_j\, e^{p_j t_s} \{1 - e^{p_j(t-t_s)}\}. \tag{IV–1}$$

The sum consists of only two components, viz. for $p_j = p_1$ and $p_j = p_2$, corresponding to:

$$V_j = \mu V_2 \tag{IV–2}$$

(of expression II–22) and

$$V_j = \mu V_3 \tag{IV–3}$$

(of expression II–23), respectively.

The calculation of expr. (6–33) will lead to a form similar to that of the second right-hand term of expression (II–21), viz.:

$$V_{aII}^{**}\,(t) = \frac{(1 - \varepsilon_a)\, R_a}{\{(1 - \varepsilon_a)\, R_a + r_a\}G'}\, \Sigma j\, V_j\, p_j\, e^{p_j t_s} \left[\frac{X_{1j}}{-p_3}\{1 - e^{p_3(t-t_s)}\} +\right.$$

$$\left. + \frac{X_{2j}}{-p_4}\{1 - e^{p_4(t-t_s)}\} + \frac{X_{3j}}{-p_j}\{1 - e^{p_j(t-t_s)}\}\right] U\,(t - t_s) \tag{IV–4}$$

Here the sum contains two terms ($p_j = p_1$ and $p_j = p_2$ resp.).
For expr. (6–34) it will be found by analogy with expr. (III–8):

$$V_{gI}^{**}(t) = \frac{R_g\,(1 - \varepsilon_a)\, R_a}{(R + R_g)\,\{(1 - \varepsilon_a)\, R_a + r_a\}G'}\, \Sigma j\, V_j\, p_j e^{p_j t_s} \left[\frac{Y_{1j}}{-p_3}\{1 - e^{p_3(t-t_s)}\} +\right.$$

$$\left. + \frac{Y_{2j}}{-p_4}\{1 - e^{p_4(t-t_s)}\} + \frac{Y_{3j}}{-p_j}\{1 - e^{p_j(t-t_s)}\}\right] U\,(t - t_s) \tag{IV–5}$$

For calculating expression (6–35), reference is made to expr. (I–5), (I–6), from which it follows that:

$$\frac{Z_{aI}}{Z + Z_{aI}} = \beta_a \frac{1 + T\, p}{1 + T_n\, p}. \tag{IV–6}$$

where

$$\beta_a = \frac{R_a}{R + R_a} \tag{IV–7}$$

$$T_n = \beta_a\, T + (1 - \beta_a)\, T_{aI} \tag{IV–8}$$

V_{gII} is given by expression (6–11):

$$V_{gII}(t) = V_1 + V_2 e^{p_1 t} + V_3 e^{p_2 t}, \tag{IV-9}$$

which is equivalent to expression (IV–1) divided by μ. (see also expressions (6–15), (6–16), and (6–17).

At $t = t_s$, $V_{gII}(t) = 0$.

thus:

$$0 = V_1 + V_2 e^{p_1 t_s} + V_3 e^{p_2 t_s}, \tag{IV-10}$$

or:

$$V_{gII}(t)\, U(t - t_s) = [V_2 e^{p_1 t_s} \{e^{p_1(t - t_s)} - 1\} + V_3 e^{p_2 t_s} \{e^{p_2(t - t_s)} - 1\}]\, U(t - t_s).$$

Transformed into a p-function:

$$V_{gII}(t)\, U(t - t_s) \equiv V_2 e^{p_1 t_s} \frac{p_1}{p - p_1} + V_3 e^{p_2 t_s} \frac{p_2}{p - p_2}. \tag{IV-11}$$

Now expression (6–35) can be written:

$$V_{aI}^{**}(t) = \beta_a \frac{1 + T p}{1 + T_n p}\left(-V_2 e^{p_1 t_s} \frac{p_1}{p - p_1} - V_3 e^{p_2 t_s} \frac{p_2}{p - p_2}\right) U(t - t_s). \tag{IV-12}$$

Determination of the corresponding time function results in:

$$V_{aI}^{**}(t) = \beta_a\, p_n \left[p_1 V_2 e^{p_1 t_s} \left\{ \frac{1 + T p_n}{-p_n(p_n - p_1)}(1 - e^{p_n(t - t_s)}) + \frac{1 + T p_1}{-p_1(p_1 - p_n)} \right. \right.$$

$$\left. (1 - e^{p_1(t - t_s)}) \right\} + p_2 V_3 e^{p_2 t_s} \left\{ \frac{1 + T p_n}{-p_n(p_n - p_2)}(1 - e^{p_n(t - t_s)}) + \frac{1 + T p_2}{-p_2(p_2 - p_n)} \right.$$

$$\left. \left. (1 - e^{p_2(t - t_s)}) \right\} \right] U(t - t_s). \tag{IV-13}$$

where,

$$p_n = -\frac{1}{T_n}. \tag{IV-14}$$

Appendix V. Discussion of the method of calculating the influence of C_{ag} on the trigger sensitivity

Referring to fig. 6–1, which represents the multivibrator circuit at the start of the first phase of the dynamic condition, it can be seen that several current generators operate on the circuit. The basic cause, which starts all transient phenomena occurring in the whole triggering action, is the application of the input trigger voltage according to fig. 3–2. This trigger voltage is transformed into a current pulse I_i, (chapter 6). It causes a current step I_{ao} between the anode of tube I and earth and another current step I_{go} between grid I and earth. Of the three current sources mentioned, I_{ao} is by far the most important, and it is this, in fact, which enables the multivibrator to be definitely triggered. This current source I_{ao} gives rise to a rather steep and large voltage change at A_I. The voltage change at A_{II} will be much smaller as no current source is directly operating at A_{II}. Only the current source $I_{go} + I_i$ at G_I will cause, via the coupling network RC, a modest change in potential at A_{II} (compare figs. 7–3 and 7–4).

The influence of the anode-to-grid capacitances is to feed back a fraction of the anode-voltage changes to the corresponding grids and via the RC-coupling elements to the other anode. The change in grid voltage because of this feedback is much more important than that at the anodes, when determining the times t_I and t_{II} (expressions 8–5 and 8–6), as the influence of the anode voltage changes is reduced by a factor μ. Moreover, to a first approximation the feedback in tube I is the only one to consider because the voltage change at A_I is the most important. However, as may be seen from section 8, in the case of the symmetrical multivibrator, it is wise to consider the feedback in both tubes, as this leads to a more elegant solution of the problem of finding the minimum trigger-voltage amplitude.

LIST OF SYMBOLS

A time constant (p. 64);
constant of the dimension voltage (p. 43).

B time constant (p. 64)
b ratio of capacitances (p. 42).

C capacitance
C_a capacitance between the anode and the cathode of a tube.
C_g capacitance between the grid and the cathode of a tube.
C_{ag} capacitance between the anode and the grid of a tube.

D time constant (p. 65).

E square of a time constant (p. 65).
E base of natural logarithm (2.71828...) (p. 24).

F time constant (p. 69).

G square of a time constant (p. 69).
g_m transconductance of a tube (p. 46)

I current
I_a anode current of a tube
I_{ao} anode current in the static condition of a multivibrator.
I_g grid current of a tube.
I_{go} grid current in the static condition of a multivibrator.

K ratio of time constants (p. 66).

L ratio of time constants (p. 67).

p operation of dimension frequency or reciprocal time (p. 64).
P ratio of time constants (p. 67).

R resistance.

R_a anode-load resistance of a tube.

R_g grid-leak resistance of a tube.

r_a internal anode resistance of a tube.

r_g internal grid resistance of a tube.

t time.

t_o rise time of the trigger pulse Vi (p. 11).

t_{II} instant at which the second phase of the dynamic condition commences (p. 12).

t_s instant at which the third phase of the dynamic condition commences (p. 13).

T time constant.

$U(t)$ unit-step function: $U(t) = 0$ at $t < 0$
 $\phantom{\text{unit-step function: }}U(t) = 1$ at $t > 0$.

V voltage.

V_a voltage between the anode and the cathode of a tube.

V_g voltage between the grid and the cathode of a tube.

V_i trigger voltage at the grids of the tubes of a multivibrator circuit (p. 11).

V_o amplitude of trigger pulse Vi (p. 11);
constant voltage (p. 20, 69).

X constant (p. 70).

x abbreviation of an exponential time function (p. 43).

Y constant (p. 74).

Z impedance.

α slope of the leading flank of the trigger pulse Vi (p. 11); slope of characteristic curve (fig. 4—3).

β ratio of resistances (p. 75).

μ amplification factor of a tube.

ε ratio of resistances (p. 18, 19).

γ ratio of time constants (p. 43).

∞ infinite (time) (p. 25).